Modelling, optimisation and control of osmotic energy extraction from natural salinity gradients using pressure retarded osmosis

A thesis submitted by

Wei He

in partial fulfilment of
the requirement of the degree of

Doctor of Philosophy

in the

School of Engineering and Material Science
Queen Mary, University of London
Mile End Road
London, E1 4NS
UK

2016

School of Engineering and Material Science

Queen Mary, University of London

PhD THESIS

DECLARATION

This thesis entitled

Modelling, optimisation and control of osmotic energy extraction from natural salinity gradients using pressure retarded osmosis

I confirm that this thesis has not been previously submitted for the award of a degree by this or any other university.

Name WEI HE

Signed

Date

Abstract

This thesis investigates the osmotic power generation from natural salinity gradients using pressure retarded osmosis (PRO), focusing on modelling, optimisation and control of the process. In this study, first, due to the lack of the model to represent the realistic scale PRO osmotic power plant, the mathematical model of a scale-up PRO osmotic power plant is developed based on the validated non-linear transport equations of water and solute flux across the membrane, and the flows in the membrane channels. The developed PRO model considers the detrimental effects in a scale-up process, namely internal concentration polarisation in the support layer, external concentration polarisation near the active layer in the draw solution channel, and the reverse solute permeation across the membrane. Then, on the basis of the developed model, the overall performance of the scale-up PRO due to the detrimental effects of the mass transfer is addressed. In a scale-up PRO process, the performance of the scale-up PRO process is significantly dependent on the dimensionless flow rate. Furthermore, with the increase of the specific membrane scale, the accumulated solute leakage becomes important. The preferred membrane to achieve the optimal performance moves to the low permeability in order to reduce the detrimental effect of the reverse solute permeation. And counter-current flow scheme results in more evenly distributed water permeation across the membrane in a scale-up PRO process, compared to the co-current flow scheme. The counter-current flow scheme is capable to increase the process performance with a higher permeable and less selectable membrane compared to the co-current flow scheme.

Moreover, different configurations and flow schemes of PRO are analysed and optimised in order to maximise the osmotic energy generation from the natural salinity gradients. Configurations includes single-stage PRO system, two-stage PRO system, hybrid reverse osmosis (RO) and PRO system, and hybrid solar photovoltaic and osmotic PRO powered RO desalination system in this work. The case study of the proposed PVROPRO plant developed based on the hourly solar data of Perth Australia in a year indicates that the highest weekly production rate is found to be almost 20 times the rate in PVRO in the same week. Annual production is increased more than nine times compared to the stand-alone PVRO plant. However, detrimental effects also potentially cause the weekly permeation production rate reduction in the range of 16-20% and the overall annual reduction is 18.07% in the case study of Perth. Moreover, in order to deal with the possible fluctuations of the

operating condition, maximum power point tracking (MPPT) control of a PRO osmotic power plant is studied. Two algorithms, perturb & observe and incremental mass-resistance method, are proposed and investigated. Both the algorithms are demonstrated to be capable of tracking the maximum power point. In order to improve the performance of the MPPT, furthermore, an optimum model-based controller (OMC) and the strategy to coordinate MPPT and OMC are developed and investigated by simulation. The results demonstrate the capability of OMC to deal with the rapid variations of the salinities.

Table of Contents

List of Figures

List of Tables

Acronyms

APD	Average power density
BP	Boost pump
CAMIX	Capacitive mixing
CPRO	Constant-pressure pressure retarded osmosis
DPRO	PRO with detrimental effects
ECP	External concentration polarisation
ERD	Energy recovery device
HP	High-pressure pump
HT	Hydro-turbine
ICP	Internal concentration polarisation
IMR	Incremental mass-resistance
INC	Incremental conductance
IPRO	Ideal PRO process
MPP	Maximum power point
MPPT	Maximum power point tracking
OMC	Optimum model-based controller
ODEs	Ordinary differential equations
P&O	Perturb & observe
PD	Power density
PRO	Pressure retarded osmosis
PV	Photovoltaic
RED	Reverse electrodialysis
RES	Renewable energy source
RO	Reverse osmosis
RSP	Reverse solute permeation
SEE	Specific extractable energy
TDS	Total dissolved solid
TFC	Thin-film composite

Acknowledgments

I would like to express profound gratitude to my academic supervisor, Dr M Hasan Shaheed, for his invaluable support, endless encouragement, enthusiastic supervision and useful suggestions throughout this research work. His wide knowledge and his logical way of thinking have been of great value for me. His moral support and continuous guidance enabled me to process my work successfully.

I wish to express my warm and sincere thanks to Dr Huasheng Wang, Dr Yi Sui, Dr Guang Li, and Dr Henri Huijbert in School of Engineering and Material Science (SEMS) at QMUL. They constantly support my PhD study by offering me demonstration works and giving me valuable advices on research and career. Their support and advice have had a remarkable influence on my entire career in the research field. During my time at SEMS, I have met a number of graduate students I am lucky to call friends today. The numerous happy hours and discussion time we had will forever be great memories of my precious PhD period.

I would like to thank the Henry-Lester Trust (UK) and the Great Britain–China Educational Trust (UK) for the generous sponsorship to my PhD project

Last but not least, a big thank you to my family who are the most special persons in my life. They, not only gave me life, but also fill it with all the love and affection one can wish for.

Introduction

1.1 BACKGROUND

Water is one of the most abundant resources on earth. However, most of it, about 97%, is salt water in the oceans, and 3% belongs to freshwater. The small percentage of water in the earth sustaining all the livings is stored in ground, lakes and rivers. Nowadays, the freshwater provision is becoming an increasingly important issue in many areas of the world [1]. In arid areas, drinking water is very scarce and water impendence has been demonstrated to be necessary in establishing a human habitat. In cities, with rapidly increasing population and environmental pollution, the demand for potable water is becoming to be rapidly stressed, especially in London whose population is estimated to grow by 12% over the next 20 years [2]. London's water supply is classed by the UK Environment Agency as "seriously water stressed" [3]. It indicates a significant potential risk of water shortage for customers in dry periods. Faced with the scarcity, desalination has been demonstrated to be one of the prominently viable methods to increase water supply [4]. Considering the huge capacity of seawater, desalination is expected to offer a

seemingly unlimited, steady supply of high quality water, without impairing natural freshwater ecosystems [5]. Currently, in remote areas, a small scale water desalination plant to provide drinking water for community has been used [6]. In cities, desalination water system has started to be a fresh water source. In London, a reverse osmosis (RO) plant desalinating 150,000 m^3 per day has been constructed in Becton in order to mitigate the gap between limited supply and increasing demand [7]. However, the major challenges for widely using desalination as a potable water source are the high economic cost and environmental risk, especially due to enormous energy consumption, carbon dioxide emission and concentrated brine discharge. High energy cost involved in desalination limits the more widely application in the world.

Among the current mature desalination technologies, RO is the most energy efficient method, which is a pressure driven membrane process. An applied pressure is exerted on the saline water side and used to drive the freshwater reversely permeate from the high concentration side to the low concentration side across a semi-permeable membrane. A high performance membrane should have maximum permeability and selectivity over the dissolved salt in the saline water. Currently, RO process is the most efficient technology among the widely used mature desalination processes. It has developed over the past 40 years to a 44% share in world desalting production capacity, and 80% share in the total number of desalination plants installed worldwide [8]. The economic cost in RO results from energy consumption, investment and maintenance cost of membrane and equipment, and labour expenses. Energy cost of pumps is reported as the major portion of the total cost and it reaches up to 45% of the water production cost [9, 10]. Consequently, it is important to reduce the energy consumption for the purpose of spreading the technology by making it affordable to more people.

One significant improvement is the availability of high performance RO membrane. After introduction of highly permeable membranes in mid 1990s with low salt passage [11], the significant improvement in energy reduction to operate the plant has become attainable according to the achievable high-permeable productivity. Since then the RO is operated at the thermodynamic restriction which is close to the theoretical operational optimum with the minimum energy consumption. In Fig. 1.1, as Wilf reported [11], when highly permeable membrane is used, the minimal applied pressure would be very close to the osmotic pressure of the RO concentration at the exit of membrane. As a result, the greatest

efficiency gains have arisen from the improvement of the membrane by modifying the structure, material, and morphology of a RO membrane to facilitate the high water permeability, salt rejection and applicability in mechanical, chemical and biological stability.

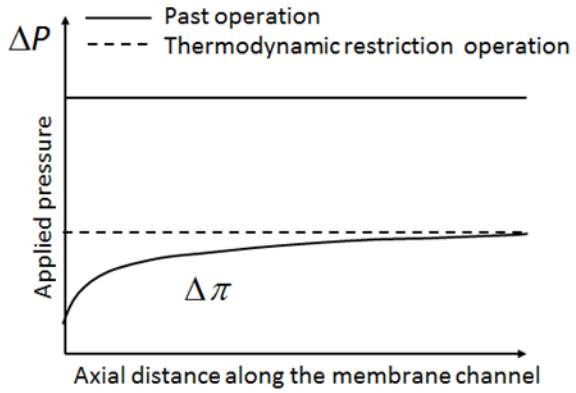

Figure 1.1: Illustration of the thermodynamic restriction of the RO operation [12].

Besides high performance membranes, optimisation in operational conditions also reduces the specific energy consumption (SEC) of a RO process. Fan et al. [12-14] analysed the RO system with respect to water recovery, energy recovery, system efficiency, feed flow and permeate flow rate, as well as the applied trans-membrane pressure. Their efforts were dedicated to decrease the SEC by increasing water recovery with a fixed feed flow rate and applied pressure. In accordance with the high permeable membrane, optimal configurations of a RO operated at the thermodynamics restriction, were systematically investigated. Zhu and his colleagues [15-17] carried out a series of investigations on theoretical framework of a RO desalination which included the optimisation of single stage RO on SEC with different water recovery ratios, brine management, constrained feed and permeate flow rate, the efficiency of pump and the pressure drop in the membrane. They reported the global minimal SEC based on the thermodynamic restriction and the variations of optimal water recovery ratios of minimal SEC in different operations. Based on energy optimisation, the two-stage RO process is more favourable than single-stage process at the same level of total water recovery. In addition, the overall energy consumption for desalinating water will be significantly reduced if the high hydraulic energy of brine water can be recovered. This can be done using a variety of energy

recovery devices (ERDs), including the Francis turbine, Pelton Wheel, turbocharger, SWEER and Pressure Exchanger [18].

Furthermore, investigations were also carried out in employing environmentally-friendly energy sources to drive the separation process desalinate seawater. The renewable energy technologies include solar thermal [19], photovoltaic (PV) [20-23], wind [24-26], geothermal energy [27, 28] and hybrid energy source [6, 29]. Since 2010, osmotic energy recovery/generation from salinities in desalination plant has attracted a huge amount of attention [30-35]. Osmotic energy, or salinity energy, released from the mixing of the salinity gradients (such as freshwater, river water and seawater) is also a source of renewable energy that is eco-friendly with no significant emission of greenhouse gases during the operation. In addition, compared to other renewable energy sources, it is less periodic and has no significant operational hazards. A remarkable amount of osmotic energy available from the salinity gradients between seawater and fresh water due to the enormous discharge of river to seawater annually [36]. Its potential energy capacity which is estimated to be around 2 TW, which is about 13% of the current world energy consumption [37]. Actually, mixing energy from natural salinity gradients has been regarded as one of renewable energy sources since 1950s [38].

Common approaches to extract osmotic energy include reverse electrodialysis (RED) and pressure retarded osmosis (PRO), which can be regarded as the reverse process of electrodialysis (ED) and RO in desalination. RED is an emerging membrane based technique that generates electrical power from the salinity gradients [5, 39]. During the RED process, the composite ions are driven by the salinity difference transporting across the ion-exchange membrane. The ion flows are converted into electron flows at the electrodes. The discharge can be seen as the flow of the solutes due to the salinity difference until the equilibrium of the solutes is reached. Prior studies of RED focused on not only an independent unit operation [40-42], but also the hybrid RED-RO plant in which RED as the pre and post treatment of RO [30].

1.2 RECENT DEVELOPMENTS IN PRESSURE RETARDED OSMOSIS

PRO is one of the most developed technologies to capture the osmotic energy from salinities, which was reported achieving both higher efficiencies and higher power densities than the RED [43]. PRO is an osmotic-pressure driven membrane process, taking advantage

of natural osmosis process to permeate water from a low concentration side to a high concentration side through a semi-permeable membrane, and expanding the pressurised water in hydro-turbine to generate electricity. PRO was invented by Sidney Loeb in 1970s' [44], and developed rapidly in recent years due to significant improvement of membrane performance [45]. In 2009, the world's first PRO plant was launched in Norway with 4kW capacity [34]. Recently, a membrane distillation (MD) and PRO hybrid desalination demonstration plant is being built in Korea, which is a five year project costing 23 million USD [46].

However, the power density and energy capacity of a PRO from natural salinity gradients are much lower than the theoretical calculation due to its low water permeability and the suboptimal structure of the support layer of membrane that is likely to be fouled and substantially reducing the water flux [47, 48]. In order to minimise the potential fouling effects, different membrane types and orientations, as well as operations of a PRO process were investigated [49]. It is noted that PRO process has been researched not only as an independent power plant [34], but also as pre or post treatment to recover osmotic energy from high concentration brine discharge in a hybrid process of RO and forward osmosis (FO) processes [50, 51]. Most of them were focused on improving water flux and power density of the process [52, 53] and only a few also focused on energy generation [32, 54]. Theoretically, the maximum energy generated by a PRO process can be calculated by the Gibbs free energy based on the second law of energy conservation [55]. Considering the irreversible loss, the viewpoint of extractable energy was incorporated into the energy analysis [32]. Compared with power density, extractable energy is also significantly influenced by the applied hydraulic pressure of draw solution. However, they are inconsistent in optimal hydraulic pressure to accomplish their optimal performance. In other words, when maximum power density of a PRO is achieved, the energy available accessed by a PRO, normally, is not fully extracted [32].

To achieve the economic viability which is estimated to be 5 W/m^2 of the membrane power density [56], previous studies mainly focused on the development of the high performance membrane and the evaluation on the lab-scale PRO process. In a lab-scale PRO process, as the limited membrane area is utilised, the performance is actually the maximum or peak power densities. With a scale-up process, the strengthened draw dilution and feed concentration accompanying with the water and solute transfer are inevitable and the realistic process performance would be totally different. Due to significantly improved

membrane performance, the realistic PRO salinity power generation has become a hot topic in the field. Also, on the basis of increasingly clear understanding of the mass transfer across the membrane, mathematical modelling has become an important approach to study the scale-up process performance and explore how much are we from the economic viability of the realistic applications (5 W/m^2). These studies aimed to evaluate process performance considering the detrimental effects in the PRO mass transfer. These detrimental effects commonly exist in osmotic-driven membrane process [57], including the internal concentration polarisation (ICP) inside the support layer, external concentration polarisation (ECP) on the draw solution side near the membrane surface, and the reverse solute permeation (RSP) across the membrane. The performance limiting effects are the main reasons that limit the efficiency of the water permeation and the energy conversion. A systematic study on these performance limiting effects of PRO was carried out by Yip et al. [33]. The flux models of the water and solute considering all the ICP, ECP and RSP were derived and verified with the experimental results of different membrane properties [58].

Therefore, numerical modelling of the scale-up PRO process can be developed on the basis of these validated transport equations to study the design and operation. Lin et al. identified the thermodynamic limits of the PRO process by evaluating the extractable energy in reversible operation and constant-pressure operation for a module-scale PRO process [59]. A further analysis of the module-scale PRO considering ICP, ECP and RSP was carried out by Straub et al [60]. In addition, inspired by the theory and design of the heat exchangers, Sharqawy and Banchik studied the RO and PRO plant as the membrane mass exchangers and derived systematic effectiveness-mass transfer units (ε-MTU) models for the future design in practice [61, 62]. The method discretises the mass transfer into several units and calculates the rate of mas transfer in the mass exchanger which is the PRO membrane module. They also investigated the overall membrane performance and identified the optimum operations of a PRO plant based on ε-MTU model considering the CP effect [63]. Feinberg et al compared the performance and operations of full-scale co-current PRO and RED in the salinity power generation and found significantly reduced performance due to the increase on the process scale [64]. An iso-watt diagram for PRO performance evaluation with respect to the membrane characteristics and site specific design parameter was constructed by simulation and demonstrated to be a useful tool for goal-oriented membrane development [65]. Also, effect of the operating temperature on

hydrodynamics and membrane parameters in PRO was studied via numerical simulation [66] and validated with the experimental results [67].

In addition to the numerical studies of the stand-alone PRO process, hybrid RO-PRO configuration is a hot topic in the field due to the inherently reciprocal advantages of the two processes. Kim et al. evaluated and compared four configurations of RO-PRO systems by numerical modelling considering the spatial distribution of concentration and velocity based on mass balance principle [68]. A module-scale PRO was studied by simulation and experiment in a hybrid RO-PRO plant [69, 70]. According to the model-based simulation, it was estimated that the maximum power density of the PRO can be approximately achieved up to 10 W/m^2 in the hybrid system by using virtual membrane [69]. In the pilot system, average experimental power densities for the RO-PRO plant ranged from 1.1 to 2.3 W/m^2 [70].

1.3 MOTIVATION

As introduced earlier, problems of current technologies in desalination, such as enormous energy consumption, carbon emission, and wastewater discharge, has raised concerns. Due to the rapid increase on the utilisation of desalination worldwide, improvement on desalination needs to be achieved to reduce the carbon footprint and environmental risk. Therefore, the motivation of this research project is to investigate the solutions to these problems in energy-water-environment nexus by investigating osmotic energy generation/recovery using PRO and its application in desalination to reduce the overall energy consumption and brine discharge in desalination. PRO is one of the promising approaches to deal with the problem of energy, water and environment simultaneously, due to its inherent combination of renewable energy generation and water treatment plant. It can be used to reduce the energy consumption in drinking water production, recycle brine and wastewater, and generate electricity.

1.4 AIMS AND OBJECTIVES

The thesis is mainly focused on the mechanism and behaviour of mass transfer in PRO, based on which further optimisation and control are carried out. The aim of this research is first to develop a mathematical model of a scale-up PRO process which is capable of considering the increase of the process scale and the detrimental effects, namely ICP, ECP and RSP. Furthermore, analysis, optimisation and control of the scale-up PRO process are

aimed to carry out in different configurations and designs on the basis of the developed model.

The objectives of this research are therefore,

- Mathematical model development of the scale-up PRO process. The developed mathematical model and numerical methodology is able to estimate the detrimental effects in the mass transfer of the PRO coupled with the increase on the process scale, including ICP in the support layer, ECP in the boundary layer at the draw solution side and the RSP across the membrane.
- Evaluation of the detrimental effects and optimisation of the operation and design in the scale-up PRO process. The overall performance of the different configurations and flow schemes of the scale-up PRO are aimed to study. And the optimum operations to achieve the well-designed system should be identified.
- Sensitivity analysis of membrane properties and process characteristics of a scale-up PRO process. Parametric study of the components in PRO, such as membrane module, pressurisation, energy generation and recovery devices, need to be developed.
- Hybrid RO and PRO membrane process. Due to the reciprocal benefiting design of the hybrid RO-PRO process, this promising configuration needs to be investigated. Because of the sophisticated interactions between the PRO and the RO, the operation of the hybrid process aims to be studied. Analysis and optimisation of operation and design should be carried out accordingly. Moreover, a solar assisted hybrid RO-PRO process is aimed to be studied in order to further improve the overall performance of the hybrid process.
- Performance control of a scale-up PRO process. In order to ensure the identified optimum operations and performance, a robust maximum power point tracking (MPPT) controller aims to be developed.

1.5 CONTRIBUTION OF THE RESEARCH

In this research, a systematic investigation is carried out for a scale-up PRO process. First the framework to simulate a scale-up PRO process is developed. On the developed framework, the non-linear process behaviour of the PRO and several hybrid processes are analysed and optimised. The main contributions of this investigation are as follows:

This study presents a thermodynamic and energy analysis of the discharge behaviour of a single-stage PRO process which is then expanded into a proposed potential two-stage process to enhance total energy extraction in a practical application. A thermodynamic model describing the operational conditions for the optimal power density and the extraction of energy from a single-stage PRO process is introduced. The discharge behaviour of the power generated from the process is analysed and the profiles of water flux, power density, and extracted energy are obtained. The membrane area is also studied with respect to different hydraulic pressure on the draw solution, and the flows of both the draw and feed solutions. The inherent inconsistencies in the operational conditions with regard to achieving maximal power density and available energy are discussed and interpreted based on the discharge behaviour. A two-stage PRO process with two alternative feed arrangements (continuous feed and divided feed) is then proposed and its operation is simulated and analysed. The results indicate favourable energetic performance of the two-stage versus the one-stage PRO process in terms of the reduced frictional loss and unused energy involved in the process.

A simplified PRO model incorporating the detrimental effects of ICP, ECP and RSP is proposed and verified using published data. The results demonstrate the accuracy of the model to address decreased water flux and power density due to the performance limiting effects. Based on the model, the discharge behaviour of a PRO process is reported with respect to different applied pressures on the draw solution and two flow schemes, co-current and counter-current flows. In the co-current flow PRO process, from the flow profiles in the draw and feed channels, it is found that the adverse effects on the process dynamics, such as water flux and power density, and required membrane area, can be regarded as a further retardation by applying ‘an extra applied pressure’ on the draw solution. In addition, the capacity of extractable energy of the full scale PRO discharge is significantly reduced due to the ICP, ECP and RSP effects. Furthermore, the termination conditions of the PRO discharge and its effects on the dynamics of the PRO process are also investigated in the case of the counter-current flow PRO process.

This work carries out a systematic evaluation of the membrane and process characteristics of a scale-up PRO. In order to meet pre-defined membrane economic viability (5 W/m^2), different operating conditions and design parameters are studied with respect to the increase of the process scale, including the initial flow rates of the draw and feed solution, operating pressure, membrane permeability-selectivity, structural parameter, and the

efficiency of the equipment. The numerical results indicate that the performance of the scale-up PRO process is significantly dependent on the dimensionless flow rate. Furthermore, with the increase on the specific membrane scale, the accumulated solute leakage becomes important. The required membrane to achieve the optimal performance moves to the low permeability in order to reduce the detrimental effect of the reverse solute permeation. Additionally, the counter-current flow scheme is capable to increase the process performance with a higher permeable and less selectable membrane compared to the co-current flow scheme. Finally, the inefficiencies of the process components including HP, ERD and HT decrease the salinity energy generation and move the optimal operation to the high dimensionless flow rate and higher specific membrane scale.

MPPT of a scale-up PRO based osmotic power generator is investigated. In fact, MPPT in renewable energy has been developed in tracking the maximum power point (MPP) for not only solar photovoltaic (PV) arrays [71-76] but also for fuel cell power plant [77, 78]. Conventional MPPT of PV arrays operated by sensing the current and voltage and the changing duty cycle of the converter to match the MPP. Popular and widely implemented MPPT techniques such as perturb and observe (P&O) [72, 73] and incremental conductance (INC) [71, 79] differ markedly in terms of convergence speed, steady state oscillations and cost effectiveness [80]. Actually, operations and power output of a scale-up PRO is similar to PV arrays. Power output of both renewable energy generation are evaluated by the product of two variables which are the pressure and the flow rate of the permeation for PRO and the current and the voltage for PV arrays. With the increase on one variable, furthermore, another variable decreases in an operating generator. Therefore, MPPT techniques are potentially applicable in tracking the MPP of a scale-up PRO by sensing the flow rate and the pressure of the permeation. Inspired by the well-known MPPT in PV array, two algorithms, perturb & observe (P&O) and incremental mass-resistance (IMR) method, are investigated. Using a series of simulations, both the algorithms are demonstrated to be capable of tracking the maximum power point (MPP). However, in both cases, the trade-off between the rise time and the oscillation is found, requiring further consideration on the selection of the step-size for perturbation pressure or incremental pressure. In order to improve the performance of the MPPT, furthermore, an optimum model-based controller (OMC) is used to estimate the initial optimum pressure for the MPPT in a scale-up PRO process. It is found that with OMC, the performance of the MPPT is improved significantly. Finally, a strategy to operate and coordinate the MPPT and OMC to deal with the rapid

variations of the salinities are proposed and evaluated in terms of individual variation of the concentration or flow rate and co-variation of the both. The simulations demonstrate the preferred performance of the proposed strategy to adjust the operation subject to the rapid changes of the salinities.

Furthermore, a methodology is developed to assess the feasibility of a RO desalination system powered by a stand-alone salinity driven PRO technology. First, the proposed hybrid RO–PRO system is analysed as a thermodynamic cycle and its feasibility is mathematically interpreted using a feasible condition (FC) number, several dimensionless operational variables and a number of constraints to represent the objective of zero brine discharge. Then, a study of the stand-alone feasibility of a hybrid seawater RO–PRO system is carried out. The results show that lower RO water recovery and higher dimensionless flow rate improve the stand-alone feasibility of the system. A subsystem, a look inside the PRO, is developed to study the applied pressure and the required membrane area to achieve the operations with optimum FC numbers. It is found that the optimum applied hydraulic pressure is inversely proportional to the dimensionless flow rate in the feasible range of stand-alone operations and more area of membrane is required by a larger FC number. Finally, a case study of a selected operation is presented based on its energy performance, and two influencing factors, the inefficiency of the components and the salinity concentration of the feed water.

In addition, a novel RO seawater desalination plant powered by PV and PRO (PVROPRO) is proposed and the feasibility of two stand-alone schemes, salinity-solar powered RO (SSRO) operation and salinity powered RO (SRO) operation, are investigated. First, the stand-alone feasibility of the plant is thermodynamically analysed. In doing so, on the basis of mathematical models describing RO, PRO and the PV array, the stand-alone feasibility is numerically investigated and the feasible operational windows for the two operation schemes, SSRO and SRO, are identified. In addition, the detrimental effects, concentration polarisation (CP) and reverse salt permeation (RSP) in the mass transfer, on the operational windows are investigated. Finally, a case study of the proposed PVROPRO plant is developed based on the hourly solar data of Perth Australia (a typical place for desalination, in which there has twelve seawater RO trains with a capacity of 160 mega-litres per day and six brackish water RO trains with a final product of 144 mega-litres per day) in a year. In such a typical place in which freshwater is desalinated from seawater and brackish water, the highest weekly production rate is found to be almost 20 times the rate

in PVRO in the same week. Annual production is increased more than nine times compared to the stand-alone PVRO plant. Furthermore, it is found that, due to detrimental effects the weekly permeation production rate is decreased in the range of 16-20% and the overall annual reduction is 18.07%.

1.6 CHAPTER OUTLINE AND ORGANISATION

Chapter 2 presents the principles of the PRO process to extract energy from the salinity gradients and the mathematical models to simulate a scale-up PRO process.

Using the models derived in Chapter 2, In Chapter 3, discharge behaviour and the influences of detrimental effects and flow schemes on the overall performance of the scale-up PRO process are evaluated considering the increasing membrane area.

On the basis of the developed mathematical model and modelling framework of the scale-up PRO process considering ICP, ECP and RSP effects, sensitivity analysis of membrane properties and process characteristics of the scale-up PRO process are investigated with different operating conditions in Chapter 4.

Furthermore, in order to ensure the PRO operated at the identified operations, MPPT algorithms and controller are studied in Chapter 5. Two algorithms are studied and implemented in the controller. In order to deal with the rapid operational variations of the salinities, a model-based controller and control strategy are investigated.

Moreover, stand-alone salinity power driven RO desalination and stand-alone hybrid solar-salinity power driven RO desalination plant are proposed, analysed and optimised. On the basis of the studies on the osmotic energy generation/recovery using the scale-up PRO process, the innovative hybrid RO-PRO process is investigated in Chapter 6. Moreover, a solar power assisted hybrid RO-PRO plant is analysed in Chapter 7 and the significant improvement is observed.

1.7 DELIVERIES

Published journal articles:

1. **He W**, Wang Y, Mujtaba IM, Shaheed MH. An evaluation of membrane sensitivity and process characteristics of scale-up pressure retarded osmosis (PRO) salinity power generation, *Desalination,* 2016, 378: 1-13.

2. **He W**, Wang Y, Shaheed MH. Maximum power point tracking (MPPT) of the scale-up pressure retarded osmosis (PRO) osmotic power plant*, Applied Energy* 2015, 158: 584-596.
3. **He W**, Wang Y, Shaheed MH. Stand-alone seawater RO (reverse osmosis) desalination powered by PV (photovoltaic) and PRO (pressure retarded osmosis). *Energy,* 2015, 86(0): 423-435.
4. **He W**, Wang Y, Shaheed MH. Enhanced energy generation and membrane performance by two-stage pressure retarded osmosis (PRO), *Desalination*, 2015, 359: 186-199.
5. **He W**, Wang Y, Shaheed MH. Modelling of osmotic energy from natural salt gradients due to pressure retarded osmosis: Effects of detrimental factors and flow schemes. *Journal of Membrane Science*. 2014;471:247-57.
6. **He W**, Wang Y, Sharif AO, Shaheed MH. Thermodynamic analysis of a stand-alone reverse osmosis desalination system powered by pressure retarded osmosis. *Desalination*. 2014;352:27-37.
7. **He W**, Wang Y, Shaheed MH. Energy and thermodynamic analysis of power generation using a natural salinity gradient based pressure retarded osmosis process. *Desalination*. 2014;350:86-94.

Conference presentation and seminar or webinar:

8. **He W**, Shaheed MH. Modelling and analysis of osmotic energy from salinity gradients. *INES Webinar on SGP Resource Analysis*, November, 2015.
9. **He W**, Shaheed MH. Modelling, optimisation and control of osmotic energy generation using pressure retarded osmosis (PRO), *Euromembrane,* 2015, RWTH Aachen, Germany.
10. **He W**. Modelling, optimisation and control of osmotic energy extraction from natural salinity gradients using pressure retarded osmosis, Association of British Turkish Academics (ABTA) 2015 Doctoral Research Awards Ceremony, May, 2015, Darwin Lecture Theatre, University London College, United Kingdom.
11. **He W**, Wang Y, Shaheed MH. Modelling and Simulation of Osmotic Energy from Salinity Gradients: A Case Study from River Thames, 2013, *ICRERA*, IEEE *international conference on renewable energy research and applications*, Madrid, Spain.

MATHEMATICAL MODEL OF THE SCALE-UP PRO OSMOTIC ENERGY POWER PLANT

2.1 INTRODUCTION

In this Chapter, mechanisms of PRO to extract osmotic energy from salinity gradients are introduced and detailed mathematical models to describe the energy conversion and evaluate the performance of both the membrane and process are also developed. To scale-up the PRO process in realistic applications, coupling effect of the membrane area increase and the mass transfer is considered and the models of discharge behaviour of the scale-up PRO process are derived.

Furthermore, detrimental effects, namely ICP, ECP and RSP, decrease the performance of the PRO process in terms of reduced power density and extractable energy. Based on prior

investigations, it was found that the effect of ICP, resulting from an asymmetric membrane structure, becomes severe with higher difference of concentration [81]. The ECP effect can be reduced with high cross-flow velocities [82] and spacers in the flow channels [83]. Moreover, several mathematical models have been developed and verified with experiments to describe the effects on power generation [31, 58, 84-87]. Accordingly, based on these models, many studies have been carried out to investigate the PRO/FO process through numerical simulation [88-91]. However, few investigations have addressed the dynamic of the PRO discharge behaviour coupled with the detrimental effects in a scale-up process in which the dilution of the draw solution and the concentration of the feed solution are considered. Therefore, the detailed models considering these detrimental effects in a scale-up PRO process are also developed.

2.2 OSMOTIC ENERGY GENERATED BY A PRO

PRO uses the natural phenomenon of osmosis to permeate water across a semi-permeable membrane from a side with low solute concentration and low hydraulic pressure to a side with high concentration and high pressure. The permeated water is then used to generate electricity in a hydro-turbine (HT). The process is illustrated in Figure 2.1. In the PRO process, the draw solution is pressurized by high-pressure pump (HP) and energy recovery device (ERD). As water is transported across the membrane, the draw solution becomes progressively diluted and the concentration of the feed solution rises.

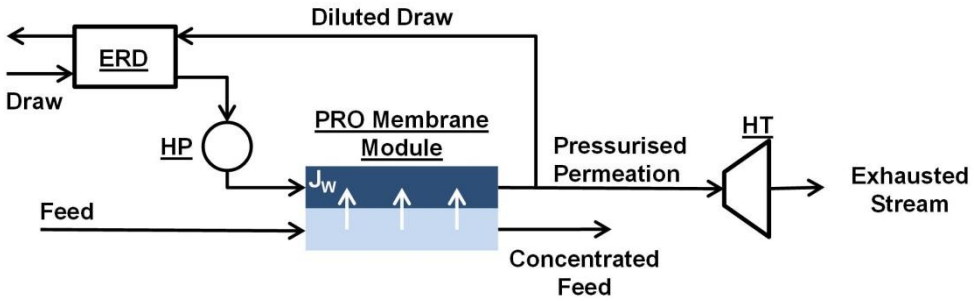

Figure 2.1: A schematic illustration of a PRO process.

Two of the key parameters determining the performance of PRO processes are the conditions of available salinity streams and the PRO operations. The two salinity streams

determine the total energy capacity that can be potentially harvested. The Gibbs free energy is the theoretical maximum when the two streams are mixing, and is converted into electricity by a PRO process. However, this energy cannot be fully harvested. In addition to the membrane performance, the efficiency of PRO process also significantly depends on the hydraulic pressure applied on the draw solution, because the applied pressure determines not only the flow rate but also the pressure head of the pressurised permeated water.

Variables in the available water conditions comprise the concentration and volume of the draw and the feed water. Power generation by a PRO process from natural salinity gradients could utilise high concentration saline water such as seawater and brackish water as draw solution. The total dissolved solid (TDS) of brackish water is in the range of 1 – 5 g/L, and the TDS of seawater is larger than 35 g/L. Normally, water with TDS smaller than 1 g/L is classified as fresh water. This includes water from rivers, sewage, private effluents and industrial wastewater, but water from such sources would require pre-treatment before use as feed water in a PRO system to prevent membrane fouling.

The available volume of draw and feed water is also very important because it significantly influences the variation of net driving force and, as a consequence, determines the change of osmotic pressure difference, water flux and power density along the membrane. The van't Hoff equation for osmotic pressure applies to dilute, ideal solutions and is given by

$$\pi = \nu RTc \tag{2.1}$$

where R is the gas constant, T is the temperature, c is the concentration of the solution, ν is the number of ionic species each salt molecule dissociates. In this chapter, for simplicity, the draw solution is regarded as seawater with 35 g/L TDS, and the feed solution is selected as freshwater with 0.1 g/L TDS. And both solutions are assumed as hypothetic solutions in order to identify the thermodynamic limit of the osmotic energy. Accordingly, the van't Hoff law is used to approximate the osmotic pressure difference between the draw and feed solutions. Thus, it can be expressed as,

$$\Delta\pi = \nu RT\Delta c = \nu RT\left(\frac{V_D^0}{V_D^0 + \Delta V}c_D^0 - \frac{V_F^0}{V_F^0 - \Delta V}c_F^0\right) \tag{2.2}$$

in which, V_D^0 and V_F^0 are the initial volume rate of draw and feed, c_D^0 and c_F^0 are the initial concentration of draw and feed, ΔV is the permeated water volume rate. Furthermore, if a dimensionless flow rate ϕ is defined as $\phi = V_F^0 / (V_F^0 + V_D^0)$, the osmotic pressure difference can be expressed as,

$$\Delta\pi = \nu RT\left(\frac{1-\phi}{1-\phi(1-\frac{\Delta V}{V_F^0})}\mathrm{c}_D^0 - \frac{1}{1-\frac{\Delta V}{V_F^0}}\mathrm{c}_F^0\right) \tag{2.3}$$

Based on Equation (2.3), the influence from the feed dimensionless flow rate on the osmotic pressure difference across the PRO membrane can be obtained. The osmotic pressure difference between seawater and freshwater as a function of dimensionless permeated volume and dimensionless flow rate based on the van't Hoff law is illustrated in Figure 2.2, at a temperature of 298 K. The results indicate that the water availability has a significant influence on the change of osmotic pressure difference. The concentration difference of draw and feed water determines the initial osmotic pressure difference and the volume affects how the difference disappears. It is obvious that all the curves originate at the same point due to the same initial concentrations of the draw and feed water. However, different dimensionless flow rates lead to different trajectories of osmotic pressure difference during energy generation by the PRO process.

2.2.1 Power density

Membrane power density is the power that can be generated per unit membrane area [87], a key factor to signify the performance of a PRO process. With a larger power density, a smaller area of membrane is needed to achieve certain level of power generation [35]. The power density in W/m^2 is the product of water flux and applied hydraulic pressure,

$$W = J_w \Delta P \tag{2.4}$$

in which the water flux can be further expressed as,

$$J_W = A(\Delta\pi - \Delta P) \tag{2.5}$$

where A is the membrane permeability, ΔP is the applied hydraulic pressure on the draw solution, and $\Delta\pi$ represents the osmotic pressure difference. The pressure drop through

the flow channel is negligible on both the feed and the draw side [62, 91]. Hence, the applied pressure is constant over the length of the both channels.

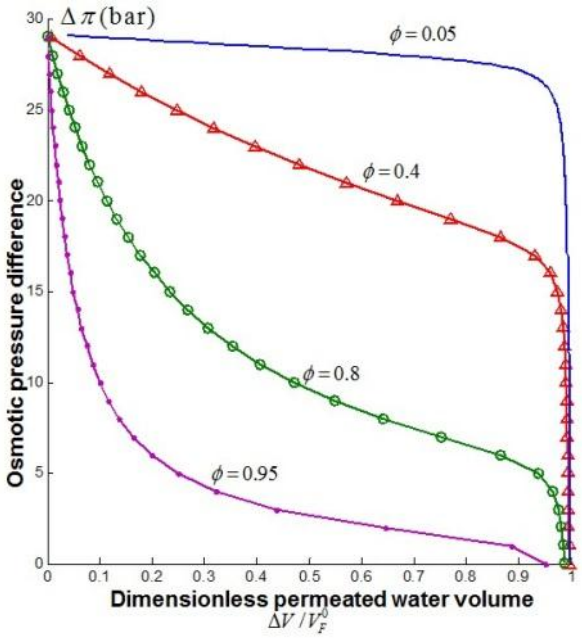

Figure 2.2: The osmotic pressure difference profile as a function of dimensionless permeated volume and dimensionless flow rate.

2.2.2 Osmotic energy generated by a PRO process

As mentioned earlier, the maximum energy released from a mixture of two different composition solutions is the difference in the Gibbs free energy between the final mixture and the two initial solutions. In fact, theoretically, it is the maximum energy generation of a reversible PRO process in which infinitesimal water flux is maintained through the osmosis process by applying a hydraulic pressure negligibly smaller than the osmotic pressure difference. It is defined as the reversible PRO (R-PRO) process energy [32]. The R-PRO energy can be represented as the integration of osmotic pressure difference through the permeating process as,

$$E_{R-PRO} = \int_0^{\Delta V_{SUM}} \Delta\pi d(\Delta \mathrm{V}) \tag{2.6}$$

in which ΔV represents the volume of the permeating water, and ΔV_{SUM} is the accumulated permeate volume when water flux is terminated. In reality, due to natural

thermodynamic inefficiency, the extracted energy is less than the R-PRO energy due to the entropy generation during the mass transfer. In an actual PRO process, a constant hydraulic pressure is applied on the draw solution. The water flux is terminated when the net driving force equals zero. Therefore, the final permeated volume of water is less than the total volume permeated in a reversible process. The work done by a constant PRO (C-PRO) process can be expressed as,

$$E_{C-PRO} = \Delta P \cdot \Delta V_{SUM} \tag{2.7}$$

in which, E_{C-PRO} is represented as the energy generated by the C-PRO process. The C-PRO energy is the energy that can be extracted in practice [32]. The difference between the R-PRO and C-PRO energy represents the irreversible energy loss due to the frictional resistance in the transportation of water inside the membrane [32]. This frictional force between the water molecules and membrane give rise to a hydraulic resistance [92], and thus a partial of osmotic driving force is consumed to compensate for the resistance. This part of energy loss is the frictional loss. Furthermore, in a C-PRO process, the actual permeate volume is smaller than the volume of water that would permeate into the draw solution without applied hydraulic pressure. Thus, the energy embedded in the "non-permeated water" cannot be extracted by a C-PRO process. This part of energy loss is unused energy. With no pressure loss assumed in the both draw and feed flow channels, the extractable energy and energy losses of the PRO process from seawater and river water are illustrated in Figure 2.3. In the figure, the area of the black rectangle represents the actual energy extracted by the C-PRO process. The frictional loss and unused energy are denoted by the blue shaded areas of the left upper region and the right bottom region of the black rectangle respectively.

Because the final permeated volume of water in a C-PRO process, ΔV_{SUM}, is a function of the applied pressure, it can be obtained by substituting $\Delta P = \Delta \pi$ into Equation (2.3). E_{C-PRO} is only dependent on the hydraulic pressure applied. Different applied hydraulic pressure on draw solution results in different capacity of extracted energy and the corresponding energy losses. The optimal applied hydraulic pressure for extracting maximal energy by a C-PRO process can be obtained by solving $dE_{C-PRO} / d(\Delta P) = 0$, based on Equation (2.7) in which the dimensionless final permeated volume $\Delta V_{SUM} / V_F^0$ is obtained by substituting $\Delta P = \Delta \pi$ into Equation (2.3). Accordingly, the optimal applied pressure can be expressed as [32],

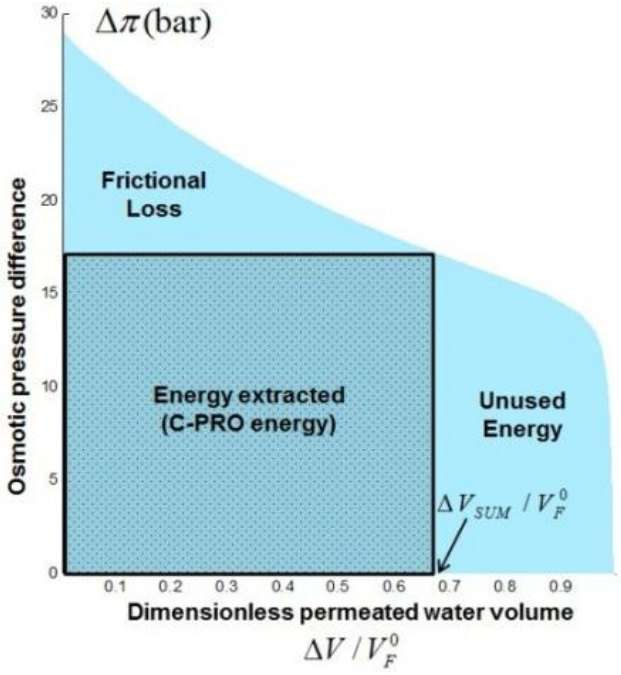

Figure 2.3: The different types of energy involved in the PRO process are illustrated**.**

$$\Delta P_{C-PRO}^{MAX} = \nu RT[(1-\phi)c_D^0 - \phi c_F^0 + (2\phi - 1)\sqrt{c_D^0 c_F^0}] \tag{2.8}$$

where ΔP_{C-PRO}^{MAX} represents the optimal applied hydraulic pressure to obtain the maximum extracted energy. Conversely, the maximum power density of a certain membrane is achieved at the applied hydraulic pressure equalling half of the initial osmotic pressure difference according to $dW/d(\Delta P) = 0$ based on Equation (2.4) [32]. The applied pressure to achieve the maximum power density of a PRO membrane is expressed as [32],

$$\Delta P_W^{MAX} = \frac{1}{2}\nu RT(c_D^0 - c_F^0) \tag{2.9}$$

where ΔP_W^{MAX} is the optimal applied pressure to obtain the maximum power density.

Therefore, based on Equations (2.8) and (2.9), the applied pressure to achieve the maximum extracted energy and power density of a PRO process with respect to the different dimensionless flow rates of feed water can be obtained. The results are illustrated in Figure 2.4. Normally, there is incompatibility in operations to achieve the optimal power density and the maximum energy extracted simultaneously excluding the dimensionless flow rate of feed equalling 0.5. In the range of dimensionless flow rate from zero to 0.5 or

from 0.5 to 1, the optimal applied pressure to achieve maximum extracted energy is different from the one to achieve maximum power density.

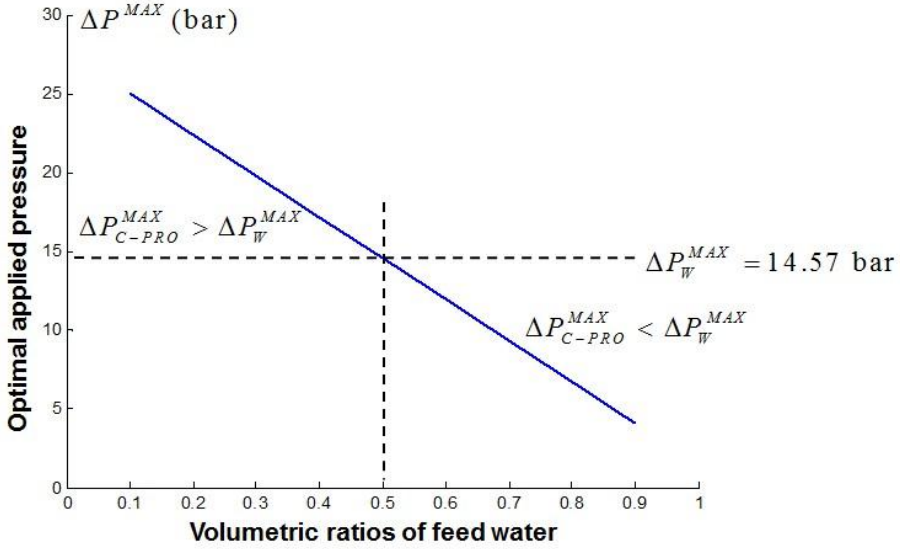

Figure 2.4: The optimal pressures to achieve the maxima of extracted energy and power density with different dimensionless flow rate.

2.3 MATHEMATICAL MODELS OF A SCALE-UP PRO PROCESS

The equations above describe the ideal power dynamic characteristic of a PRO process with ideal draw and feed solutions. However, in practice, the osmotic pressure difference between the two sides of the membrane, $\Delta\pi - \Delta P$, is lower than the osmotic pressure difference between the bulk draw and feed solutions due to the polarisation effects of ICP within the porous support layer, ECP near the membrane surface in the draw solution side and RSP which is common phenomenon in membrane processes [87]. The polarisation will reduce the flow rate of the permeation and result in lower power density of the membrane and less energy generation from the harvesting process. Although effects of CP and RSP are inevitable in the mass transfer of both water and salt across the membrane, ideal PRO process is the thermodynamic limit of the osmotic energy extraction using PRO. With the continuous improvement on the membrane properties, the PRO is approaching the ideal performance. Therefore, both models of the PRO are developed considering the increase of the membrane area, including the ideal PRO (I-PRO) model in which concentration polarisation effects are neglected and the salt concentration near the membrane surface is equal to the bulk concentration of the flow stream, and the PRO model considering detrimental effects of ICP, ECP and RSP (D-PRO).

2.3.1 *I*-PRO models

Ideally, without any consideration of concentration polarisation effects, the concentration of the solution near the membrane surface is equivalent to the concentration of the bulk flow. In this case, the concentration of the solutions near the membrane can be approximated as

$$c_{D,m} = c_{D,b}; c_{\mathrm{F},m} = c_{\mathrm{F},b} \tag{2.10}$$

in which $c_{D,b}$ and $c_{F,b}$ represent the concentration of the bulk flow of the draw and feed solutions. Therefore, the water flux of the I-PRO process is,

$$J_W = A(\nu RT(c_{D,b} - c_{F,b}) - \Delta P) \tag{2.11}$$

And with the permeation across the membrane, the updated concentrations of the draw and the feed are,

$$\begin{aligned} c_{D,b} &= \frac{\mathrm{c}_{D,b}^0 V_D^0}{V_D^0 + \Delta V_P} = \frac{\mathrm{c}_{D,b}^0 (1-\phi)}{1-\phi(1-\Delta V_P / V_F^0)}; \\ c_{F,b} &= \frac{\mathrm{c}_{\mathrm{F},b}^0 V_F^0}{V_F^0 - \Delta V_P} = \frac{\mathrm{c}_{F,b}^0}{1 - V_P / V_F^0} \end{aligned} \tag{2.12}$$

Based on the preceding analysis, it can be observed that the required operation for maximizing power density is not usually synchronized with the one for achieving maximal extracted energy. Actually, the mismatch on the optimal applied hydraulic pressure between the power density and extracted energy is determined by their different physical representations. Power density represents the utilisation efficiency of the membrane. Conversely, extracted energy is the efficiency of salinity energy harvesting by a C-PRO process with given water conditions of both draw and feed solutions. Power density is related to the water flux of the membrane. In contrast, the extracted energy is determined by the accumulated permeate water volume from the feed side to the draw side along the membrane. The water flux of a steady-state PRO process is, in fact, the velocity of permeated water flow along the membrane. From this viewpoint, the water flux can be expressed as,

$$d(\Delta V) = J_w d(A_M) \tag{2.13}$$

where A_M is the area of the membrane. Furthermore, if the expression for water flux with respect to dimensionless permeated water volume, $\Delta V^* = \Delta V / V_F^0$, is considered, combining Equation (2.13) with Equations (2.11) and (2.12), an ordinary differential equation (ODE) for the dimensionless permeated water volumetric rate ΔV^* along the membrane can be obtained as,

$$J_W = \frac{d\Delta V}{dA_m} = A(\nu RT(\frac{(1-\phi)c_D^0}{1-\phi(1-\Delta V^*)} - \frac{c_F^0}{1-\Delta V^*}) - \Delta \mathrm{P}) \tag{2.14}$$

The solution to this differential equation represents the accumulated water permeated volume along the membrane during the discharge of the PRO process.

2.3.2 D-PRO model

The ideal condition is difficult to be achieved because of the existence of ICP, ECP, and RSP. Due to these detrimental effects, the osmotic driving force is lower than the osmotic pressure difference between the bulk draw and feed solutions. Several mathematical models have been developed to represent the concentration difference between the two sides of the membrane in terms of bulk concentrations. One of these models, which was developed by McCutcheon et al. [84, 85], was for osmotic flux and incorporated a dense, symmetric membrane. Elsewhere, the effect of draw solution concentration, draw solution flow rate, feed water flow rate, and membrane orientation on PRO water flux performance and derived PRO water flux equations combining the ICP effect was studied by Xu [81]. Recently, a derivation of the complete water flux equation for a PRO process, taking all ICP, ECP and RSP effects into consideration was presented by Yip [58]. According to the study, the concentration difference between the two sides of the membrane can be represented as:

$$c_{D,m} - c_{F,m} = \frac{c_{D,b}\exp(-J_W / k) - c_{\mathrm{F},b}\exp(J_W S / D)}{1 + \frac{B}{J_W}[\exp(J_W S / D) - \exp(-J_W / k)]} \tag{2.15}$$

where D is the bulk diffusion coefficient, $k = D/\delta$ is the boundary layer mass transfer coefficient in which δ boundary layer thickness, and $S = t_s\tau/\varepsilon$ is the support layer structural parameter in which t_s is the thickness of the support layer, τ and ε are the tortuosity and porosity of the support layer of the membrane respectively. In Equation

(2.15), the effects of ECP and ICP are described by the first and the second terms of the numerator on the right hand side, whilst the denominator accounts for the effect of RSP at the membrane interface [33]. According to their work, the water flux, J_W, based on the D-PRO models was obtained

$$J_W^{D-PRO} = A(C_{os}(\frac{c_{D,b}\exp(-J_W^{D-PRO}/k) - c_{F,b}\exp(J_W^{D-PRO}S/D)}{1+\frac{B}{J_W^{D-PRO}}(\exp(J_W^{D-PRO}S/D) - \exp(-J_W^{D-PRO}/k))}) - \Delta P) \tag{2.16}$$

In addition, when the RSP effect is considered, the reverse solute flux, J_S, is also included,

$$J_S = B(c_{D,m} - c_{F,m}) = B(\frac{c_{D,b}\exp(-J_W^{D-PRO}/k) - c_{F,b}\exp(J_W^{D-PRO}S/D)}{1+\frac{B}{J_W^{D-PRO}}(\exp(J_W^{D-PRO}S/D) - \exp(-J_W^{D-PRO}/k))}) \tag{2.17}$$

Taking advantage of the accumulated water permeation by integrating the volumetric water flux along the membrane channel, at the steady-state, the mass rates of water and reverse solute permeation can be derived.

$$d(\Delta V_P) = J_w d(A_m); \quad \Delta q_P = \rho_P \Delta V_P \tag{2.18}$$

where ΔV_P and Δq_P are the volumetric and mass rate of permeated water, and ρ_P is the density of permeating water. In addition, when RSP effect is included in the modelling, the transporting rate of the reverse solute permeation is also crucial and can be expressed as

$$d(\Delta V_S) = J_S d(A_m); \quad \Delta m_S = \rho_S \Delta V_S \tag{2.19}$$

where ρ_S is the density of the draw solution, ΔV_S and Δm_S are the volumetric and mass rate of the reverse solute. However, when the RSP effect is considered, the mass balance will be changed to

$$\begin{aligned} c_{D,b} &= \frac{c_{D,b}^0 q_D^0 - \Delta m_S}{q_D^0 + \Delta q_P} = \frac{c_{D,b}^0(1-\phi) - \phi\Delta m_S / q_F^0}{1-\phi(1-\Delta q_P / q_F^0)}; \\ c_{F,b} &= \frac{c_{F,b}^0 q_F^0 + \Delta m_S}{q_F^0 - \Delta q_P} = \frac{c_{F,b}^0 + \Delta m_S / q_F^0}{1-\Delta q_P / q_F^0} \end{aligned} \tag{2.20}$$

2.4 PRELIMINARIES FOR SIMULATION

2.4.1 Membrane *parameters*

Thin-film composite (TFC) polyamide membranes are widely utilised in separating and salt-rejecting membrane processes [5]. In general, with a given structural parameter, increasing the membrane water permeability and decreasing the salt permeability will increase the specific power density [91]. However, achieving high performance is limited by the permeability-selectivity trade-off relationship of the TFC polyamide membrane [33, 93], such that an increase in the membrane water permeability, A, is commonly accompanied by a corresponding increase in salt permeability, B. The trade-off relationship between the permeability and selectivity can be approximated by a non-linear empirical relation proposed by Yip and Elimelech [33]. In addition, the range of the values of the structural parameter, S, is also restricted by the types and functions of the membrane. The structural parameter usually ranges from 10-10,000 μm, including conventional TFC reverse osmosis membranes ($S = 10000\ \mu m$) [58], hollow fibre membranes ($S = 600 - 1400\ \mu m$) [94], hand-cast flat sheet membranes ($S = 300 - 3000\ \mu m$) [95] and nano-fibre composite membranes ($S = 80 - 110\ \mu m$) [96]. Some current membrane properties from selected publications are listed in Table 2.1.

Table 2.1: Membrane properties selected from the literature**.**

No	Reference	Water permeability, A ($L \cdot m^{-2} \cdot h^{-1} \cdot bar^{-1}$)	Salt permeability, B ($L \cdot m^{-2} \cdot h^{-1} \cdot$)	Structural parameter, S, (μm)
1	[97]	0.44	0.27	481
2	[31]	0.74	0.63	480
3	[58]	1.74	0.16	307
4	[98]	1.90	0.48	776
5	[99]	3.32	0.14	460
6	[100]	4.02	1.65	350
7	[58]	5.81	0.88	370
8	[58]	7.55	5.45	327

2.4.2 Flow parameters

The geometry of the simple cross-flow chamber model used in this chapter is shown in Figure 2.5. A feed solution with low salt concentration flows through a channel with a PRO membrane side wall. On the other side of the semi-permeable membrane, a draw solution

with higher salinity flows in the same direction (co-current scheme in Figure 2.5(a)) or in the opposite direction (counter-current scheme in Figure 2.5(b)).

The flow parameters are determined by local water conditions that comprise concentration and mass flow rates of both the high and low concentration solutions.

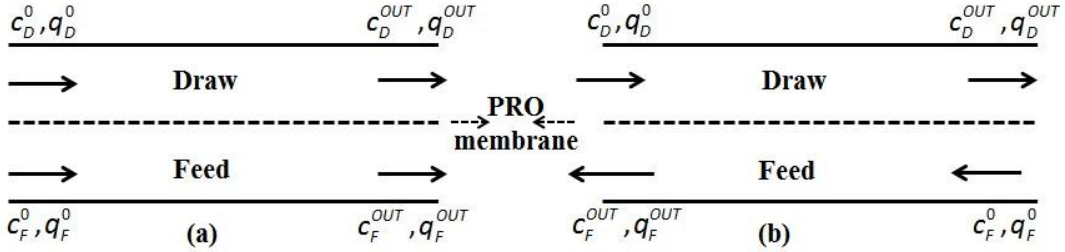

Figure 2.5: Illustrative flow schemes of a PRO chamber in co-current cross-flow (a) and counter-current cross-flow (b).

2.4.3 Modelling framework of the scale-up PRO process

For both I-PRO modelling and D-PRO modelling, the flowchart to simulate the scale-up PRO process is shown in Fig. 2.6. First, the parameters initialisation is needed to setup the simulations The parameters include salinities' conditions which are concentrations and flow rates of the draw and the feed solutions, membrane parameters of membrane water and salt permeability coefficient, structural parameter and mass transfer coefficient, and PRO operation parameter which is mainly the hydraulic pressure applied on the draw solution. After initialising these parameters, by updating the salt concentrations of the draw and feed solutions represented by Equation (2.12) and the water flux profile represented by Equation (2.11) into permeated water mass flow rate expressed by Equation (2.14), an ODE describing permeated water flux based on I-PRO model can be obtained. When the detrimental effects are included, considering the reverse solute flux represented by Equation (2.17), a system of ordinary differential equations (ODEs) on mass rate of permeated water and reverse solute permeation also can be obtained. Moreover, with the inlet and outlet conditions of the PRO, the ODEs can be solved and water flux and power density can be obtained. The flowchart of simulating the PRO discharge is illustrated in Figure 2.6. Both models are implemented in MATLAB and the ODEs are solved using ode

solvers in MATLAB. The detailed methodology and code implementation of the MATLAB ODEs solvers can be found in MathWorks[1].

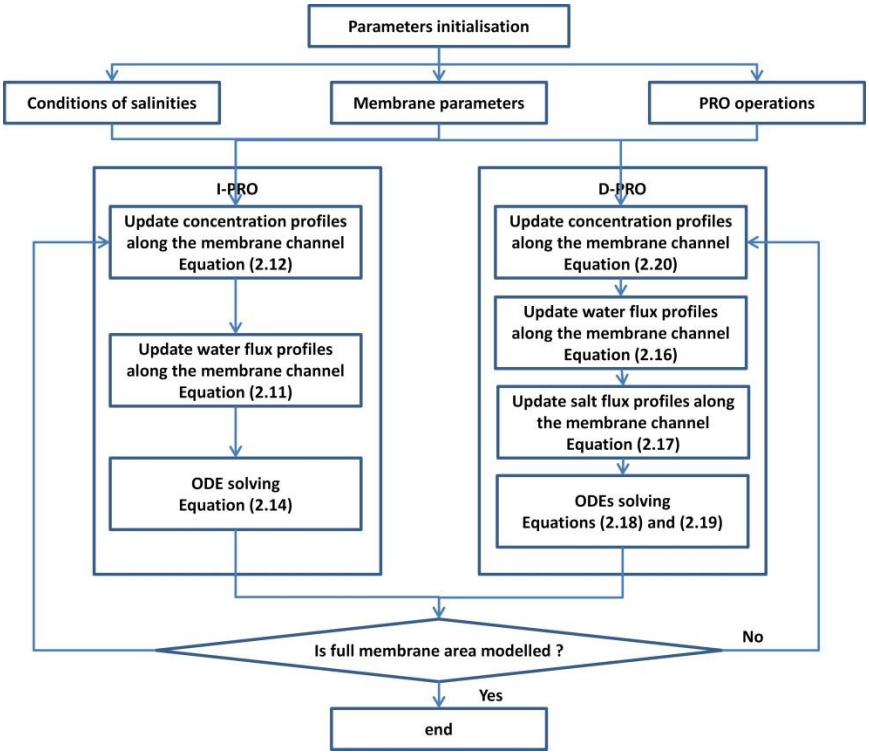

Figure 2.6: Flowchart of the PRO modelling.

2.5 SUMMARY

As presented in this chapter, the principles of the PRO process are introduced in both perspectives of membrane and process. Through the theoretical analysis, it is found that 1) water availability is a significant factor affecting the performance of a PRO process, including the concentration and the volume of the feed and draw water available. 2) With a certain level of water availability, applied hydraulic pressure needs to be varied to achieve better performance with different operational conditions. And for different optimal objectives, different applied pressure can be selected. Furthermore, detailed mathematical models of the scale-up PRO process are derived considering the effect of the membrane area increase, including the I-PRO modelling presenting the thermodynamic limiting performance and the D-PRO modelling which evaluates the detrimental effects of ICP, ECP

[1] MathWorks, http://uk.mathworks.com/help/matlab/math/choose-an-ode-solver.html.

and RSP. Both the models allow the numerical methods to be carried out to investigate the discharge behaviour of the PRO in scale-up applications.

THERMODYNAMIC ANALYSIS OF SCALE-UP PRESSURE RETARDED OSMOSIS OSMOTIC POWER PLANT

3.1 INTRODUCTION

In general, content of this Chapter can be divided into two parts. One is the thermodynamic analysis of power and energy discharge behaviour of the scale-up PRO process with respect to different operations and system designs by I-PRO modelling. The other is evaluations of the detrimental effects of ICP, ECP and RSP in the scale-up PRO.

First, a thermodynamic analysis of the discharge behaviour of a PRO process is carried out to investigate the relationship between the power density and the extracted energy is presented in this chapter. Based on the models of the PRO process introduced in Chapter 2 the study in this chapter focuses on the influences of different parameters and operational conditions on the discharge behaviour of the process and the theoretical analysis of the PRO process. Furthermore, similar to the energy efficient advantages in two-stage RO configurations [101], two-stage PRO process is potentially efficient in salinity energy harvest. The configuration is able to decrease the frictional loss by altering the hydraulic pressure applied on the draw solution, and increase the energy generation due to the two-stage generation by increasing the water permeation and reducing the unutilised energy

loss. However, a review of the literature reveals no investigations to date of two-stage PRO processes, or analysis of their potential for increased total energy extraction. Therefore, a study of two-stage PRO process is also developed as presented in this chapter. Relevant targets for study include the analysis and optimisation of the possible configurations and operations of two-stage processes. To address this omission, the current investigation defines and analyses the performance of a two-stage PRO with two different feed water operations: continuous feed two-stage PRO and divided feed two-stage PRO. The results show the characteristic of preferable energy generation capacity of the two-stage PRO process and the influences on the performance due to variation in operational conditions and the available volumes of feed and draw water for use in the PRO process.

Moreover, this chapter also presents the investigation of two fundamental influencing factors, detrimental effects and flow schemes, and numerical evaluation of their impact on the water flux, power density and extractable energy for a PRO process based on its discharge behaviour. For the purpose of simplifying calculations, a simplified PRO model is proposed to approximate the water flux considering the effects of the ICP, ECP and RSP and is verified using both a classic PRO model and experimental data. Besides, on the basis of the PRO models, the framework of modelling the PRO discharge is provided, and the discharge behaviour of PRO is presented with respect to different hydraulic pressure applied on the draw solution and two flow schemes, the co-current and counter-current cross-flows. Finally, water flux, power density and concentration profiles have been derived.

3.2 DISCHARGE BEHAVIOUR OF THE SCALE-UP PRO PROCESS

Based on the flowchart of I-PRO modelling as shown in Fig. 2.6, a study to find the changing discharge processes with different operations is therefore carried out. To develop the simulations, several assumptions are made: i) Pressure drop through the flow channel is negligible in the case of both feed and draw solutions of the both flow channels. A constant hydraulic pressure is applied on the draw solution, and no pressure is applied on the feed solution; ii) Osmotic pressure is linearly proportional to the concentration difference in the range of salt concentrations used in this study; iii) Mass flow rates are averaged in the cross-section area of the two flow channels. Accordingly, it becomes a one dimensional problem in each flow channel, and the mass transfer coefficient is constant when the effect of ECP is considered; iv) Membrane fouling or deformation does not occur. These assumptions are used throughout the works within this thesis.

In this chapter, draw solution is seawater and feed solution is fresh water with a dimensionless flow rate of 0.5. The membrane area is assumed large enough and thus the full-scale PRO discharge and the corresponding required minimum area can be studied. The influence of different applied pressure on water flux is depicted in Figure 3.1. At each operation, for both the water flux and power density, due to the largest net driving force between the two sides of the membrane is reached at the entry of the membrane module and decreases gradually along the membrane. The water flux at the entrance decreases with increased applied pressure through different trajectories, resulting different required area of membrane to terminate the water permeation. The power density at the entrance is not proportional to the applied pressure and the maximum power density at the entrance is achieved with the applied pressure equalling to half of the initial osmotic pressure difference. The variations of the water flux profile are due to the different water permeation determined by the applied pressure. As shown in Fig 3.1, with applied pressure of 0 and 7 bar, the water flux reduce rapidly with the increase of the membrane area. This is because of the high water permeation across the membrane, accelerating dilution of the draw solution, concentration of the feed solution, and termination of the net driving force.

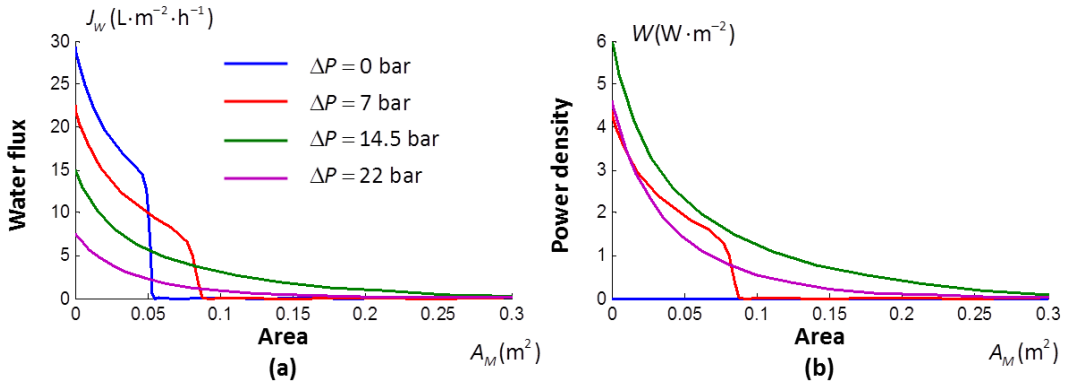

Figure 3.1: Calculated water flux and power density curves with respect to different applied hydraulic pressure are represented in (a) and (b), respectively.

However, in practice, membrane properties are the major constraints to affect the water flux and power density [102]. It significantly affects the membrane performance and determines the membrane area required in the energy generation. In this Chapter, the water permeability of the PRO membrane is selected as 1 $L \cdot m^{-2} \cdot h^{-1} \cdot bar^{-1}$ which is in the range of the membrane performance from the current studies. The consistency is obtained by comparing the obtained results of the water flux and power density with the previous studies using similar water permeability membrane [34, 58]. Power densities of different

PRO processes from some selected publications are illustrated in Table 3.1. The selected data indicates that the higher power density is not guaranteed with the higher water permeability as the high performance of a membrane is a result of the trade-off between permeability and selectivity. Furthermore, experimental results also indicate that the detrimental effects would reduce the theoretical water flux and power density significantly [87].

Table 3.1 Power density from selected publications with membrane having similar water permeability.

Reference	**Water permeability** $L \cdot m^{-2} \cdot h^{-1} \cdot bar^{-1}$	**Draw**	**Power density** $W \cdot m^{-2}$
[95]	1.88	Seawater	6.1
[98]	1.4	Seawater brine (1.0 M)	8.9
	1.7		9.2
	1.9		11
[58]	1.74	Seawater	6.09
	1.42		5.24
	4.12		5.71
[34]	0.72	Seawater	2.4
	2.23		5.5

The harvest of salinity energy from seawater and freshwater during the PRO discharge is illustrated in Figure 3.2, including the extracted energy, frictional loss and unused energy in kWh per cubic meter of feed water by a C-PRO process. According to the results, the distribution of the extracted energy and energy losses is different with respect to different hydraulic pressure applied. In Figure 3.2(a), due to low applied pressure, the net driving force of water permeation is high. Therefore, less area is required to harvest the salinity energy by a C-PRO process. Although most of the salinity energy is used according to the low unused energy, only part of the energy is extracted by the C-PRO process as a result of high frictional loss. Based on the results in Figure 3.2(b) and 3.2(c), with the increased hydraulic pressure, frictional loss decreases and unused energy increases with the increase of hydraulic pressure.

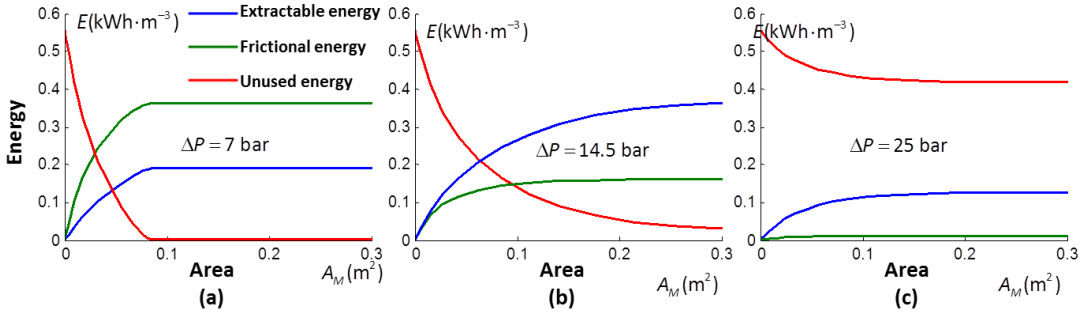

Figure 3.2: The discharge behaviour of the PRO process with different applied hydraulic pressures are represented in the figure, in which applied pressure equalling to 7 bar in (a), 14.5 bar in (b) and 25 bar in (c).

With the discharge behaviour of the PRO process in Figures 3.1 and 3.2, it is easy to understand the mismatch in hydraulic pressure to obtain the maximal power density and maximal energy extraction as described in Figure 2.4, because they are different inherently although closely interrelated. The general definition of power density (Equation 2.4) is dependent on the water flux. It is a transient characteristic of the PRO membrane. In contrast, extracted energy is an accumulated PRO property along the membrane at its steady state. It is the performance of a full-scale PRO discharge. In Figure 2.4, the power density is a value representing the efficiency of unit membrane at the entrance. In contrast, extracted energy is the integration of the power generation of the entire system.

The required membrane area of a full scale PRO process varies with different hydraulic pressure applied on the draw solution as illustrated in the Figures 3.1 and 3.2. The relation between the water permeation and the membrane area is non-linear as described in Equation (3.1). In fact, the membrane cost of a PRO process depends on some influencing factors, including the hydraulic pressure applied on the draw solution, the dimensionless flow rate and membrane permeability. Consequently, the problem can be represented mathematically as follows, $A_M^{FULL} = A_M|_{J_w=0}$. Through the operational pressure between 0 bar and ΔP^{MAX} which is the maximum of the applicable hydraulic pressure on the draw solution that it is the osmotic pressure difference at the entrance, i.e. $\Delta P^{MAX} = \nu RT(c_D^0 - c_F^0)$. In the simulation, three dimensionless flow rates, 0.2, 0.5 and 0.8, are selected and represented for the possible flow rates of the available salinity gradients in different regions. In addition, two membrane permeability parameters listed in Table 3.1, 1.74 $L \cdot m^{-2} \cdot h^{-1} \cdot bar^{-1}$ and 1.9 $L \cdot m^{-2} \cdot h^{-1} \cdot bar^{-1}$, from Ref. [98] are studied. The results are shown in the Figure 3.3.

The results indicate that the required membrane area for a full-scale permeation with different applied pressure has a maximum which varies depending on the dimensionless flow rate. For a certain dimensionless flow rate, when the applied pressure increases from zero, the membrane consumed in a full scale PRO discharge first increases and reaches its maximum, then decreases to zero when the maximum hydraulic pressure is applied. In addition, higher water permeability of the membrane reduces the required membrane area according to increased water flux across the membrane at each applied hydraulic pressure. Furthermore, comparing the profiles of the required membrane area in different dimensionless flow rates, it is found that the maximum of the membrane area changes. This is due to the extraction of the salinity energy during the full scale PRO discharge in which the optimal pressure is different with respect to the dimensionless flow rates as illustrated in Figure 3.3.

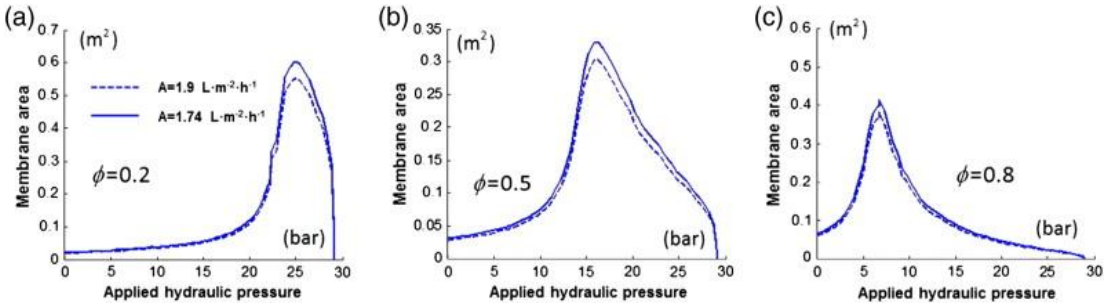

Figure 3.3: The schematic illustration of the required membrane area of a full-scale PRO process with different hydraulic pressure applied on the draw solution, dimensionless flow rates and water permeability.

3.3 ANALYSIS OF TWO-STAGE PRO PROCESS

In this section, a two-stage PRO process and its several operations are proposed in order to further increase the efficiency in terms of the energy harnessed. The two-stage PRO process is illustrated in Figure 3.4. In the figure, two PRO processes are series connected in draw water flow. The dilute draw solution from the first stage PRO process is the first partially used in pressurizing the raw draw solution, then combined and fully used to be the draw solution in the second stage PRO process. Depending on the different feed water flows two kinds of two-stage PRO processes are defined. In one case, the concentrated feed water from the first stage is continuously used as the feed water to the second stage. Different operations, such as hydraulic pressures, can be applied in the two stages in order to improve the overall performance by reducing the frictional loss and unused energy loss. It is defined as a continuous feed two-stage PRO process which is illustrated in Figure 3.4(a).

The other is a different feed flow scheme, because the feed water is divided into two flows at the beginning and is used as feed water to two PRO processes separately. In this configuration, excluding the control of applied pressure in both stages, distribution of the salinities between the two stages is also considered. It is defined as divided feed two-stage PRO process and is illustrated in Figure 3.4(b). In this section, the performance of the two-stage PRO process and single-stage PRO process with the same water availability among different feed water flow schemes and operations are analysed and compared.

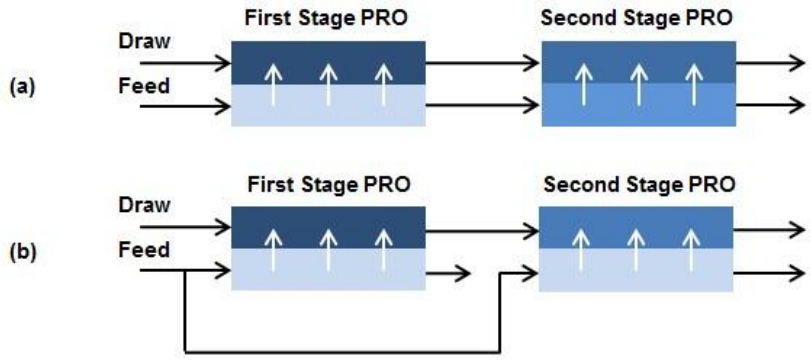

Figure 3.4: The schematic illustration of two-stage PRO process.

3.3.1 CONTINUOUS FEED TWO-STAGE PRO PROCESS

In the case of the continuous feed two-stage PRO process, the feed water is used to generate power twice through the two PRO processes. With the maximal C-PRO energy extraction in both two PRO processes, the total energy generation is illustrated in Figure 3.5(a). The energy generated by the first stage PRO process is represented by the area of the left dashed rectangle, and the energy generated by the second stage is denoted by the area of the right dashed rectangle. It is noted that, with the same water availability at optimal operation, the operation and performance of the first stage PRO process in the continuous feed two-stage configuration is exactly the same as that of the single-stage PRO process. In other words, the energy generated by the second stage PRO process is the extra energy from the continuous feed two-stage PRO process as compared to the single PRO process, which is the further extraction from unused energy of the first stage PRO process.

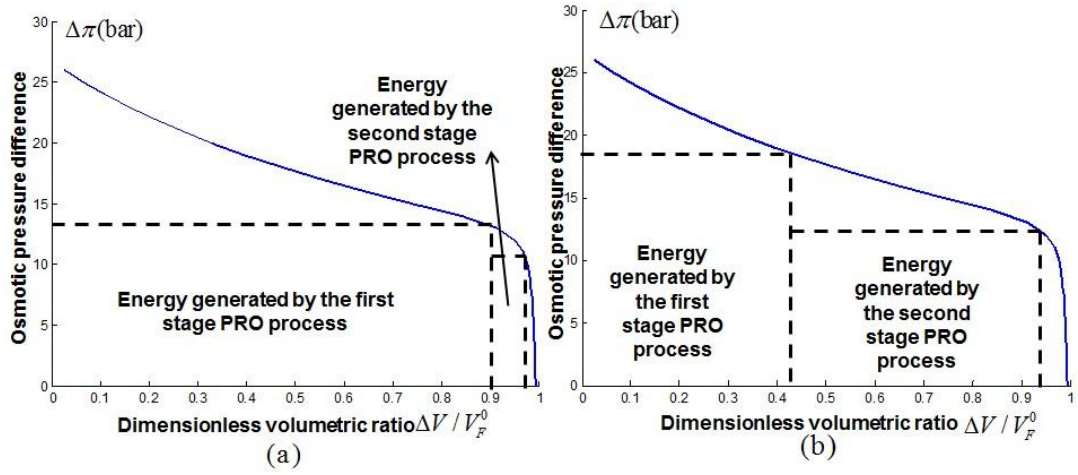

Figure 3.5: Illustration of energy generated by the continuous feed two-stage PRO process**.**

From the viewpoint of overall energy generated from a continuous feed two-stage PRO process, being operated at its optimal condition separately, the overall C-PRO energy extraction is not guaranteed to the global maximum. If the operation of the first stage varies, the total C-PRO energy and performance of the second stage PRO will also change. As in Figure 3.5(b), when the applied pressure is increased, it results in the variations in both the two stages' performance. Therefore, an investigation is carried out to find the optimal operation which achieves the maximal C-PRO generation by a continuous feed two-stage PRO process. In order to emphasize the potential energy capacity generated by the continuous feed two-stage PRO process, the comparison between continuous feed two-stage PRO and single-stage PRO process is analysed on the basis of the same water condition. The extra energy generated by a continuous feed two-stage PRO process compared to the maximum extracted energy by the single-stage PRO (0.3335 kWh/m^3) is depicted in Figure 3.6. The draw solution is seawater (32 g/L), the feed is freshwater (0.1 g/L) and the dimensionless flow rate is 0.5. From the figure, the energy extracted by the continuous feed two-stage PRO process is more than the maximum energy harvested by the single-stage PRO for most of its operations. Furthermore, it can be seen that the optimal conditions separately do not result in the overall maximal energy generation of the two-stage PRO. If the applied hydraulic pressure keeps increasing, the total energy generation increases as well. The overall maximal energy generated by the continuous feed two-stage PRO process is achieved at the applied pressure equalling about 18 bar (respectively, the optimal applied pressure in the second stage is about 12.6 bar).

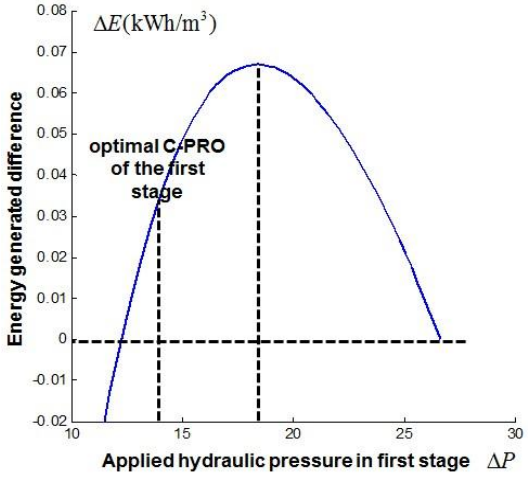

Figure 3.6: Energy generation difference between continuous feed two-stage PRO and single PRO process with respect to different operational pressure on the draw water in the first stage PRO process.

3.3.2 DIVIDED FEED TWO-STAGE PRO PROCESS

In the case of the divided feed two-stage PRO process, the feed water is used to generate power separately and the draw water is used continuously by the two PRO processes. The energy generated by the divided feed two-stage PRO process with equally distributed feed water is illustrated in Figure 3.7. Each PRO process is operated at its optimal C-PRO energy condition. Similarly, the energy generated by the first and the second stage PRO process is represented by the area of two dashed rectangles. As indicated in the figure the divided feed two-stage PRO process takes advantage of the two operations to rearrange the distribution of the energy. The extra energy is generated by reducing frictional loss and unused energy compared to that of the single-stage PRO process.

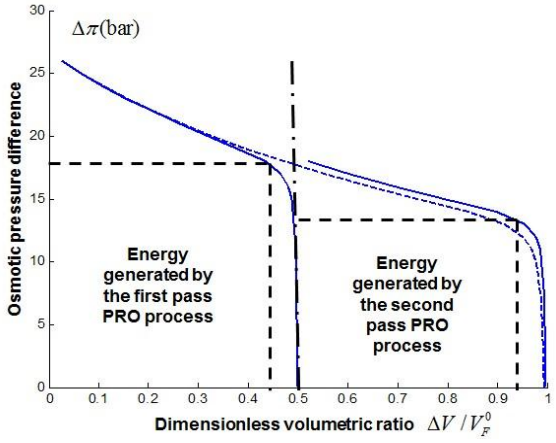

Figure 3.7: Illustration of energy generated by the divided feed two-stage PRO process.

In divided feed water condition, the influence from the first stage to the second stage is less significant than the one in continuous feed two-stage PRO process because only draw solution is utilised continually. Therefore, an investigation is carried out on the water distribution of divided feed two-stage PRO process when the two PRO processes are operated at their optimal C-PRO energy conditions. The water distribution factor here is defined as the fraction of water utilised in the first stage PRO process. The divided feed two-stage PRO process is simulated with different water distribution and the results are presented in Figure 3.8.

The performance of divided feed two-stage PRO process in terms of energy generation with different water distribution is presented and compared to that of the single-stage PRO process operated at its optimal C-PRO condition. From the figure, it is evident that the energy generated by the divided feed two-stage PRO process is larger than the maximum extracted energy of the single-stage PRO process for all the operations. The maximal C-PRO energy in this operation is achieved when about 42% of the feed water is allocated to the first stage PRO.

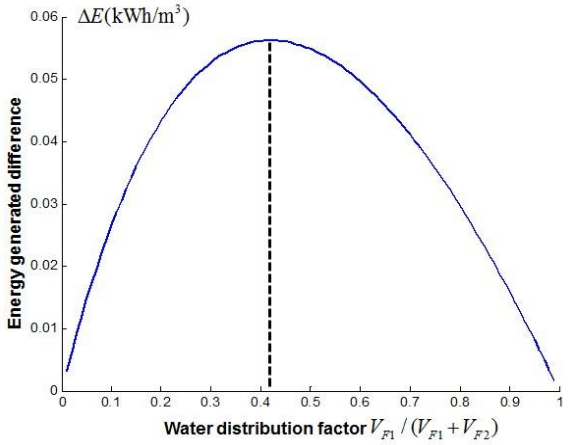

Figure 3.8: Energy generation difference between divided feed two-stage PRO and single PRO process with respect to different water distribution factors on the draw water in the first stage PRO process.

Therefore, based on the results, both continuous feed two-stage and divided feed two-stage PRO processes have shown their ability to harness more energy from a certain level of water availability. And it is necessary to note that more energy could be recovered with more stages but with an additional economic cost.

3.4 DETRIMENTAL EFFECTS OF ICP, ECP AND RSP

In addition, based on the D-PRO models, simulations to evaluate the detrimental effects are carried out with the similar assumptions to the I-PRO modelling above. Excluding the realistic mass transfer across the membrane, the non-ideal effect of the solutions is also considered in D-PRO modelling. The classical van-t Hoff law is developed based on the assumption of ideal solutions and only applies to the dilute solutions. Therefore, a modified van't Hoff law is used to address the non-ideal effect of the solution. According to the modified van't Hoff's law [62], the osmotic pressure difference can be represented as

$$\Delta\pi_m = C_{os}(c_{D,m} - c_{F,m}) \tag{3.1}$$

where C_{os} is the van't Hoff coefficient, $c_{D,m}$ and $c_{F,m}$ are the concentration of the draw solution and the feed solution on the two sides of the membrane respectively. The classical van't Hoff law ($C_{OS} = \nu RT$) is restricted to use on dilute, ideal solutions [103, 104]. Actually, in the salinity range of 0-70 g/kg, the modified van't Hoff law is used to approximate the linear osmotic pressure. The approximation is validated and the maximum deviation is 6.8% [61, 62].

3.4.1 THE APPROXIMATED D-PRO (AD-PRO) MODEL

Due to the high non-linear relation of the D-PRO model represented by Equation (2.16), it is difficult to solve the ODE of permeated water mass transfer rate based on the D-PRO model. An equation such as this usually needs to use iterative methods to solve a non-linear equation in each position along the membrane channel to get the changing water flux. In order to reduce the computational effort, the water flux represented by Equation (2.16) can be simplified by using the first order Taylor series which means that Equation (2.16) can then be written as

$$J_W^{AD-PRO} = \frac{A\left(\frac{C_{os}(c_{D,b} - c_{F,b})}{1 + BS/D + B/k} - \Delta P\right)}{1 + \frac{AC_{os}(c_{D,b}/k + c_{F,b}S/D)}{1 + BS/D + B/k}} \tag{3.2}$$

On the basis of the permeability-selectivity trade-off and the membrane properties discussed earlier (section 2.4.1), three membranes from Table 2.1 were selected for the

verification of the proposed AD-PRO model (membranes 3, 5, 7) representing a low permeability (LP) PRO membrane, a medium permeability (MP) PRO membrane and a high permeability (HP) PRO membrane respectively. The parameters used in the calculation are: temperature 298 K, mass transfer coefficient 138.6 $L \cdot m^{-2} h^{-1}$ [58], diffusion coefficient 1.49×10^{-9} $m^2 \cdot s^{-1}$ [87], and van't Hoff coefficient 0.7345 $bar \cdot kg \cdot g^{-1}$ [62]. From the previous studies, it is shown the insignificant effect of density variation on the solutions obtained in the range of salinity studied [105, 106], for simplicity, a constant density of the water is used for both draw and feed solutions [107], which is 1,000 kg m^{-3}. Mass fraction of the draw and feed solution can be obtained in terms of the solution concentration on the surface of the membrane, such as $c_{D,m}$ and $c_{b,m}$. The water flux and power density of the three membranes based on the I-PRO, D-PRO and AD-PRO model are shown in Figure 3.9.

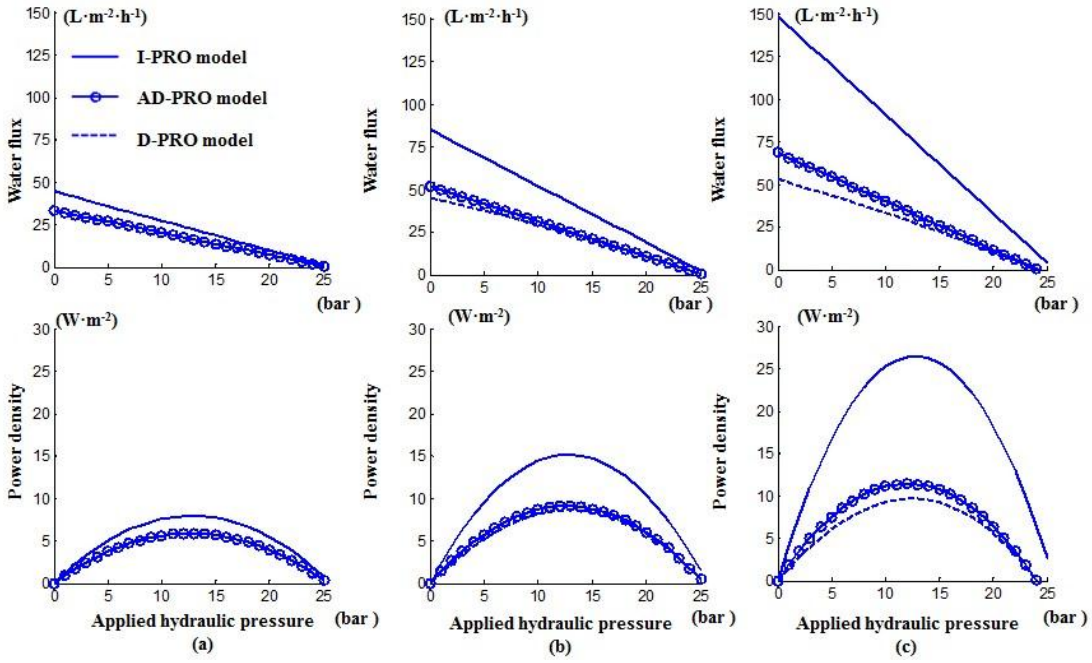

Figure 3.9: Modelled water flux and power density as a function of applied hydraulic pressure based on I-PRO, D-PRO and AD-PRO models. Validations of the AD-PRO using three membranes, LP, MP and HP membranes are shown in (a), (b) and (c), respectively.

Because the D-PRO model has been verified using experimental data with satisfactory consistency [32], the effects of ICP, ECP and RSP can be estimated by the difference between the solid and dashed curves in Figure 3.9 representing water flux and power density, respectively. It is observed from Figure 3.9 that the water flux and power density of a PRO process with detrimental effects, are significantly reduced compared to the ideal water flux for all the LP, MP and HP membrane selected. In addition, the difference in

water flux and power density between the I-PRO and D-PRO model increases with the membrane of higher water permeability. According to Equation (2.16), this is due to more severe ICP, ECP and RSP effects caused by the increased water flux.

From the results as shown in Fig 3.9, it can be concluded that a linearised AD-PRO model can be used to describe the water flux and power density of the LP membrane with very high accuracy because of the very close values obtained by both AD-PRO and D-PRO modelling. Thus, as D-PRO modelling as a reference, very high accuracy of the AD-PRO modelling is achieved when LP membrane is used. And the accuracy decreases with more severe effects of the ICP, ECP and RSP in the cases of high water permeability membranes. In Figure 3.9(a), the circled line is almost overlapped by the dashed line for all the applied hydraulic pressure. This is the same as the situation in the modelling of power density of the LP membrane in Figure 3.9(a). The deviations of the results between the two models become larger with respect to the increase on the membrane permeability. In Figures 3.9(b) and 3.9(c), although the water flux and power density based on AD-PRO model are higher than the values on D-PRO model, the water flux and power density based on AD-PRO model still addressed the significant decrease caused by the effects of ICP, ECP and RSP. Therefore, in the later investigation, the AD-PRO model was used to address the three detrimental effects in simulating the PRO processes. The LP membrane was selected to further study the discharge behaviour of the PRO process due to its high accuracy.

In addition to the comparison with existing D-PRO model, the AD model is also verified with experimental data. The results are shown in Figure 3.10 in which the water flux and power density based on the AD-PRO model are validated using experimental data [108]. The membrane parameters list in this study were water permeability, A, 1.35 $L \cdot m^{-2} \cdot h^{-1} \cdot bar^{-1}$, salt permeability, B, 0.28 $L \cdot m^{-2} \cdot h^{-1}$, and structure parameter, S, 149 μm. The results show satisfactory agreement between the model and experimental data in the case of both the mixture of seawater and brackish water, and the mixture of the seawater and river water.

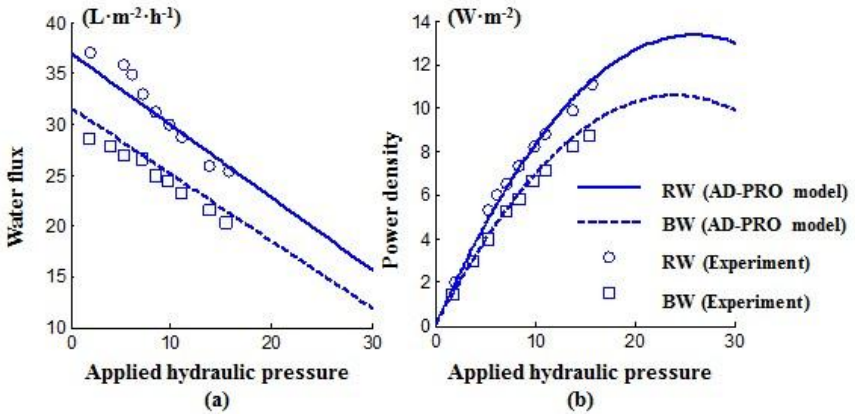

Figure 3.10: Verification of the AD-PRO model with the experimental data.

3.4.2 Co-current flow scheme

In the co-current flow scheme, the two respective streams of the draw and feed solution, c_D^0 and c_F^0, are in the same direction with mass flow rates of q_D^0 and q_F^0, respectively. Here, a dimensionless water flux is defined for the use of inlet and outlet conditions in all cases. The dimensionless water flux, J_W^* is represented as

$$J_W^* = \frac{J_W}{J_W^{MAX}} = \frac{J_W}{AC_{os}(c_D^0 - c_F^0)} \tag{3.3}$$

where J_W^{MAX} is the maximum water flux in PRO with zero hydraulic pressure. Therefore, the inlet condition and outlet condition can be expressed as

$$\begin{aligned} J_W^{*,IN} &= \frac{J_W^{IN}}{J_W^{MAX}} = \frac{c_{D,m}^0 - c_{F,m}^0 - \Delta P/(C_{os})}{c_D^0 - c_F^0}; \\ J_W^{*,\mathrm{OUT}} &= \frac{J_W^{OUT}}{J_W^{MAX}}; \end{aligned} \tag{3.4}$$

where J_W^{IN} and J_W^{OUT} represent the water flux at the inlet and outlet respectively. Theoretically, for a full scale PRO discharge, the water flux reduces to zero at the outlet. However, it is very difficult to reach absolute zero flux numerically, especially when the salt concentration of the feed solution is zero or very diluted. Also mathematically numerical error during the modelling makes it difficult to reach the absolute zero. Thus, a relatively small value which is considerably larger than the magnitude of numerical error is selected as a reference to compare the different PRO operations. In this study, when the water flux

at the outlet is reduced to that of $J_W^{*,OUT} = 0.01$, it is assumed to be a full scale PRO discharge (actual water flux is approximately 0.5 $L \cdot m^{-2} \cdot h^{-1}$ with the given initial condition of the salinity gradients).

- **WATER FLUX AND POWER DENSITY**

In this chapter, the draw solution is selected with a concentration of 35 g/kg and the feed solution, fresh water, with a concentration of 0.1 g/kg. A dimensionless flow rate (feed fraction) of 0.5 is assumed by default. For simplicity, the initial flow rate of the feed solution is assumed to be 1 $kg \cdot h^{-1}$.

Based on the flowchart of the D-PRO modelling as shown in Figure 2.6, the water flux and power density with three different applied hydraulic pressures are shown in Figures 3.11 and 3.12, respectively. The difference between the water flux shown in Figure 3.9 and the water flux profiles shown in Figure 3.11 is that the results presented in Figure 3.9 are the transient water flux for the membrane area approaching zero. While Figure 3.11 shows the profiles of water flux along the channel with enough membrane area during the discharge of the PRO process. First of all, with increased applied hydraulic pressure, less deviation between the two profiles of water flux with and without consideration of ICP, ECP and RSP effect is obtained. As illustrated in Figure 3.11(a), with 20 bar applied on the draw solution, the majority of the two profiles are almost overlapping. The insignificant reduction on the water flux is a result of the lower water flux caused by the higher applied pressure. Similarly, looking at a water flux profile of the PRO discharge in Figure 3.11(a), a large deviation of the AD-PRO process from the I-PRO process results in at the inlet in all the operations with different hydraulic pressures and then reduces in accordance with the decreasing water flux. Actually, the overall performance limiting effects are reflected by the reduction on the net driving force. In this context, the water flux can be expressed as

$$J_W^{D-PRO} = A(\Delta\pi_m - \Delta P) = A[\Delta\pi_b - (\Delta P + \Delta\pi_b - \Delta\pi_m)] \tag{3.5}$$

where $\Delta\pi_b$ is the osmotic pressure difference of the bulk solutions. The performance limiting effects on the water flux can be regarded as the effect of 'an extra applied pressure' to further retard the water transportation across the membrane. As such, in Figure 3.11(a), all the dashed curves representing the water flux considering detrimental effects, start at a lower value and behave similarly as the profiles of water flux with a higher hydraulic

pressure applied on the draw in an I-PRO process. Although the 'extra applied pressure', $\Delta\pi_b - \Delta\pi_m$, varies along the membrane channel, an averaged pressure can be implemented on the draw solution of the I-PRO process to approximate the profile. This is in comparison to Figure 3.11(b) where the detrimental effects can be approximated by applying a constant 'extra pressure' on the I-PRO model. In Figure 3.11(b), the water flux based on the I-PRO model with $\Delta P = 9$ bar is relatively closer to the profile of water flux considering the detrimental effects.

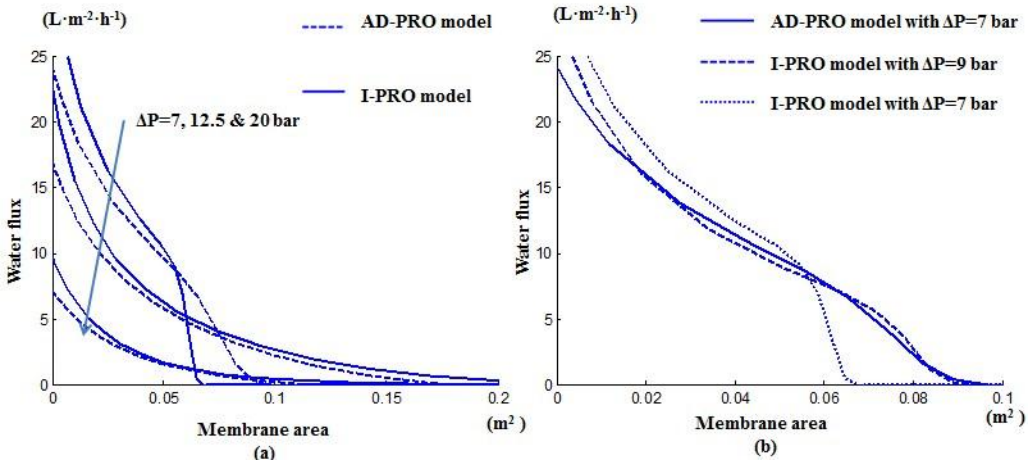

Figure 3.11: Water flux along the membrane during the steady-state co-current cross-flow PRO discharge with different applied hydraulic pressures in (a) and the approximated decreased water flux by 'an extra applied pressure' in (b).

It is seen from Figure 3.12 that the power density also changes with different applied pressure, a result of water flux change based on Equation (2.2). In addition, the effects of ICP, ECP and RSP also lower the power density at the start. Moreover, the 'extra pressure approximation' of the performance limiting is still validated in the power density due to the close relation between the water flux and the power density.

- **EXTRACTABLE ENERGY**

The extractable energy of a PRO plant is assessed from the view of the full scale discharge. In addition to the energy loss of the friction and un-permeation in the osmotic-driven water transportation, the extractable energy of a PRO process can be obtained [32] as presented by Equation (2.7). Based on the full scale PRO discharge behaviour, the extractable energy of the PRO process considering ICP, ECP and RSP is shown in Figure 3.13 in which three dimensionless flow ratios of 0.2, 0.5 and 0.8 are studied to represent the different salinity

gradients available worldwide. For the purpose of comparison, the extractable energy profiles of the three conditions in I-PRO process are also presented.

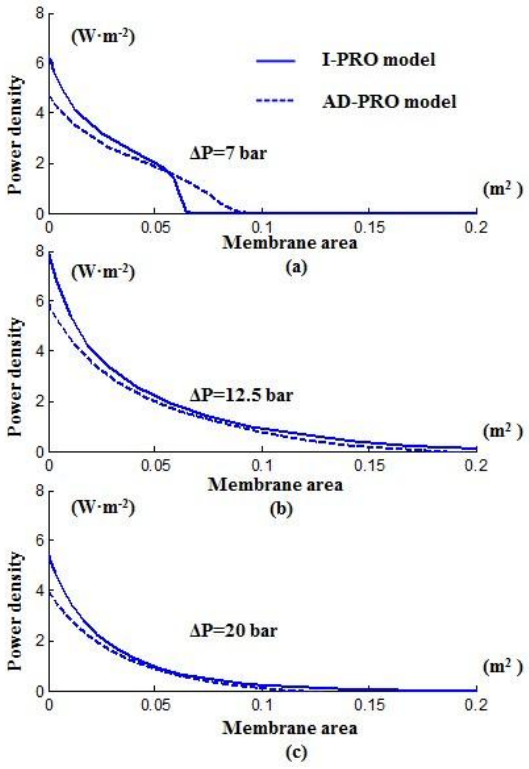

Figure 3.12: Power density along the membrane during the steady-state co-current cross-flow PRO discharge with different applied hydraulic pressures.

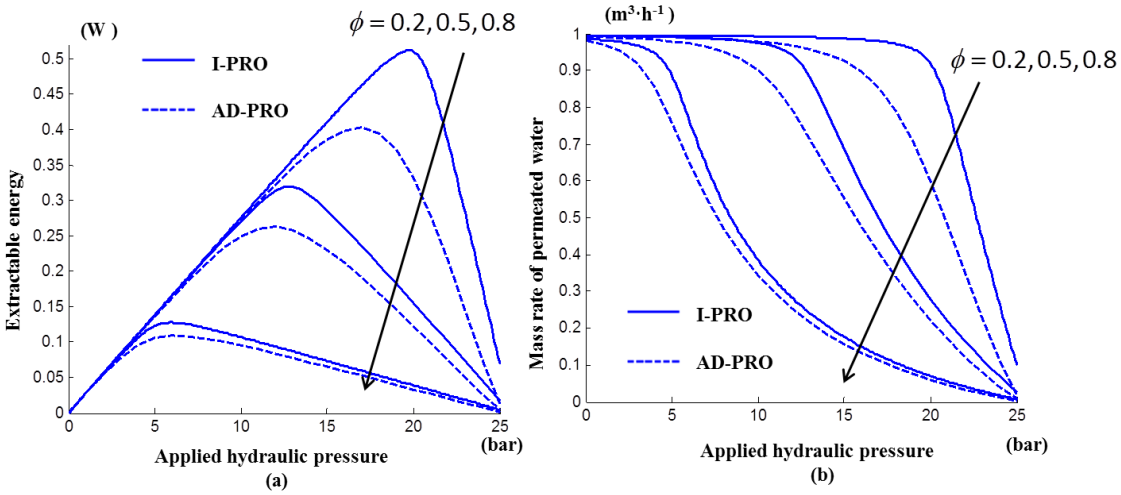

Figure 3.13: Effects of ICP, ECP and RSP on the extractable energy capacity of the full scale PRO discharge.

The results clearly indicate the significant reduction on the extractable energy capacity of the full scale PRO discharge on all the salinity gradient conditions. With the constant hydraulic pressure on the draw solution, the ICP, ECP and RSP effects on the process-based extractable energy is only determined by the reduced mass rate of permeated water as presented in Figure 3.13(b). The decrease is a result of an accumulating effect of the reduced water flux along the membrane caused by the overall effect of ICP, ECP and RSP.

- **REQUIRED MEMBRANE AREA FOR PRO DISCHARGE**

The water flux and power density obtained above in Figure 3.9 reveals the change of profiles with different hydraulic pressure applied on the draw solution. It is also observed that the detrimental effects drive the water flux and power density away from the ideal behaviour of the PRO process. But the required membrane area of a PRO process cannot be easily differentiated in the cases of 12.5 and 20 bars as demonstrated in Figures 3.11 and 3.12. Thus, the change on required membrane area of a PRO process is needed to be studied further. The concept is to describe the minimum area required to reach the predefined outlet condition. By rearranging Equation (3.7), the required membrane area can be expressed as

$$A_M = \int \frac{1}{J_W} d\Delta V_P \tag{3.6}$$

Previously, it has been shown that the water flux keeps decreasing after entering a co-current PRO process. Therefore, the required membrane area of a full scale PRO discharge used is the minimum area that allows the dimensionless water flux reduced to 0.01. The required membrane area of a full PRO discharge is shown in Figure 3.14.

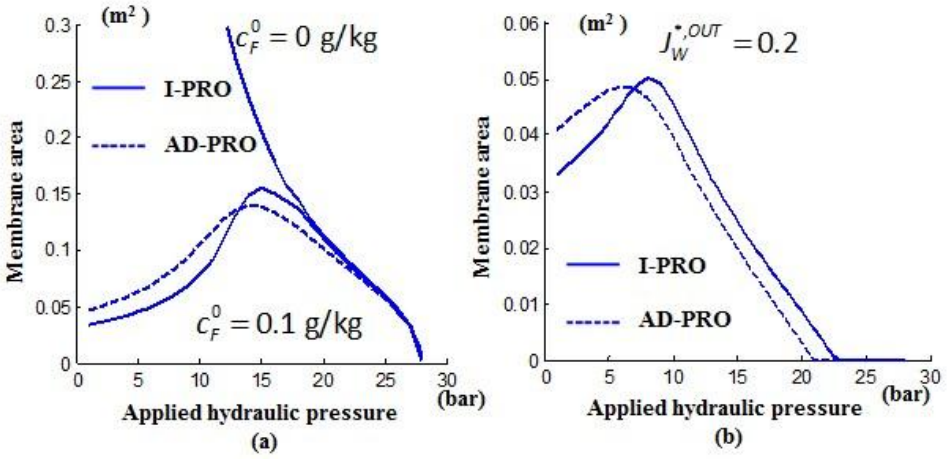

Figure 3.14: Required membrane area in the PRO discharge**.**

Theoretically, if there is no RSP and with a zero salt concentration in the feed solution, the permeated flux will never reach zero, except for infinite membrane area, because the driving force on the feed solution side will not vanish when the water is permeating. In Figure 3.14(a), with a zero salt concentration feed solution (DI water in practice), huge amount of the area is required at lower range of the hydraulic pressure even to reach the "pseudo zero water flux" ($J_W^{*,OUT} = 0.01$). With a non-zero salt concentration (0.1 g/kg illustrated in Figure 3.14(a)) in the feed solution, the hypothetic infinite membrane area of an I-PRO process without RSP is not needed.

Comparing the two PRO models in the modelling of required membrane area, it is found that the curve of the area representing the full scale AD-PRO discharge can be approximated by a translational curve of area representing the full scale I-PRO process towards the lower hydraulic pressure. It is a demonstration of the 'extra pressure approximation' of the overall effects of ICP, ECP and RSP on the dynamics of the PRO. Because in an I-PRO process, with respect to the range of the available lower hydraulic pressure, and with the increase on the pressure, more membrane area is required for a full scale discharge. Thus, for an AD-PRO process approximated by applying 'an extra pressure' on the draw solution in the I-PRO process, more area is required in the lower range of the hydraulic pressure. Conversely, less area is required for the operations in the higher range of applied pressure. Furthermore, the deviation of the area required in the different PRO operations between the two processes also varies because of the different magnitude of water flux. When water flux is lower, the detrimental effects are insignificant. As shown in

Figure 3.14(a), the two curves of area are almost overlapping when the applied pressure is larger than 20 bar.

In addition, the required area of different scale of PRO discharge is also evaluated. In Figure 3.14(b), the outlet condition is 0.2 dimensionless water flux (approximate 10 $L \cdot m^{-2} \cdot h^{-1}$). The results demonstrate that the overall detrimental effects on the required area are significant in all the operations. It is also clear from the results that the approximation of the AD-PRO by applying 'an extra pressure' on draw solution of the I-PRO is more feasible.

- **SALINITY CONCENTRATION AND DRIVING FORCE PROFILE**

An average salinity concentration variation along the membrane can be also obtained according to mass balance. Besides, if the concept of osmotic driving force of each solution on the two sides of the membrane is defined as the difference between the osmotic pressure and the hydraulic pressure, then the driving force of water flux across the membrane is the difference of the driving force between the membrane surfaces in the two solution channels. Therefore, the driving force of a solution is defined as

$$DF_i = \pi_i - P_i \tag{3.7}$$

where DF_i is the driving force and π_i and P_i are the osmotic pressure and hydraulic pressure, respectively. Higher osmotic driving force in each side allows higher permeating rate of water from the opposite side of the membrane. Accordingly, the driving force of the draw and feed solution along the membrane in the I-PRO process are illustrated in Figure 3.15 with three hydraulic conditions.

From Figure 3.15, it is observed that during the PRO discharge, the driving force of the draw solution decreases and the corresponding increase occurs in the feed solution. Water permeation terminates when the two driving forces are equalised. In addition, the profiles of the driving force are different with different values of the applied hydraulic pressure. With a lower applied pressure such as 7 bar illustrated in Figure 3.15, the terminated driving force at the outlet of the flow channel is a consequence of the rapidly increasing driving force on the feed side due to the lack of the feed solution. In such a case, the variation on the driving force of the feed solution side dominates the termination of the PRO discharge. This is also the reason why the large membrane area is required when the feed salt concentration is zero in the PRO operations with a lower hydraulic pressure. In

contrast, when a higher hydraulic pressure is applied, the equilibrium of the concentration between the two sides across the membrane is mainly a result of the dilution effect of the draw solution.

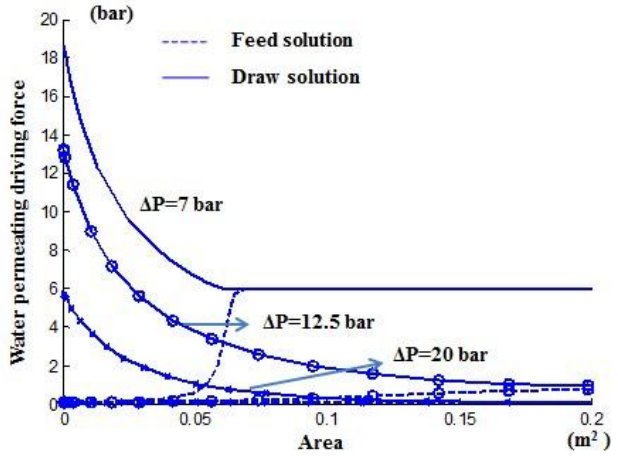

Figure 3.15: The driving forces of the draw and feed solution along the co-current flow PRO membrane module.

3.4.3 Counter-current flow scheme

In the case of a counter-current flow scheme, the two streams of the draw and the feed solution flow in the opposite directions. The inlet and outlet conditions of the two channels should be considered separately, and depending on different applied hydraulic pressure, the terminated condition of the water flux varies.

Similarly, the initial concentrations of the draw and the feed solutions are c_D^0 and c_F^0, respectively, and the mass flow rates are q_D^0 and q_F^0, respectively. Because of the different positions of the two streams' inlets and outlets, from the view of the dimensionless water flux, two conditions can be expressed as

$$\begin{aligned}\text{condition 1: } J_W^{*,\text{IN}} &= \frac{c_{D,m}^{OUT} - c_{F,m}^0 - \dfrac{\Delta P}{C_{os}}}{c_D^0 - c_F^0};\ J_W^{*,OUT} = \frac{c_{D,m}^0 - c_{F,m}^{OUT} - \dfrac{\Delta P}{C_{os}}}{c_D^0 - c_F^0} \\ \text{condition 2: } J_W^{*,\text{IN}} &= \frac{c_{D,m}^0 - c_{F,m}^{OUT} - \dfrac{\Delta P}{C_{os}}}{c_D^0 - c_F^0};\ J_W^{*,OUT} = \frac{c_{D,m}^{OUT} - c_{F,m}^0 - \dfrac{\Delta P}{C_{os}}}{c_D^0 - c_F^0}\end{aligned} \tag{3.8}$$

where $c_{D,m}^{OUT}$ and $c_{F,m}^{OUT}$ are the concentration of the draw and feed solution on the surface of the membrane at their outlets. In the case of condition 1, the zero water flux is reached

at the outlet of the feed solution channel. In contrast, the termination of the water flux happens at the outlet of the draw solution channel in the case of condition 2. Based on the solute balance in an I-PRO process and the termination conditions above, the applied hydraulic pressure is divided into three parts

$$\begin{aligned} \Delta P_0 &= C_{os}[(1-\phi)c_D^0 - \phi c_F^0] && \text{condition 1\&2} \\ \Delta P = \Delta P_1 &< \Delta P_0 && \text{condition 1} \\ \Delta P = \Delta P_2 &> \Delta P_0 && \text{condition 2} \end{aligned} \tag{3.9}$$

where ΔP_0 represents the applied hydraulic pressure when both conditions 1 and 2 are satisfied simultaneously, and ΔP_1 and ΔP_2 represent the two range of hydraulic pressure and conditions 1 and 2 are satisfied separately in an I-PRO process.

- **WATER FLUX AND POWER DENSITY**

Similarly, with the inlet and outlet conditions of a counter-current flow scheme, the ODE describing the water permeation can be solved and then the water flux and power density can be obtained based on Equations (2.16) and (2.2) during the steady-state discharge of the I-PRO process. The resulting water flux and power density are studied. Due to these two conditions, the results of each flow with three different applied hydraulic pressures are shown in Figure 3.16.

The positions of the zero water flux are different in the case of two termination conditions. According to Equation (3.9), with condition 1 applied, the water flux terminates at the outlet of the feed solution. In contrast, condition 2 is reached at the outlet of the draw solution. This is illustrated in Figure 3.16 where (a) and (b) represent condition 1, and (c) and (d) represent condition 2. The zero points of the area-axis (x-axis) in Figure 3.16 represent the inlet of the draw solution. Thus, all the results are presented in the same x-axis direction of the flow of the draw solution, namely from the left to the right as illustrated in Figure 2.5(b). In PRO operations under condition 1, the water flux at the outlet of the feed solution is always zero for a full scale PRO discharge. As noted in Figure 3.16(a), from the inlet of the feed solution, the water flux starts at a non-zero value, increases gradually during the PRO discharge until its maximum is reached. Then the water flux decreases to zero rapidly before flowing out of the feed channel. In addition, the starting value on the right hand side of Figure 3.16(a) decreases with the increase of the applied

pressure in the range of ΔP_1. When the value of ΔP_1 approaches to ΔP_0 (in this case, $\Delta P_0 = 12.817$ bar), the starting water flux also gets closer to zero as illustrated in Figure 3.16(a) when 12.5 bar is applied on the draw solution. In such a case, water flux at both ends is nearly zero. Conversely, in the PRO operations applying hydraulic pressure in the range of ΔP_2, the termination of the full scale discharge occurs at the outlet of the draw channel. The profiles of the water flux in a counter-current scheme (Figure 3.16) PRO process are more even comparable to that in co-current flow scheme (Figure 3.11) because of the lower maximal value and the larger minimal value. Moreover, according to Thorsen and Holt's findings [55], the power yielding from a membrane module is similar for co-current and counter-current cross-flow in practice. However, the more evenly distributed water flux of the counter-current means its maximum water flux is lower than that of the co-current scheme, and therefore, comparatively, it possesses a lower possibility to be fouled at the higher water flux. From this point of view, counter-current flow scheme is preferred.

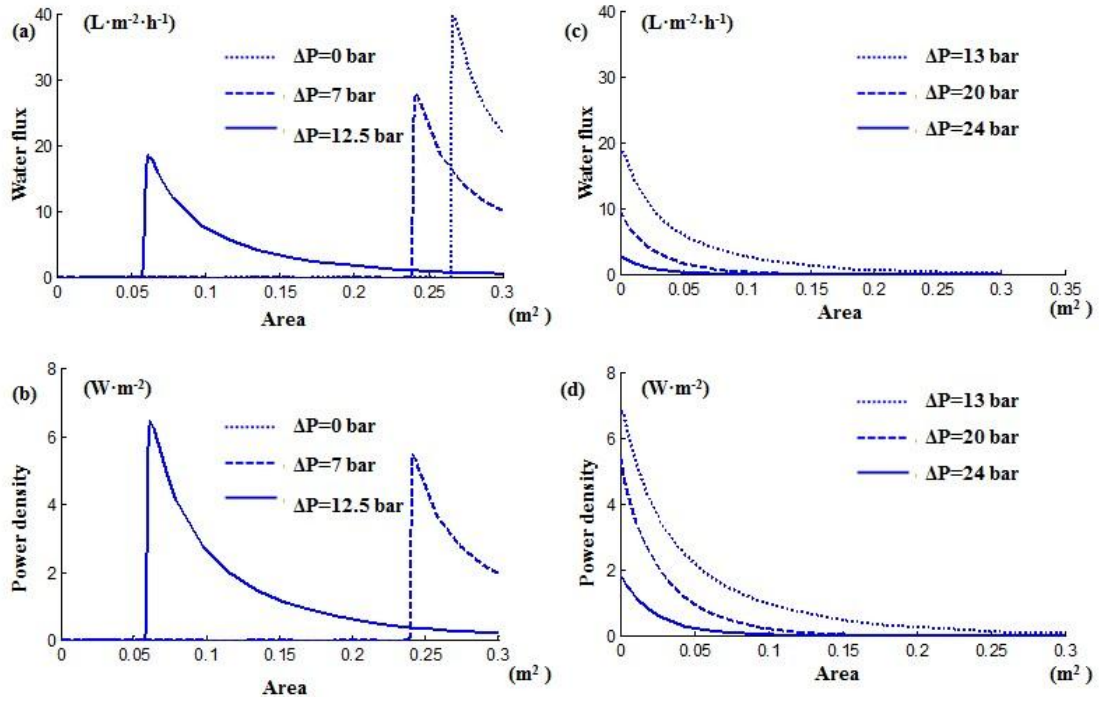

Figure 3.16: Water flux and power density along the membrane during the steady-state counter-current cross-flow PRO discharges with different applied hydraulic pressure.

- **DRIVING FORCE PROFILE**

The driving forces of the two solutions along the membrane were also studied. The results of I-PRO process with two conditions are presented in the Figures 3.17(a) and 3.17(b), respectively. Also the driving force profiles of the counter-current flow PRO process are shown using the same area-axis (x-axis) as Figure 3.16.

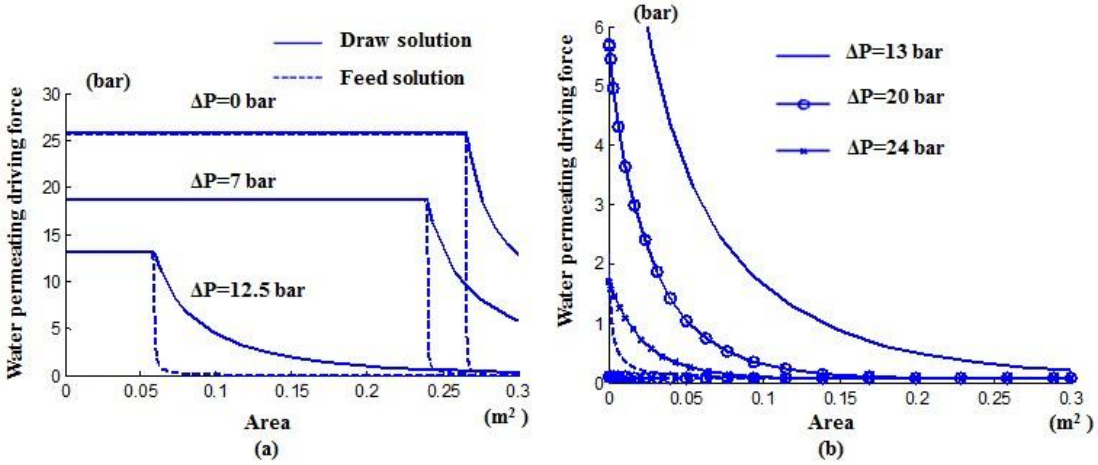

Figure 3.17: The driving forces of the draw and feed solution along the counter-current flow PRO membrane module.

From Figure 3.17, it is evident that the driving forces of the draw and feed solution changes along the membrane in the same direction. This can be seen where both the driving force decreases from the left hand side to the right hand side of the membrane module (flow direction of the draw solution as illustrated in Figure 2.5(b)). Condition 1, as represented by Figure 3.17(a), clearly indicates more retarded water permeation due to the reduced net driving force with a higher applied pressure. Also, the different applied hydraulic conditions induce different driving force profiles along the membrane for both the conditions as represented in Figures 3.17 (a) and (b). Based on the profiles of the driving force of the water permeation in the counter-current PRO flow scheme, it is found that the difference between the two termination conditions is due to the disappearance of the net driving force for different reasons. Similar to the co-current flow scheme, in the case of condition 1 (lower range of available hydraulic pressure, ΔP_1), the water flux is terminated as a result of the shortage of the feed solution near the outlet of the feed solution. The 'over-permeation' of the feed solution increases its concentration rapidly and terminates the water flux sharply. Conversely, the dilution of the draw solution reduces the driving force

gradually and terminates the water permeation in condition 2 when the applied pressure is in the higher range as denoted by ΔP_2.

3.5 SUMMARY

An analysis of the PRO processes for energy production from natural salinity gradients has been compared between the PRO process with and without detrimental effects. The I-PRO and D-PRO models are introduced and an approximated AD-PRO model is proposed and compared with published data. Furthermore, water flux and power density of the PRO processes with co-current and counter-current flow schemes have been studied and analysed. In addition, the driving force profiles along the different membrane modules and operations with different applied hydraulic pressure are also analysed. Based on the results of this chapter, the following conclusions can be drawn: 1) the operations of a two-stage PRO processes is advantageous in harnessing more energy from the same level of water availability compared with a single-stage PRO process. 2) the proposed AD-PRO model can be used to approximate water flux and power density of the PRO process incorporating the effects of ICP, ECP and RSP. Especially, for the PRO process with low water permeability membrane where a very high accuracy is achieved; 3) during the discharge of a full scale PRO process, the detrimental effects further retard the water permeation and power generation and both water flux and power density start at much lower values and behave similar as that with an 'extra pressure' applied on the draw solution in an ideal PRO process; 4) the capacity of the extractable energy from a full scale PRO discharge is significantly reduced due to the ICP, ECP and RSP effects; 5) termination of the water permeation is a result of the run out of the draw solution or the feed solution, determined by the hydraulic pressure applied on the draw solution in both co-current and counter-current flow PRO processes; and 6) the water flux of the counter-current flow PRO process varies more evenly along the membrane channel compared to that of the flux of the co-current flow PRO process.

AN EVALUATION OF MEMBRANE PROPERTIES AND PROCESS CHARACTERISTICS OF SCALE-UP PRESSURE RETARDED OSMOSIS (PRO) PROCESS

4.1 INTRODUCTION

The challenge in a scale-up PRO process is the decreased average power density with the increase of the process scale [64]. According to the analysis carried out by Statkraft [56], the satisfactory power density should be no less than 5 W/m^2 to achieve economic viability. Due to inherent trade-off challenge between power density and specific energy in a full-scale PRO process [60], optimising the process configuration, membrane properties, operating conditions and components efficiency including HP, ERD and HT are crucial to balance these two objectives and to improve the performance of PRO process. For accelerating the implementation of PRO process, therefore, the process dynamics and the influential factors of the scale-up PRO process need to be investigated and figured out.

Moreover, membrane is the core component in the PRO process and its performance determines the overall economic and energy performance of the system. Several investigations focusing on the membrane fabrication reported the existence of permeability-selectivity trade-off relationship. These studies also addressed the optimum membrane properties and the resulting maximum peak power densities by developing sensitivity analysis of membrane properties in a lab-scale PRO [33]. Furthermore, in a scale-up PRO, the existing trade-off relationship of the membrane permeability and rejection is coupled with the spatial variations of the flow, heat and mass transfer, making the problem more complicated. In order to improve the particular membrane properties for a scale-up PRO, a balanced membrane performance needs to be identified considering different operating conditions and the increase of the process scale. However, there is no reported published work on the sensitivity analysis of membrane properties on the scale-up PRO performance with respect to different operating conditions. Only a particular membrane with a selected set of membrane water permeability coefficients, solute permeability coefficients and structural parameters was selected for studying the module-scale or scale-up PRO process in previous studies [59-62, 69, 109-111]. Therefore, in this chapter, a sensitivity analysis of the membrane properties aims to be developed in a scale-up PRO to investigate the optimum properties in different operating conditions, such as different flow schemes (co-current and counter-current flow scheme) and flow fractions of the salinities. Additionally, in a system-level, energy losses in energy generation, water pumping and pressurization significantly affect the overall performance of the scale-up PRO. Therefore, in this study, the effects of the inefficiencies of the components (HP, ERD and HT) are also addressed in this chapter.

4.2 MASS TRANSFER IN PRESSURE RETARDED OSMOSIS

In this chapter, sensitivity analysis and process characteristics of PRO with respect to operating condition, membrane properties and components (HP, ERD and HT) are aimed to be studied. The analysis can be achieved through a series of simulations with different parameters. In each simulation, all the parameters are given and the process performance in terms of specific extractable energy and average power density can be evaluated. The average power density is the mean power density over all the membrane area used and the specific extractable energy is the extractable energy per flow rate of the initial feed flow rate. In a PRO process, in order to efficiently utilise the membrane and low concentration

salinity, these two objectives are used. The flowchart of the numerical work is illustrated in Figure 4.1.

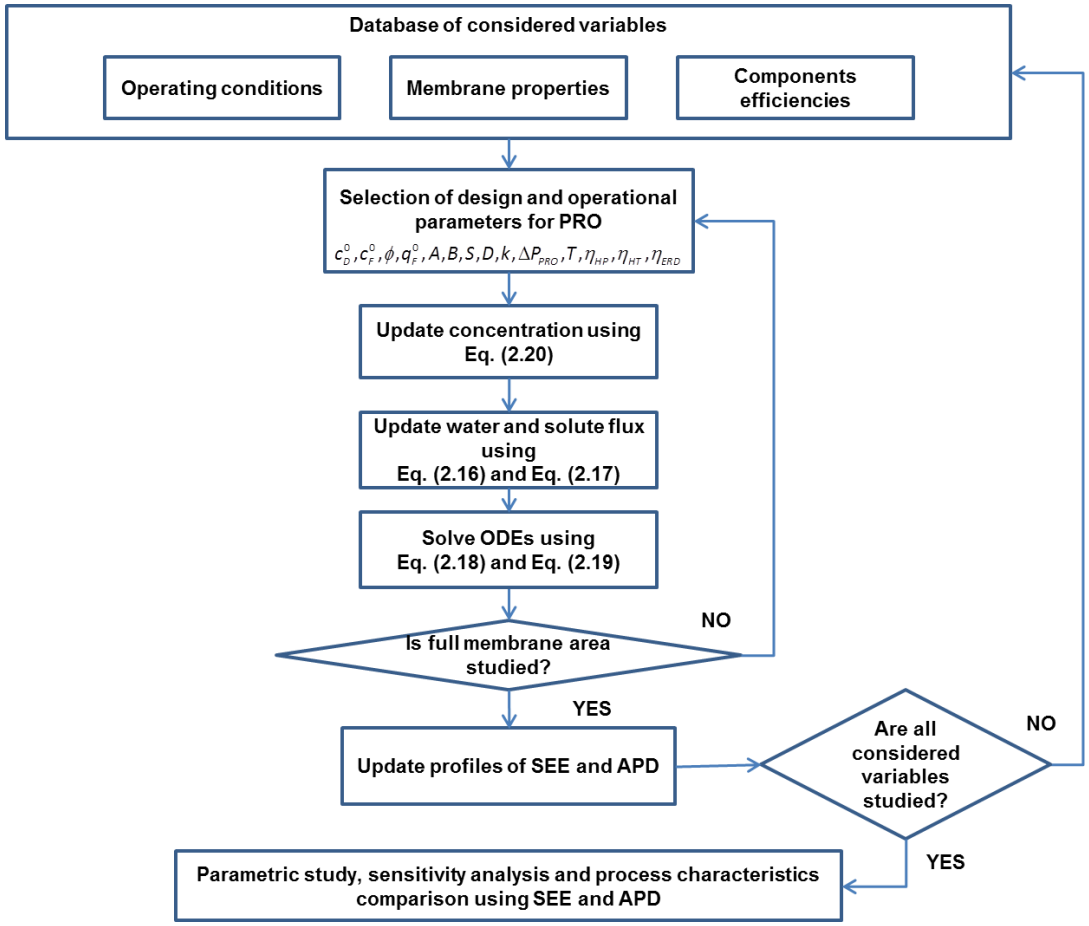

Figure 4.1: Flowchart of the sensitivity analysis and process characteristics of PRO in this work.

A database of PRO process variables including operating conditions, membrane properties, and components efficiencies is identified first. For each case study, a particular combination of the variables is selected. In the simulation, with selected design parameters and operations in the simulations, the salt concentration of the draw and feed solution are updated by substituting water flux and reverse solute flux into permeated water mass flow rate and accumulated solute permeation rate, similar to the simulation developed in previous chapters. On the basis of D-PRO modelling, a system of ODEs on mass rates of permeated water and reverse solute permeation can be obtained to describe the steady-state PRO process. Moreover, with the inlet and outlet conditions of the co-current and counter-current flow PRO discharge, the ODEs can be solved, and profiles of water flux and power density can be obtained. Then, the specific extractable energy and the average power density can be obtained. After the evaluation of a particular PRO process

performance, the next combination of the variables is selected for the simulation. If all the combinations of the pre-defined variables are studied, the simulation stops and all the results of the specific extractable energy and average power density are used to be compared and analysed to address the influences of operating operation, membrane properties and components efficiencies.

4.3 INFLUENCE OF OPERATING CONDITIONS ON PERFORMANCE OF THE SCALE-UP PRO PROCESS

The flow parameters are determined by local water conditions that comprise concentration and mass flow rates of both the high and low concentration solutions. In this chapter, the draw solution was selected with a concentration of 35 g/kg and the feed solution (fresh water), with a concentration of 0.1 g/kg.

One of the important operating conditions is the hydraulic pressure applied on the draw solution. A constant hydraulic pressure difference is applied in the PRO process. For a full scale PRO discharge, the balance is established between the osmotic pressure difference and the hydraulic pressure difference at the outlet of the membrane module. In a co-current flow scheme, due to the same flow direction of the two streams, the concentration of the feed solution and the dilution of the draw solution are accumulated from the same inlet to the same outlet. Conversely, in the counter-current flow scheme, depending on the different hydraulic pressure, the balance of the net driving force in a full scale PRO process is achieved at different places, according to the results in Chapter 3. With a low hydraulic pressure, the mass transfer across the membrane is dominated by the concentration of the feed solution. The outlet of the zero net driving force is achieved at the outlet of the feed solution. In contrast, with a high hydraulic pressure, the termination of the driving force is determined by the concentration of the draw solution in the full scale permeation. Therefore, the balance is achieved at the outlet of the draw solution.

Furthermore, the influences of the hydraulic pressure on the specific extractable energy and the average power density are studied in both the co-current and the counter-current flow PRO processes. The results are shown in Figure 4.2 in which the specific extractable energy is represented by colour-map and the average power density is represented by contour-line. Three cases of the dimensionless flow rates, 0.2, 0.5 and 0.8, are selected for representing the low, medium and high dimensionless flow rates. The selection of these three ratios aims to represent different feed fractions of the possible salinity gradients. The

scale of the membrane area is studied in terms of specific membrane area which is the membrane area per initial flow rate of the feed solution. The investigated specific membrane area is up to 0.4 m^2 per 1 $L \cdot h^{-1}$ feed solution which is sufficient for a full scale PRO discharge in different operations. In addition, the membrane used in this section has the following specifications [33]: water permeability 1.74 L $m^{-2} \cdot h^{-1} bar^{-1}$, salt permeability 0.16 L $m^{-2} \cdot h^{-1}$, and structural parameter ($S = t_s \tau / \varepsilon$ which is introduced in Chapter 2) 307 μm. Other parameters used in the calculation are same to those used in Chapter 3.

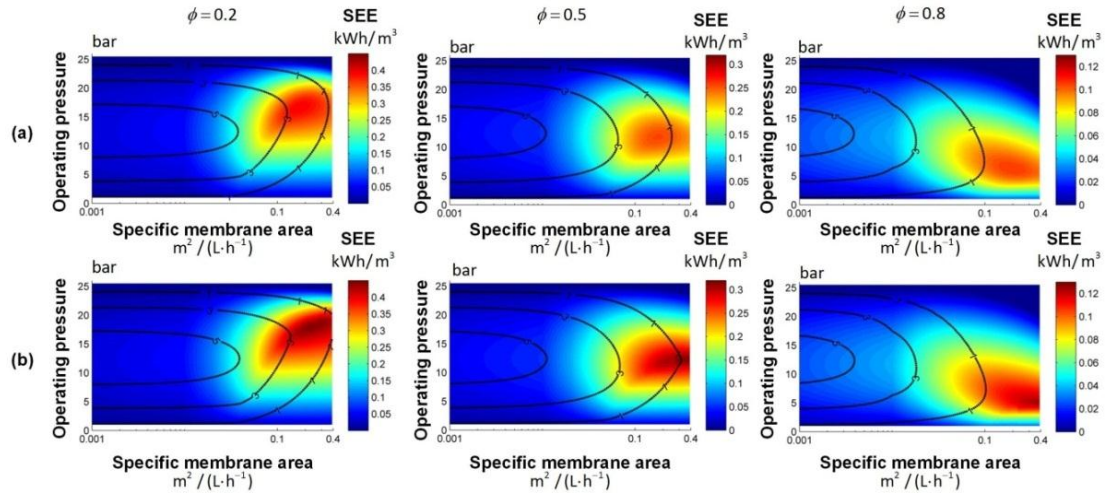

Figure.4.2: Influence of the applied hydraulic pressure on the performance of the scale-up PRO process. SEE is shortened for specific extractable energy. Two flow schemes, co-current and counter-current, are shown in (a) and (b), respectively.

According to the results, at the same dimensionless flow rate, the trade-off relationship between the specific extractable energy and the average power density can be found. When a large scale of the membrane is used, the specific extractable energy is found to be high while the average power density is found to be low. Conversely, at a small specific membrane scale, the specific extractable energy is very low when the average power density is high. It is the result of the vanishing net driving force of the permeation due to the dilution of the draw and the concentration of the feed during the PRO discharge. Thus, in order to increase the membrane efficiency and reduce the membrane cost, a high average power density should be aimed to achieve with the loss in the specific extractable energy. In addition, comparing the specific extractable energy between the two schemes, it is easy to find the advantageous efficiency of the counter-current flow scheme in the energy extraction. On the basis of the colour-map of specific extractable energy, the specific extractable energy of the counter-current flow scheme is larger than that of the co-current flow scheme at a particular dimensionless flow rate, especially in a high specific

membrane scale. In contrast, the differences of the average power density between the two flow schemes are not obvious, especially in the range of high average power density. Comparing the contour-line of average power density 3 and 5 W/m^2, the range of the dimensionless flow rate and the membrane scale are quite similar. At the dimensionless flow rate 0.2, the range of the average power density larger than $1W/m^2$ has a slightly wider validated specific membrane area in the counter-current PRO process. Therefore, from the perspective of the average power density, there is no obvious difference between the co-current and the counter-current flow scheme in the range of high average power density. Conversely, with the increase on the specific membrane scale, in the range of the low average power density, enhanced performance of the average power density can be achieved in the case of the counter-current flow scheme.

However, operating pressure and membrane usage in a PRO process are always concerned. A high pressure operation requires high performance membrane module with proper spacer, membrane property and design. And a large membrane usage significantly affects the capital investment and maintenance cost. Based on the map of specific extractable energy and average power density shown in Fig. 4.2, as a result, the PRO process can be possibly operated at a lower pressure with less membrane scale to achieve the same average power density if the loss of part of the specific extractable energy is acceptable. The appropriate operations can be selected along the contour lines of average power density in the range of lower hydraulic pressures and smaller specific membrane area.

Moreover, according to the results shown in Fig. 4.2, the most important influential factor to determine the specific extractable energy and average power density of a membrane module is the dimensionless flow rate. In Fig. 4.2, the most validated operations to achieve the economically viable average power density (≥ 5 W/m^2) is largest in the process with a dimensionless flow rate 0.2. In contrast, in the case of dimensionless flow rate 0.8, there is the smallest range of the preferred operations whose average power density is economically viable. And the maximum specific extractable energy is significantly large when the dimensionless flow rate is 0.2. Therefore, from the perspective of the salinity energy generation and the overall membrane performance in the membrane module, a low dimensionless flow rate is preferred.

4.4 INFLUENCE OF MEMBRANE PROPERTIES ON THE PERFORMANCE OF SCALE-UP PRO PROCESS

At the heart of the membrane process, membrane performance is always one of the hottest topics in the field. Previous studies have demonstrated that the enhanced PRO membrane performance was attributed to the high water permeability of the active layer coupled with a moderate salt permeability and the ability of the support layer to suppress the leakage of the salt into the porous support layer [58]. Several detailed studies on the membrane properties and the influences on a coupon-scale PRO process can be found in the literature [33, 58, 87]. However, the sensitivity analysis of the membrane properties has not been studied in the case of a scale-up PRO process. Therefore, in this section the performance of the scale-up PRO process with different membranes is presented.

4.4.1 Trade-off relationship between the water and solution permeability of PRO membrane

A systematic study to determine the permeability-selectivity trade-off relationship for the thin film TFC polyamide membranes can be found in [33]. According to their study, a trade-off relationship between the water and salt permeability coefficients of TFC polyamide membranes subject to chlorine-alkaline modification can be expressed as

$$B = \frac{L^{\beta}}{\lambda}\left(\frac{R_g T}{M_W}\right)^{\beta+1} A^{\beta+1} \tag{4.1}$$

where L is the thickness of the active layer, M_W is the molar mass of water, R_g is the gas constant, T is the absolute temperature, λ and β are the fitting empirical parameters. A set of the fitting parameters are obtained based on the data from publications on the hand-cast polyamide PRO membranes [33]. With this relationship between the permeability and selectivity of a TFC membrane, a number of permeability-selectivity paired coefficients can be obtained. The fitting parameters used are shown in Table 4.1. Other parameters include temperature 298 K, molar mass of water 18 g·mol^{-1}, and the gas constant 8.314 J·K^{-1}·mol^{-1}.

Table 4.1: Fitting parameters for the permeability-selectivity trade-off relationship of the TFC membrane [33].

Parameter	Value
β	2
λ	0.37×10^{-7} cm^4/s^2
L^{β}/λ	6.11×10^{-3} s^2/cm^2

4.4.2 Sensitivity analysis of membrane properties

As discussed in Chapter 2, on the basis of the permeability-selectivity trade-off of the TFC membrane properties, from recent literatures, membranes with satisfactory performance can be divided into low, medium and high permeable membrane according to the water permeability in the range of 1.42 – 7.76 L $m^{-2}{\cdot}h^{-1}bar^{-1}$ [33], as shown in Table 2.1. In addition, the range of the structural parameter, S, is also restricted by the types and functions of the membrane. Therefore, membrane with water permeability coefficient in the range of 0 to 8 L $m^{-2}{\cdot}h^{-1}bar^{-1}$ and the structural parameter of 10-10000 μm are selected to represent the possible membrane properties. According to the trade-off relationship represented by Equation (4.1), the corresponding membrane solute permeability coefficient is in the range of 0 to 6.29 L $m^{-2}{\cdot}h^{-1}$. Thus, on the basis of the selected range of the permeability, selectivity and structural parameter of the membrane, the sensitivity analysis of membrane properties on the performance of the scale-up PRO process can be carried out.

In order to achieve high average power density of the membrane which is close to the economic viability, based on the results in section 4.3, three specific membrane scales, 0.01, 0.5 and 0.1 $m^2/(L{\cdot}h^{-1})$, are selected. For simplicity, dimensionless flow rate 0.5 is selected and the results are shown in Figure 4.3 in which both the co-current and the counter-current flow schemes are presented in row (a) and (b), respectively. The optimum properties of the membrane properties achieving the maximum specific extractable energy and average power density at a particular structural parameter are presented by the dashed lines in all scaled-up PRO processes studied. According to the results, generally, the enhanced performance is attributed to the increased water permeability of the active layer coupled with a moderate salt permeability and the ability of the support layer to suppress the accumulation of the leakage salt. On the left of the dashed line, the increase on the membrane water permeability coefficient benefits the PRO process because it allows a higher volume of water permeation, and hence, the specific extractable energy increases to the maximum. In contrast, on the right of the dashed line, the salt leakage accumulated in the porous layer overwhelms any benefit from a higher water permeability membrane due to the inherent trade-off relationship.

Consequently, at a very small scale of the PRO process 0.01 $m^2/(L{\cdot}h^{-1})$, such as the coupon-scale or lab-scale PRO process, the dilution of the draw and the concentration of

the feed are not significant. Thus, the specific extractable energy between the co-current and the counter-current process are similar to the investigated peak power densities with the different membrane properties in [33]. Furthermore, with the increase on the specific membrane scale, different level of influences of membrane properties on the scaled-up process performance is observed. In both the co-current and the counter-current flow PRO processes, with the increase of the specific membrane scale, the maximum specific extractable energy occurs at a lower membrane water permeability coefficient especially in the range of low structural parameter. For example, in the co-current PRO process as shown in row (a), the maximum specific extractable energy profile (dashed line) occurs at a lower membrane permeability coefficient with the low structural parameter. The optimum membrane permeability represented by the dashed line is nearly 8 L m^{-2} $h^{-1}bar^{-1}$ in PRO scale 0.01 $m^2/(L\cdot h^{-1})$, is nearly 4 L m^{-2} $h^{-1}bar^{-1}$ in PRO scale 0.05 $m^2/(L\cdot h^{-1})$, and is slightly higher than 2 L m^{-2} $h^{-1}bar^{-1}$ in PRO scale 0.1 $m^2/(L\cdot h^{-1})$ at the structural parameter 10 µm. Similar trend has been also found in the counter-current flow scheme. This indicates that with the different specific membrane scale of the PRO process, the balance of the trade-off between the permeability and selectivity to achieve the maximum specific extractable energy varies. The detrimental effect of the RSP plays a more significant role with the increase on the specific membrane scale. And thus, the increased specific membrane scale requires the preferred membrane properties to move to the higher selectivity of the membrane to mitigate the solute leakage and to achieve the maximum specific extractable energy extraction. In addition, comparing the dependency of the membrane properties in the case of the two flow schemes, the membrane performance is also different. It is found that the maximum specific extractable energy profile occurs at slightly higher membrane permeability in the counter-current flow scheme. When the structural parameter is low, the preferred membrane permeability shifts to the high value obviously, as shown in Figure 4.3. This means that the ability to increase the specific extractable energy by enhancing the membrane permeability is better for the counter-current flow scheme. A higher reverse solute permeability coefficient is acceptable for the counter-current PRO process to access a higher permeable membrane. As a result, the counter-current flow scheme performs better than the co-current flow scheme and more specific extractable energy and average power density can be achieved in the counter-current flow schemes with the same salinity gradients by using a higher permeable membrane.

Additionally, from the perspective of development and selection of the high performance membrane in a scale-up PRO process, the requirements may be different from those for the maximum salinity energy extraction. First, due to the accompanying increase in the solute leakage, high permeable membrane is not always the better choice for the energy extraction when the scale of the process increases. For a large scale PRO process, a medium or a low permeable membrane may be more efficient in order to reduce the accumulated solute leakage. Furthermore, different flow schemes of the PRO process are suited to different membranes for the maximum specific extractable energy extraction. Therefore, for a specific flow scheme, the selection of the membrane should be considered.

Due to the accumulative reverse solute leakage, high permeable membrane may result in a poor performance in a scale-up PRO process, according to the specific extractable energy and average power density shown in Figure 4.3.

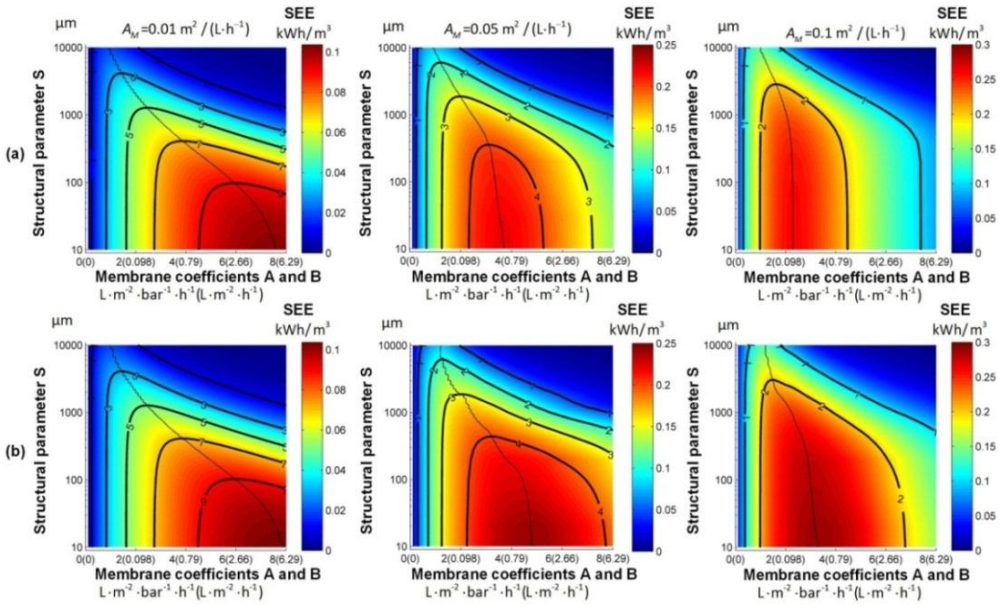

Figure 4.3:. Influence of membrane properties on the performance of the scale-up PRO process. Two flow schemes, co-current and counter-current, are shown in (a) and (b), respectively.

Moreover, there is no operation to meet the targeted economically viable average power density (5 W/m^2) in specific membrane scale 0.05 and 0.1 $m^2/(L{\cdot}h^{-1})$. Does it mean the technology is difficult to scale-up? Actually, Equation (4.1) and the fitting parameters shown in Table 4.1 to describe the trade-off permeability-selectivity of membrane are an empirical correlation and parameters. These empirical correlations are built up mainly based on membrane developed no later than 2011. Recently, with the rapid development

of the high performance membrane, the trade-off permeability-selectivity of the membrane has been considerably improved. However, in order to meet the economic viability, how much improvement do we need? An analysis is presented in this section to find a solution.

Therefore, a series of the PRO processes with different membranes and operating conditions are studied. It includes the ideal PRO process that has no CP or RSP, and the PRO process using different membranes. Generally, the goal for an ideal membrane should have maximum water permeability, minimum solute permeability and minimum structural parameter [70]. For current membranes, if the selectivity of the membrane can be improved with no loss on the water permeability, the performance of the scale-up PRO process can be enhanced and shifts the economically viable PRO towards the larger specific membrane scale. Therefore, four virtual membranes are selected to represent the further improvement on the membrane. The virtual membranes have 0%, 10%, 30% and 50% of the solute permeability coefficient based on the trade-off permeability-selectivity relationship represented by Equation (4.1). In other words, with the same water permeability of the membrane, the selectivity is improved at different levels for the four virtual membranes. In addition, two specific membrane scales, 0.05 $m^2/(L\cdot h^{-1})$ and 0.1 $m^2/(L\cdot h^{-1})$, are selected for the simulation. For convenience, only the performance of the co-current PRO process is illustrated. The results are shown in Figure 4.4 in which several figures are shown with respect to the performance of the PRO process with different membranes and operating conditions. The specific extractable energy and average power density are represented in colour-map and contour-line, respectively. The dimensionless flow rate is 0.5.

The results of I-PRO modelling without the CP or RSP indicate the limiting performance of the specific extractable energy and average power density in the PRO processes of the selected two scales. From the results shown in Figure 4.2, it is found that the specific membrane scale significantly affect the average power density. The economic viability of the membrane can only be achieved at a small specific membrane scale. However, as indicated earlier, the specific extractable energy is increased when more membrane is used in PRO process. As shown in I-PRO modelling, the maximum specific extractable energy of the PRO process with specific membrane scale 0.1 $m^2/(L\cdot h^{-1})$ is slightly higher than that with the small scale 0.05 $m^2/(L\cdot h^{-1})$. In fact, the rapid reduction on the average power

density along with the increase in the membrane scale is due to significantly reduced efficiency of the mass transfer. The maximum water flux occurs at the inlet and reduces rapidly along the membrane channel. As a result, the limiting maximum average power density is significantly decreased when the scale of the PRO process increases. The limiting maximum average power density is only 3.1821 W/m^2 in PRO of specific membrane area 0.1 $m^2/(L \cdot h^{-1})$. This means that the economic viability of power density can never be achieved in this configuration with the selected salinities.

Comparing the results of PRO process with different membrane solute permeability coefficients, the effect of the accumulated solute leakage on the different scale of the PRO can be evaluated. If there is no RSP in which membrane with zero solute permeability coefficient, the higher permeable membrane results in better performance of PRO process at a particular structural parameter. However, the CP effects cause significant reduction in the overall performance of the scale-up PRO process. Especially in the PRO process using high permeable membrane, the maximum average power density reduces rapidly with the increase in the structural parameter. Furthermore, compared to the remaining results shown in Figure 4.3, the overall performance of the scale-up PRO process with the less membrane permeability coefficient is improved. Generally, a large solute permeability has two negative impacts on the performance: it reduces the peak water flux at the inlet and accelerates the solute leakage from the draw to the feed along the flow channel. In such a case, a low peak water flux occurs at the inlet and declines very fast due to the increasing feed concentration. Thus, due to the rapidly reducing net driving force across the membrane, the water permeation is significantly decreased compared to the I-PRO. As a result, both the specific extractable energy and average power density are reduced with the increase in the solute permeability.

In fact, for a scale-up PRO process, in order to meet the economically viable power density, a complex issue needs to be addressed. On one hand, for maximizing the specific extractable energy, the scale of PRO process should be increased to reach the maximum water permeation from the draw to the feed. On the other hand, the increasing scale significantly reduces the economic viability of the membrane. Thus an optimum specific membrane scale for PRO process is constrained for the economic viability.

	Ideal PRO without CP or RSP	0% of solute permeability coefficient B	10% of solute permeability coefficient B	30% of solute permeability coefficient B	50% of solute permeability coefficient B
A_M^1	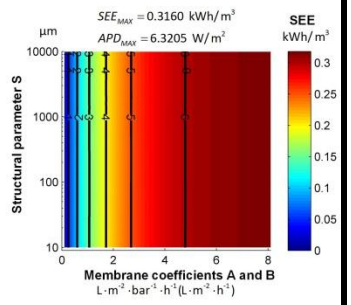	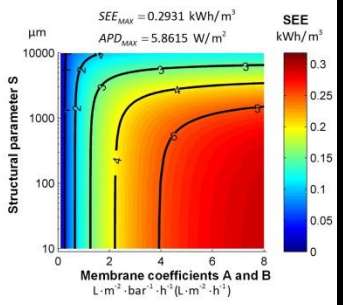	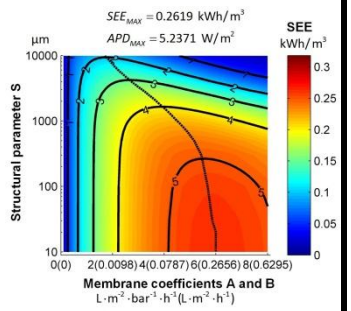	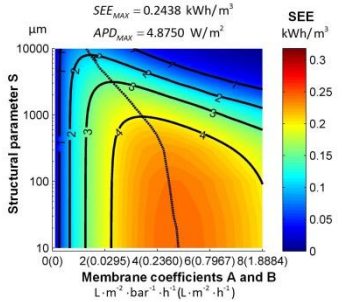	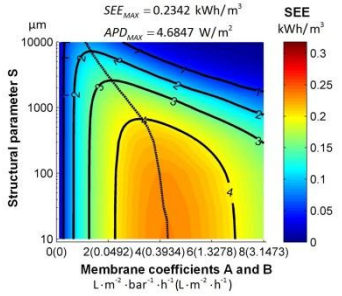
A_M^2	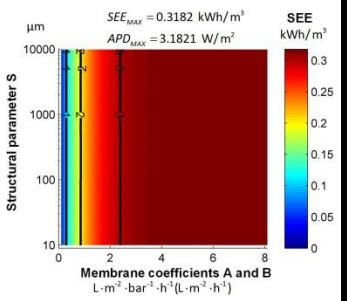	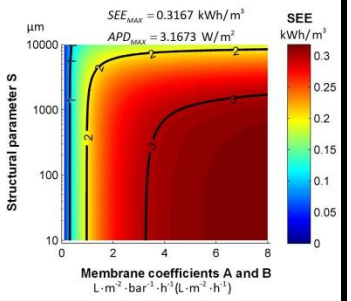	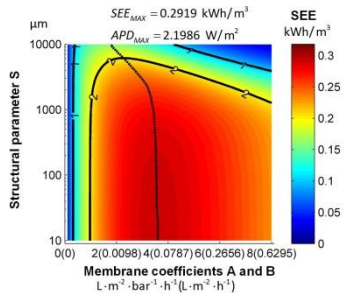	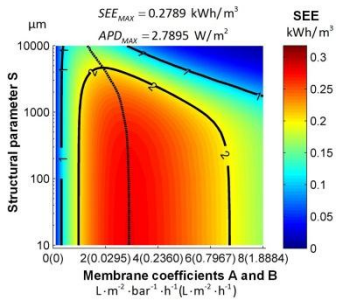	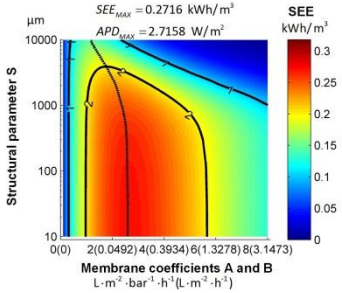

Figure 4.4: Membrane sensitivity and process characteristics of co-current PRO. A_M^1 and A_M^2 are the selected specific membrane scales which are 0.05 and 0.1 $m^2/(L \cdot h^{-1})$, respectively.

Moreover, in addition to other influential factors, such as hydraulic efficiency of the components, the membrane properties have an important influence on the optimum scale. At a particular specific membrane scale, a high water permeability membrane is necessary to achieve a high average power density. However, simultaneously, high solute permeability is often accompanied. The reverse solute leakage significantly decreases the maximum average power density of a PRO process. If the maximum average power density is less than the economically viable power density, the membrane scale should be further decreased for the higher average power density. Therefore, the better membrane used in PRO process, with very high water permeability, very low solute permeability and structural parameter, the larger scale of the process meeting the economic viability can be achieved. For example, as shown in Figure 4.4, under the selected flow conditions and salinities, the maximum average power density of the PRO with specific membrane scale 0.05 $m^2/(L \cdot h^{-1})$ is 5.2371, 4.8750 and 4.6847 W/m^2 for the three membranes with 10%, 30% and 50% of the solute permeability based on the trade-off relation represented by Equation (4.1). It indicates that the economic viability of the PRO process using the membrane with 10% of the solute permeability can be achieved in the specific membrane scale 0.05 $m^2/(L \cdot h^{-1})$. In contrast, using another two membranes, the specific membrane scale needs to be further reduced to meet the economically viable power density. Therefore, the economic viability is an overall result of the specific membrane scale, membrane properties, and conditions of salinities and flows.

Furthermore, the analysis and discussion above is on the basis of the constant membrane properties with respect to different operating conditions. In fact, from literatures, it is reported that the membrane permeability-selectivity significantly decreased when a high pressure is applied on the draw solution, due to the membrane deformation [70]. Also, in a long-term operation, membrane fouling results in the reduction on the membrane permeability. Several recovery strategies, such as backwashing, need to be adopted. These potential detrimental effects on the membrane further reduce the performance of the scale-up PRO process and increase the economic cost [112]. Therefore, in order to achieve the economic viability, further improvement on the membrane performance still needs to be investigated.

4.5 INFLUENCE OF PROCESS COMPONENTS EFFICIENCIES ON THE PERFORMANCE OF THE SCALE-UP PRO PROCESS

In the simulations of the scaled-up PRO process above, the performance is evaluated from the membrane module level, the inefficiencies of the process components are not considered. The HP, ERD and HT are all considered with 100% efficiency. However, in real applications, the energy losses in these components have a significant impact on the performance of the process. The efficiencies of the HP, ERD and HT are represented by η_{HP}, η_{ERD} and η_{HT}. Therefore, considering these machines' inefficiencies, the average power density of a PRO process can be changed to

$$e_{C-PRO}^{Eff} = \frac{\Delta P_{PRO} \Delta V_P \eta_{HT} - V_D^0 \Delta P_{PRO} (1-\eta_{ERD}) / \eta_{HP}}{A_M} \tag{4.2}$$

For simplicity, with the negligible change on the density of the water during the PRO process, the ratio of the volumetric rates can be represented by the dimensionless flow rate, ϕ. Accordingly, the average power density of the PRO process considering the inefficiencies can be further written as

$$e_{C-PRO}^{Eff} = e_{C-PRO}\eta_{HT} - \frac{(1-\phi)\Delta P_{PRO}(1-\eta_{ERD})V_F^0}{A_M \phi \eta_{HP}} \tag{4.3}$$

where e_{C-PRO} is average power density of PRO with 100% efficiency components.

According to Equation (4.3), it indicates the energy losses due to the inefficient machines can be divided into two main categories: energy loss in the salinity energy generation by HT which is considered by $e_{C-PRO}\eta_{HT}$, and energy loss in pressurizing the draw solution by ERD and HP which presented by the second part in Equation (4.3).

At the early stage for a preliminary analysis of the scale-up PRO process, for simplicity, constant efficiencies of the machines are assumed. Therefore, several sets of the possible efficiencies of the components are selected for further study, which are listed in Table 4.2 to represent the different components operated at the possible conditions (EFF1-EFF8) and an ideal condition (EFF9). The influence of the inefficiencies of the components is studied in the scaled-up PRO process in terms of the average power density considering different specific membrane area. In the simulation, due to the unchanged initial flow rate of the

feed solution, the specific extractable energy can be estimated based on the average power density and the specific membrane scale. Three dimensionless flow rates are selected for representing the low, medium and high dimensionless flow rates. The membrane properties are the same to the membrane used in Section 4.3. First the co-current flow scheme is considered.

TABLE 4.2 Selected sets of the components for the analysis of the machines' efficiencies.

Efficiency NO	**EFF1**	**EFF2**	**EFF3**	**EFF4**	**EFF5**	**EFF6**	**EFF7**	**EFF8**	**EFF9**
Efficiency of HP	70%	70%	70%	80%	90%	70%	70%	90%	100%
Efficiency of HT	80%	80%	80%	80%	80%	85%	90%	90%	100%
Efficiency of ERD	98%	95%	90%	90%	90%	90%	90%	98%	100%

The results are shown in Fig. 4.5 in which the nine sets of the machines are evaluated. The results clearly indicate that the hydraulic energy losses play a significant role in the PRO process. Theoretically, with the ideal machines (EFF9), because there is no energy loss of the pressurization, the maximum average power density of a PRO process with a particular dimensionless flow rate should be achieved at the infinite small membrane area and is close to its peak power density as shown in Fig. 4.5(l). It is due to the maximum specific extractable energy achieved when a small amount of the feed solution mixed with the infinite draw solution in the level of the membrane module, namely at low dimensionless flow rate. As shown in Fig. 4.2, the maximum average power density is located at the low dimensionless flow rate and low specific membrane scale. However, when the inefficiencies of the pressurization and expansion are considered in the system level, these hypothetical conclusions of the theoretical optimum cannot be realized in practice as illustrated in Fig. 4.5(a) – 4.5(h). For example, as shown in Fig. 4.5(h), although highly efficient machines are used, the average power density characteristic of scale-up PRO process is significantly changed.

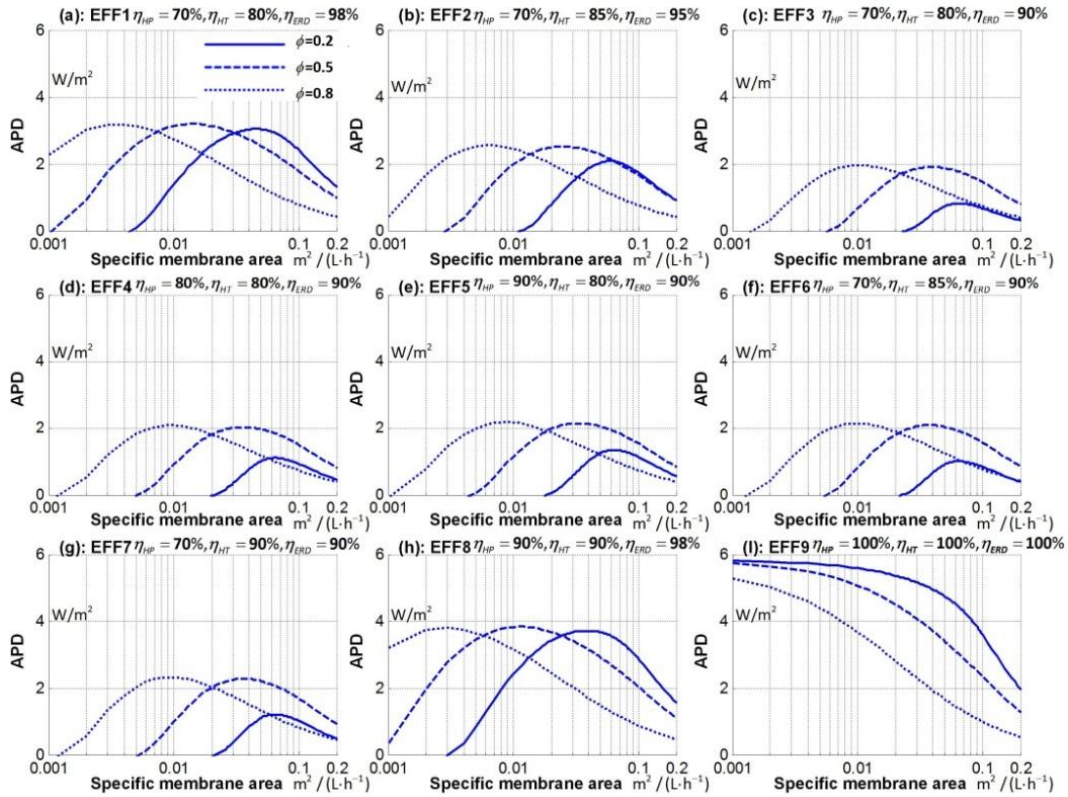

Figure 4.5 Influence of the inefficiencies of the HP, ERD and HT on the scaled-up PRO process. Results of nine sets of machines with different efficiencies are shown (a)-(I), respectively.

At a small membrane scale PRO process with a low dimensionless flow rate, the flow rate of the draw solution is relatively bigger than the flow rate of the feed solution. Although high average power densities can be achieved in the membrane module level at a low dimensionless flow rate, it reduces significantly considering the energy losses in the pressurization components in the system level. It is a result of the high flow rate of the draw solution being pumped and pressurized. Actually, at the small dimensionless flow rate, the energy loss during pumping and pressurizing the large volume of the draw solution overwhelms the salinity energy extracted from the permeation. Especially in the PRO at small specific membrane area, because of the limited salinity energy generated (limited specific extractable energy at the small specific membrane area as shown in Fig. 4.2), average power density is significantly decreased. According to the results shown in Fig. 4.5(a) – 4.5(h), by using the set of components without 100% efficiencies, significantly reduced average power densities are observed in all cases at the small specific membrane area. And with the increase on the inefficiency of the machines, the reductions of the specific membrane area are enlarged and the maximum of the average power densities move to a large specific membrane area.

Furthermore, with the increase on the dimensionless flow rate, although average power densities are reduced in the membrane module level, energy losses are also decreased due to the low flow rate of the draw solution. As a result, the overall average power density might be higher than that with a lower dimensionless flow rate. As shown in Fig. 4.5, it clearly indicates that the average power densities of the PRO at the dimensionless flow rate 0.2 change significantly from (a) – (h) compared to those at the dimensionless flow rate 0.5 or 0.8. Due to the significantly decreased performance of the PRO at the low dimensionless flow rate, the PRO process with higher dimensionless flow rate, such as 0.5, shows better performance of the membrane in terms of average power density at several studied cases. For example in Fig. 4.5(c), 4.5(d), 4.5(e), 4.5(f) and 4.5(g), the average power densities of PRO with dimensionless flow rate 0.5 are larger than those with dimensionless flow rate 0.2. Thus, the optimum operation is shifted to a higher dimensionless flow rate. Furthermore, comparing the average power densities of the PRO at dimensionless flow rate 0.5 and 0.8, it is found that the maximum average power densities of the two operating conditions are similar in the study cases as shown in Fig. 4.5(a) – 4.5(h) but the optimum specific membrane areas are smaller for the scale-up PRO with the dimensionless flow rate 0.8.

In addition, compared the three machines considered, HT, HP and ERD, the efficiency of ERD is more sensitive to the performance of the PRO process. It is due to the fact that the pressurization of the initial draw solution is mainly done by the ERD by recycling the hydraulic energy of the brine and only the extra energy consumed by HP to cover the energy loss in the recycling due to the inefficiency of ERD. As shown in Fig. 4.5(a), 4.5(b) and 4.5(c), with the efficiency of ERD reduced from 98% to 95% and 90%, significant reductions of average power density are found in all three operating conditions. However, according to the results of different HPs which are shown in Fig. 4.5(c), 4.5(d) and 4.5(e) and the results of different HTs which are shown in 4.5(c), 4.5(f) and 4.5(g), changes on the average power density are less obvious.

Results shown in Fig. 4.5 are based on co-current flow scheme. Comparison between the two flow schemes are shown in Fig. 4.6 in which two sets of efficiencies are selected. The results show the increasingly preferred performance of the counter-current flow scheme when the specific membrane area increases. It is a result of the enhanced performance of the counter-current flow as shown in Fig. 4.2 to increase the salinity energy generation in the first part of Equation (4.3).

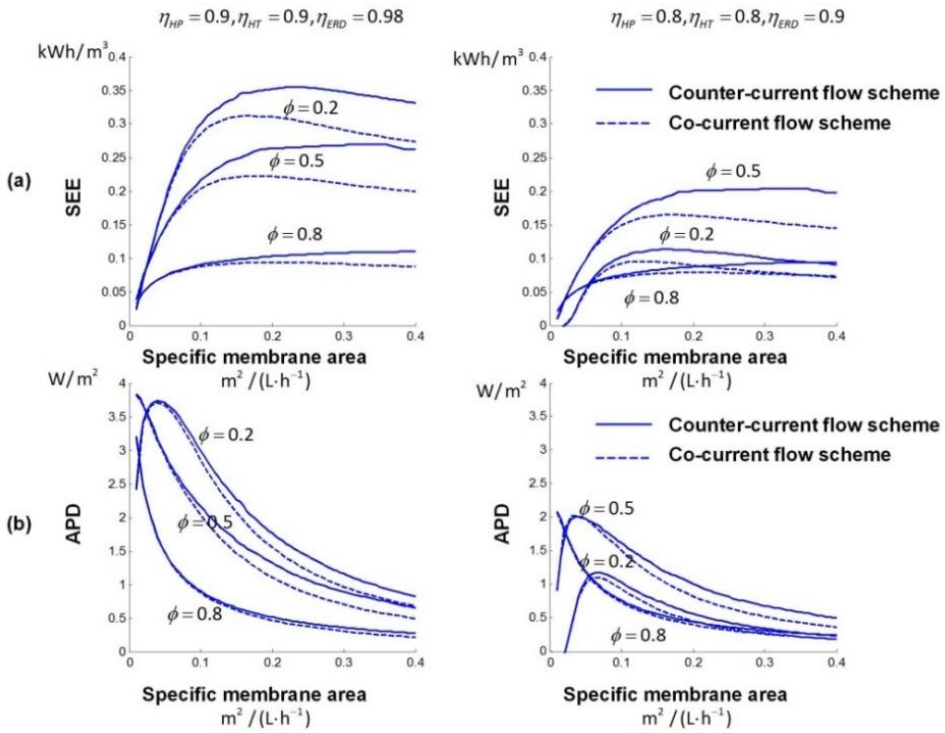

Figure 4.6: Influence of the inefficiencies of the HP, ERD and HT on the scale-up PRO process in different dimensionless flow rates. Two flow schemes, co-current and counter-current, are shown in (a) and (b), respectively.

4.6 SUMMARY

A systematic evaluation and comparison between the co-current and the counter-current scaled-up PRO process is developed as described in this chapter. The significant operating conditions and design parameters of a scaled-up PRO process are investigated. It includes the hydraulic pressure applied on the draw solution, the initial flow rates of the draw and the feed solution, the permeability and selectivity of the membrane, structural parameter, and the inefficiencies of the process components such as HP, ERD and HT. On the basis of the results, some conclusions can be drawn: 1) dimensionless flow rate has an important role in the performance of the scaled-up PRO process in terms of both the specific extractable energy and the average power density in the membrane module level. At a particular dimensionless flow rate, the process performance between the co-current and the counter-current flow scheme is not significantly different in high average power density operations; 2) In a scaled-up PRO process, with the increase on the specific membrane scale, the detrimental effect of the RSP becomes significant. The accumulated solute leakage shifts the maximum specific extractable energy occurring at the lower membrane permeability in a larger scale PRO process. The ability to increase the specific extractable

energy by enhancing the membrane permeability is better in the case of the counter-current flow PRO process.; 3) The machines' inefficiencies drive the maximum average power density occurring at a higher dimensionless flow rate to reduce the energy losses in pumping and pressurisation and a higher specific membrane scale to increase the salinity energy generation. The energy losses caused by the inefficiencies shrunk the salinity energy generation, especially at the small dimensionless flow in a small scale process.

MAXIMUM POWER POINT TRACKING (MPPT) OF A SCALE-UP PRESSURE RETARDED OSMOSIS (PRO) OSMOTIC POWER PLANT

5.1 INTRODUCTION

On the basis of the increasing development on the scale-up PRO plant, it has been demonstrated that the overall performance of a scale-up PRO considering the detrimental effects can be estimated by numerical modelling. The understanding of the process dynamics of PRO has also become clearer and deeper. However, in real applications, disturbances, fluctuations and degradation of the components and process are also unavoidable. For example, due to the seasonal rainfalls, the concentration of both sea water and river water may fluctuate. It is reported that at a particular location in central San Joaquin Valley, the total dissolved solids content deviated up to 52% from its annual

average [113]. Also in future as a stand-alone renewable energy generator or a part of hybrid energy generation, time-dependent strategy for bidding in market may need to change the PRO operation from state to state subject to the electricity price. In addition, the degradation of the membrane performance according to membrane fouling and the backwash and maintenance also affect the performance of the PRO salinity energy generation. Therefore, a maximum power point tracking (MPPT) control to extract maximum power from the PRO plant at each sample instant of real time becomes indispensable in salinity energy generation.

An investigation on the development of MPPT controller for scale-up PRO osmotic power plant is presented in this chapter. First, the characteristics of the scale-up PRO plant is studied and the performance curve of flow rate and pressure ($\Delta V - \Delta P$) and curve of power output of pressure ($W - \Delta P$) are investigated subject to different operational conditions and initial salinity conditions. Based on the process characteristics, two MPPT controllers based on P&O and INC-like algorithms are developed and tested by simulation. Furthermore, in order to improve the performance of the MPPT controllers, an optimum model-based controller is developed to select an appropriate initial operating pressure. And a strategy to operate and coordinate the MPPT and OMC subject to the rapid changes of the salinities is proposed. Finally, the improvements of the strategy are evaluated by simulations.

5.2 CHARACTERISTICS OF A SCALE-UP PRO SALINITY POWER PLANT

5.2.1 Mathematical model of PRO

As discussed in previous chapter, in a PRO plant, the membrane power density is determined by the trans-membrane hydraulic pressure and the water permeation flux across the membrane [56] and the overall performance is evaluated by integrating the water flux and power density over the entire membrane used. The modelling framework of the scale-up PRO can be found in Chapter 2.

5.2.2 $\Delta V - \Delta P$ and $W - \Delta P$ characteristics

The non-linear nature of PRO systems is apparent from its mathematical model. Also, the performance depends on a large number of influential factors, such as membrane performance, salinity conditions, process configuration, operating condition and

efficiencies of components. The complex relationship between the membrane, operating condition and salinities results in highly non-linear permeation-pressure characteristics. In this section, the complex power output characteristics are studied in different conditions by simulation.

- **MEMBRANE PROPERTY**

Due to the permeability-selectivity trade-off relationship, high permeability always results in low selectivity of the membrane. Several recent high performance membranes specifically for PRO have been found in literature and are listed in Table 5.1. In Table 5.1, membranes, from M1 to M6, are fabricated membranes as reported in the recent literature and membrane M7 is a virtual membrane. The virtual membrane properties are assumed by Prante et al. to evaluate the membrane sensitivity on the overall performance of the PRO osmotic energy harvest for estimating the further improvement on the overall performance [69]. The virtual membrane, in fact, can be used to approximately identify the limiting performance with the ideal membrane.

The overall performance of a scale-up PRO plant with the membranes listed in Table 5.1 is evaluated by simulation. The results of the permeation and the specific extractable energy of a PRO plant are shown in Figure 5.1. In the simulation, concentration of the draw solution and the feed solution are 35 g/kg and 0.1 g/kg, respectively. The dimensionless flow rate is assumed to be 0.5 in this section. The specific membrane area is 0.1 m^2 per 1 L/h feed solution. The other parameters are same to those used in Chapter 3 and 4. The efficiency of the pressurization components in a PRO process, including HP, ERD and HT, are considered as 100%.

The results shown in Figure 5.1, clearly indicate that the membrane properties have a significant influence on $\Delta V - \Delta P$ and $W - \Delta P$ characteristics of PRO. The specific influence on the PRO process with respect to the membrane permeability, selectivity or structural parameter is not the topic of this chapter and it can be found in previous chapters focusing on the high performance membrane development. The results shown in Figure 5.1 are theoretical performance at constant temperature without no membrane deformation and fouling. In fact, the fluctuation of the temperature affects the permeability and selectivity of the membrane [67]. Anastasio et al. reported that the permeability coefficients of water and solute increase from 0.589 L/(m^2·bar·h) and 0.319 L/(m^2·h) to 1.12 L/(m^2·bar·h) and

0.580 L/(m^2·h) respectively, when the temperature of the draw solution increases from 20 ^{0}C to 40 ^{0}C [114]. In addition, membrane properties may vary with respect to the hydraulic pressure on the draw solution due to the membrane deformation [31, 115]. Wan et al. tested a TFC membrane from 5 bar to 20 bar at an increment of 5 bar and found that the water permeability was at a constant 3.5 L/(m^2·bar·h) while the salt permeability increased monotonically from 0.28 L/(m^2·h) at 5 bar to 0.36 L/(m^2·h) at 20 bar [116]. Therefore, for real applications, different membrane results in different process characteristics of PRO. Furthermore, the fluctuations and the uncertainty of the membrane condition make it difficult to predict the optimum performance and track the MPP of the process.

Table 5.1: Selected membrane properties from recent publications.

NO	Publications	A [L/(m^2·bar·h)]	B [L/(m^2·h)]	S [μm]
M1	[117]	2.5	0.9	405
M2	[118]	3.12	0.55	1022
M3	[70]	5.11	0.087	310
M4	[119]	4.3	0.47	640
M5	[108]	4.1	1.74	150
M6	[99]	3.32	0.14	460
M7	[69]	67.32	0.04	6.87

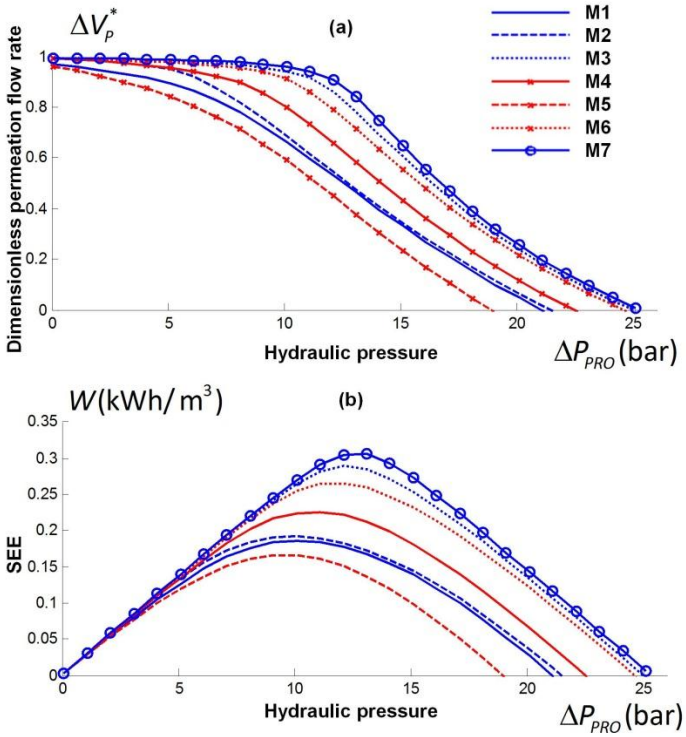

Figure 5.1: The permeation-pressure ($\Delta V_P^* - \Delta P$) and the specific extractable energy-pressure ($W - \Delta P$) characteristic curves of the PRO plant subject to different membrane properties

- **CONCENTRATIONS OF SALINITY AND DIMENSIONLESS FLOW RATE**

Due to the seasonal rainfalls, the concentration of the natural salinities may fluctuate both for seawater and river water. The example in the central San Joaquin Valley indicates significant fluctuations of the concentration [113]. In addition, for hybrid RO-PRO plant, if the brine from RO is used as the draw solution for PRO, the concentration of the draw is determined by the operation of RO. With different water recovery ratio achieved in RO, the brine with different concentration and rate flows into PRO. Similarly, due to the seasonal rainfalls and the changes in the salinities source, the available volumes of the two salinity gradients may change. Moreover, for maximizing the efficiency of using the feed solution, such as river water, the flow rate can be adjusted by changing the resistance of the valves. As a result, the process characteristic curves of the PRO process also change with respect to these variations.

The variation in $\Delta V - \Delta P$ and $W - \Delta P$ characteristics of the PRO are shown in Figure 5.2. In Figure 5.2(a) and 5.2(b), four dimensionless flow rates are selected for different flow rates from the low to the high dimensionless flow rate. And in Figure 5.2(c) and 5.2(d), three salinities are chosen, representing the seawater to the concentrated brine. The results clearly indicate the influences of the salinities on the performance of the PRO process. In addition, it is noted that the variation of these two profiles are different with respect to different variables. And due to highly non-linear mass transfer and osmotic energy extraction in PRO, the performance varies significantly when the changing variable is different. However, a MPP can be found in each condition demonstrated in Figure 5.2(b) and 5.2(d).

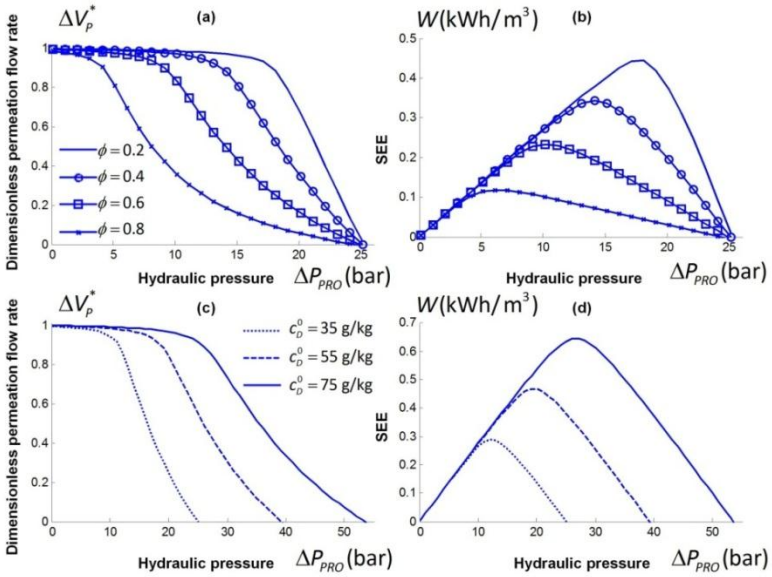

Figure 5.2: The permeation-pressure ($\Delta V_P^* - \Delta P$) and the specific extractable energy-pressure ($W - \Delta P$) characteristic curves of the PRO plant subject to different concentration and flow rate of the salinities.

5.3 MPPT FOR PRO

As shown in Section 5.2, many influential factors affect the osmotic energy extraction of the PRO process. The aim of employing MPPT is to ensure that at any operational condition, maximum power is extracted from the PRO plant. Similar to the conventional MPPT of solar PV that operates by sensing the current and voltage, MPPT of a PRO is achieved by changing the applied pressure on the draw solution based on the measurement of the osmotic power output. An illustrated diagram of the MPPT controller is shown in Figure 5.3. The MPPT evaluates the osmotic power generated by the HT and adjust the applied hydraulic pressure on the draw solution. The pressure transition can be achieved by using the variable frequency drive to change the speed of the HP [120]. This study aims to investigate the MPPT performance by simulation. Thus, at the early stage, the algorithm of the MPPT is considered with the available measured osmotic power output. And the targeted pressure can be actuated on the draw solution by a fast and stable controller.

In this investigation, two general methods, P&O and incremental mass-resistance (IMR), are applied for the MPPT of PRO. These two methods are extensively utilised in MPPT of solar PV in which IMR is an INC-like method. They can be classified into online methods, also known as model-free methods, in which, usually, the instantaneous values of measured variable are used to generate control signals.

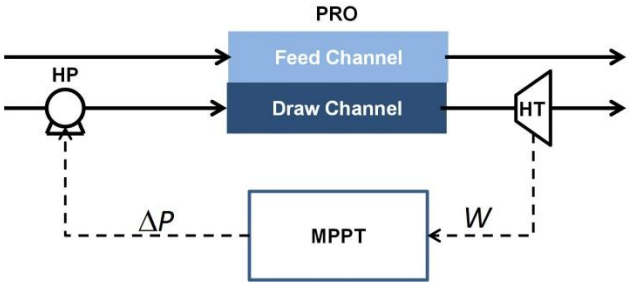

Figure 5.3: Schematic diagram of MPPT in PRO.

5.3.1 Perturb & observe (P&O) method

P&O can be implemented by applying perturbation to the reference hydraulic pressure applied on the draw solution. A flowchart illustrating this method is depicted in Figure 5.4, where pressure is the reference signal. Therefore, the goal of this algorithm involves pushing the reference pressure signal towards MPP thereby causing the instantaneous pressure to track the MPP. As a result, the output power will approach MPP. To this end, a small but constant perturbation is applied to the hydraulic pressure, which is "C" in the flowchart.

The hydraulic pressure is changed by applying a series of small and constant perturbations denoted by (C=ΔP) on a step-by-step basis in order to change the operating point of the PRO process. Following each perturbation, the output osmotic power variation (ΔW) is measured. If ΔW is positive, osmotic power will approach the MPP, therefore, a hydraulic pressure perturbation of the same sign must be applied in the following stage. A negative ΔW, on the other hand, implies that osmotic power has shifted away from the MPP, and a perturbation of opposite sign will have to be applied. This repeating process is stopped until the MPP is reached.

The MPPT using P&O algorithm has two main drawbacks. First, the selection of the perturbation applied to the system determines the oscillations as well as the convergence of the tracking. Larger perturbation results in faster tracking MPP but with larger oscillation as well. If the applied perturbation is too small, on the other hand, the oscillation around MPP will be reduced, but the rate of the convergence reduces. Therefore, inherent trade-off between the oscillation and the response rate exists in this algorithm. In addition, P&O is prone to tracking errors if the operating point changes quickly.

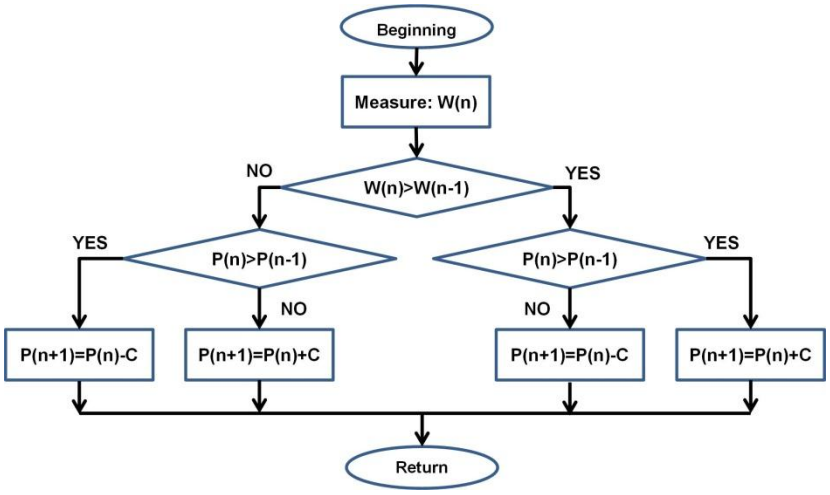

Figure 5.4: Flowchart of MPPT using P&O algorithm.

5.3.2 Incremental mass-resistance (IMR) method

The INC method in MPPT of PV employs the slope of the PV array power characteristics to track MPP. Similarly, in PRO, this method is also on the basis of the fact that the slope of the specific extractable energy curve is zero at the MPP, positive for values of the specific extractable energy smaller than the MPP, and negative for values of the specific extractable energy greater than the MPP.

The maximum specific extractable energy, $w_{MPP} = \Delta P_{MPP} \Delta V_{MPP}$, is achieved by differentiating the specific extractable energy with respect to hydraulic pressure and setting the result to zero. Accordingly, the relation of the deviations of the pressure and the permeation can be obtained, which is

$$dV / dP \cong \Delta V / \Delta P = -V_{MPP} / P_{MPP} \qquad \text{at MPP when } dW / dP = 0 \tag{5.1}$$

Therefore, by evaluating the derivative one can test whether the PRO is operating at or near or far away from the MPP. The strategy of the evaluation is shown below,

$$\begin{aligned} dV/dP = 0 &\longrightarrow \Delta V/\Delta P = -V/P \longrightarrow \text{At MPP} \\ dV/dP > 0 &\longrightarrow \Delta V/\Delta P > -V/P \longrightarrow \text{Left of MPP} \\ dV/dP < 0 &\longrightarrow \Delta V/\Delta P < -V/P \longrightarrow \text{Right of MPP} \end{aligned} \tag{5.2}$$

In the INC method, the conductance of the PV array is represented by “I/V”. Compared to that, a similar concept of “mass-resistance” is defined as “V/P” and used in the MPPT of PRO. As a result, the MPP can be tracked by comparing the instantaneous mass-resistance

("V/P") to incremental mass-resistance ($\Delta V / \Delta P$) as shown in Figure 5.5. And it is proposed to call the method incremental mass-resistance method. In Figure 5.5, the hydraulic pressure is the reference variable at which the PRO is ensured to operate. At the MPP, referencing pressure equals to P_{MPP}. In the algorithm, a parameter ε_{IMR} is used to control the tolerance of the convergence. The large tolerance results in mitigated oscillation. Once the MPP is reached, the operation of the PRO is maintained at this point unless a change in permeation occurs as a result of a change in operating condition leading to MPP transition. The algorithm, then, tracks the MPP by applying decrement or increment. A constant deviation of the referencing pressure is illustrated in Figure 5.5. Therefore, fast tracking can be achieved by applying larger increments, but the system may not operate stably at the MPP and oscillation around the MPP may result. Similar trade-off between the convergence speed and the oscillation is also involved in IMR.

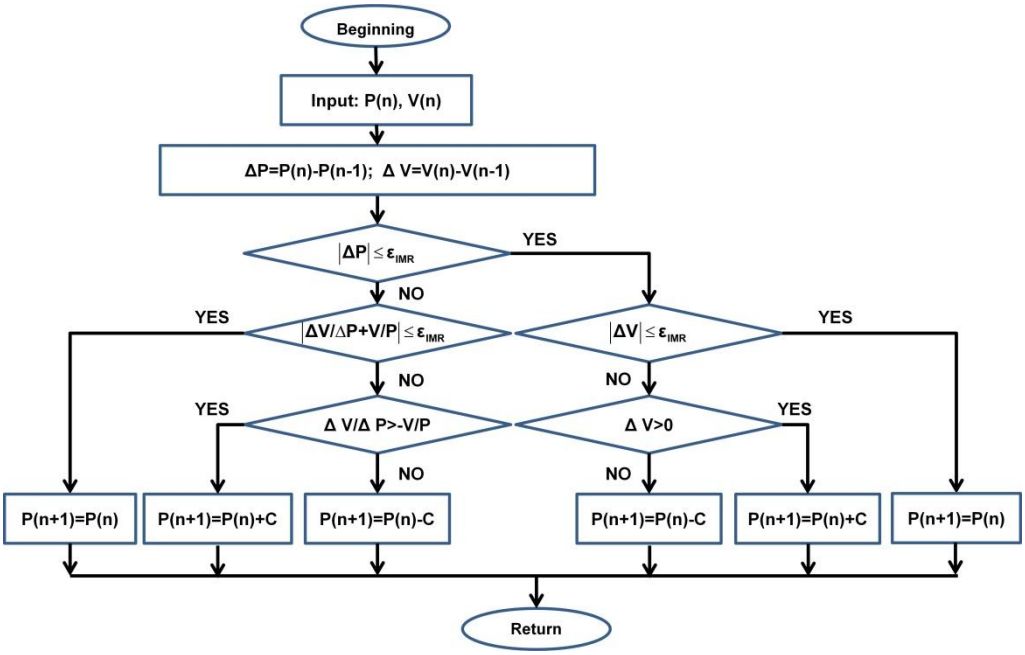

Figure 5.5: Flowchart of IMR algorithm.

5.3.3 Simulation and results

The two methods, P&O and IMR, are tested in MPPT of a PRO process by simulation. MPPT aims to track the MPP without any information of the PRO plant. The initial pressure is set to be 1 bar. And several step-sizes of the perturbation and increment are studied. The MPPT applies the initial hydraulic pressure on the draw solution, and adjusts the pressure depending on the measured osmotic power output. As shown in Figure 5.3, the

performance of the PRO plant is obtained by simulation on the basis of the model derived in Chapter 2. Membrane M3 is selected for the simulation of the PRO plant because of its high performance. And other parameters are same to the parameters used in Section 5.2.2.

The results of the osmotic power output with MPPT using P&O and IMR are presented in Figure 5.6. Three step-sizes of the perturbation and pressure increment, 2, 1 and 0.5 bar, are studied and the results are presented in Figure 5.6(a), 5.6(b) and 5.6(c), respectively. For the IMR methods using the three increments, the values of ε_{IMR} are set as 1×10^{-2}, 1×10^{-2} and 1×10^{-3}, respectively. The results in literature suggested that the transition from one steady state to another steady state for RO process changes in different process scales. Bartman et al. changed the flow rate within a wide range of operation less than ~1 min in UCLA experimental RO membrane water desalination system [121]. Sassi et al. pointed out that pseudo steady-state model of RO can be assumed for time steps more than 0.25 h [122]. For PRO, no literature studying the transition between the operations is reported. But due to the inherent similarity to RO desalination plant, the range of the transition time can be estimated. In this chapter, a general sample instant is used for representing the sensing period at the early stage.

The results clearly indicate that the performance of both the methods is parameter dependent. With the larger step-size of the perturbation and increment, a faster convergence of the MPPT is achieved. In Figure 5.6(a), both the MPPT approach near to MPP within 10 sample instants. In contrast, for finer step-sizes, 1 and 0.5 bar, the required numbers of sample instants to near the MPP are approximately 10 and 20, respectively. Furthermore, comparing the results of P&O and IMR, it is found that the convergence of IMR is better than P&O. The oscillations in all the three tested cases are significantly mitigated compared to the results of P&O. In this study, P&O method has only one manipulated parameter, perturbation on pressure, to control the MPPT. The oscillation of the PRO plant close to the MPP increases when the perturbation of the hydraulic pressure is large. As shown in Figure 5.6, from (a) to (c), the oscillation reduces significantly with the decrease on the perturbation. In contrast, two parameters, increment and parameter ε_{IMR}, are used in IMR to control the performance. The parameter ε_{IMR} changes the tolerance of the convergence and manipulates the oscillation. The control of the convergence makes the IMR flexible in MPPT. If a particular deviation of the MPP is acceptable, the stability of the MPPT might be improved by adjusting the parameter ε_{IMR}.

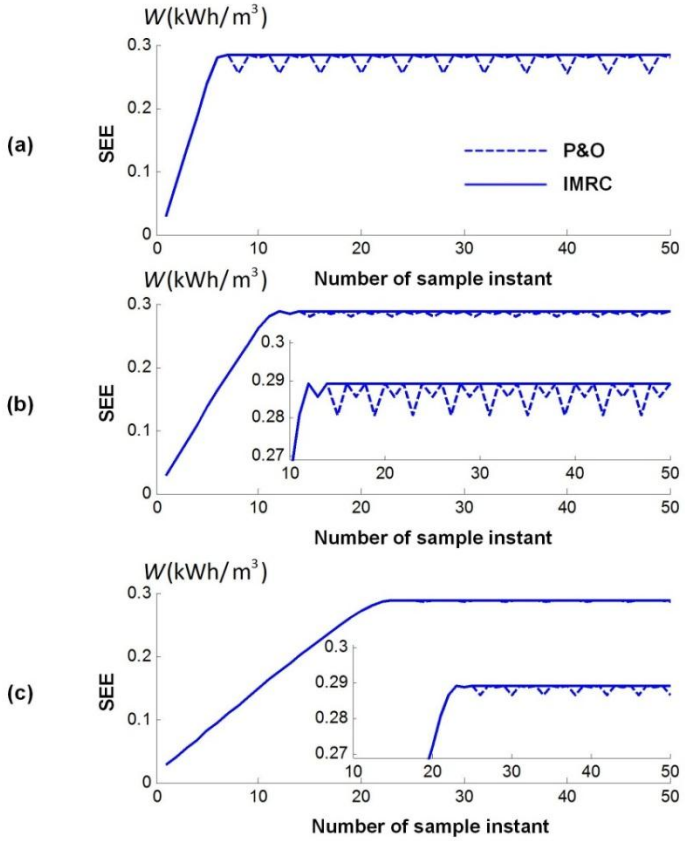

Figure 5.6: Osmotic power output with MPPT using P&O and IMR. Three step-sizes of the perturbation pressure, 2, 1 and 0.5 bar, are shown in (a), (b) and (c), respectively.

In addition, both the methods have advantages of low cost, independence of the PRO plant, easy implementation, stable and robust performance. Based on the experiences of MPPT using P&O and INC in PV array, both the methods are most commonly used and easy to implement. P&O method can be implemented using either an analogue circuit or a digital circuit and INC is commonly implemented using a digit circuit. These experiences can be extensively used in MPPT of PRO using P&O and IMR. Also, for PV array, rapid changes of the solar irradiation and temperature cause the MPP transitions fast and periodic. However, the changes in PRO may be more gradual compared to solar PV. The properties of membrane change in a continuous and gradual way due to deformation and fouling. The permeability and selectivity of the membrane commonly decrease monotonically with respect to time, resulting in the new optimum MPP may still in the vicinity of the previous MPP. Therefore, the two robust and simple methods will be less susceptible to confusion by system dynamics in MPPT of PRO with respect to membrane performance degradation.

5.4 AN OPTIMUM MODEL-BASED CONTROLLER (OMC)

Compared to the PV array, the PRO process needs more time to achieve the transition from one steady-state to another steady-state. Therefore, in order to achieve a fast response of the MPPT, adaptive and variable step-size in P&O and INC have been used in MPPT of PV array. An adaptive strategy is achieved by using a parameter or several parameters to change the step-size of the perturbation or increment according to the change of the measurements. Manual tuning of the parameter(s) is tedious and the obtained optimal results may be valid only for a given system and operating condition [74]. It means that with the changing operating environments, a constant pre-optimised parameter may fail to track the MPP efficiently. In this chapter, an optimum model-based controller (OMC) is used to determine the initial optimum hydraulic pressure with several operating variables of the PRO plant.

5.4.1 Development of OMC

In a PRO plant without considering CP or RSP, the optimum hydraulic pressures to achieve the peak power density of a coupon scale PRO and the specific extractable energy of a full scale PRO have been investigated by Yip et al. [32] and discussed in Chapter 2. According to their study, on the basis of the parameters and assumptions, the optimum pressures can be represented as,

$$\begin{aligned} \Delta P_{IPRO}^{PD} &= \frac{1}{2}(C_{OS}(c_D^0 - c_F^0)); \\ \Delta P_{IPRO}^{SEE} &= C_{os}[(1-\phi)c_D^0 - \phi c_F^0 + (2\phi - 1)\sqrt{c_D^0 c_F^0}] \end{aligned} \tag{5.3}$$

where ΔP_{PRO}^{PD} and ΔP_{PRO}^{SEE} represent the optimum pressure to achieve the peak power density and optimum specific extractable energy in an ideal PRO process with no CP or RSP. The subscript IPRO denotes the ideal PRO process with no CP or RSP. The pressure for the peak power density is the optimum theoretical pressure for the membrane unit at inlet. And the pressure for the maximum specific extractable energy is based on the full-scale PRO process in which the net driving force is zero at outlet. In fact, these two pressures can be used to be the initial pressure for the MPPT. In a small scale PRO, selecting ΔP_{PRO}^{PD} for the initial pressure is better, and ΔP_{PRO}^{SEE} is better for a large scale PRO which is close to achieve full-scale PRO discharge.

However, for a PRO plant considering CP and RSP effects, the optimum pressures may deviate from the theoretical pressure represented by Equation (5.3). In order to find the optimum pressure further close to the realistic pressure, the OMC is further improved. Previous studies have already carried out works on identifying the optimum operating pressures numerically with respect to the detrimental effects in a scale-up PRO [111]. For a hydraulic pressure to achieve the peak power density considering CP and RSP effects, the optimum pressure can be quickly found by numerical analysis. But for the optimum pressure of the specific extractable energy for a scale-up PRO, the calculation is more tedious considering the scale of the membrane utilisation, because the evaluation of each PRO operation needs to integrate all the water flux along the flow channel, which is time consuming for on-line control.

In this study, therefore, an approximation of the optimum pressure of the specific extractable energy considering CP and RSP in a scale-up process is proposed. For a stable high-performance membrane, the membrane permeability, selectivity and structural parameter should not be varied significantly. The accumulative CP and RSP effects gradually and continuously affect the scale-up PRO performance. Thus, the optimum pressure of the scale-up PRO process considering CP and RSP can be estimated in terms of the membrane unit performance and the theoretical process dynamics. An approximation of the two pressures in the ideal PRO and PRO considering CP and RSP is represented as

$$\frac{\Delta P_{DPRO}^{SEE}}{\Delta P_{DPRO}^{PD}} \cong \frac{\Delta P_{IPRO}^{SEE}}{\Delta P_{IPRO}^{PD}} \tag{5.4}$$

where the subscript DPRO denotes the PRO process considering detrimental CP and RSP effects. Therefore, the approximation of the pressure to achieve the maximum specific extractable energy in a scale-up PRO considering CP and RSP can be derived as,

$$\Delta P_{DPRO}^{SEE} = \frac{\Delta P_{IPRO}^{SEE}}{\Delta P_{IPRO}^{PD}} \Delta P_{DPRO}^{PD} \tag{5.5}$$

The schematic diagram of the PRO plant with MPPT and OMC is illustrated in Figure 5.7. The OMC senses the initial flow rates and concentrations of the draw and the feed solution, and determines the initial pressure for the MPPT based on the pre-measured membrane properties, A B and S. Then, the MPPT using P&O or IMR algorithm tracks the MPP locally

around the estimated optimum pressure with a small step-size of the perturbation or increment.

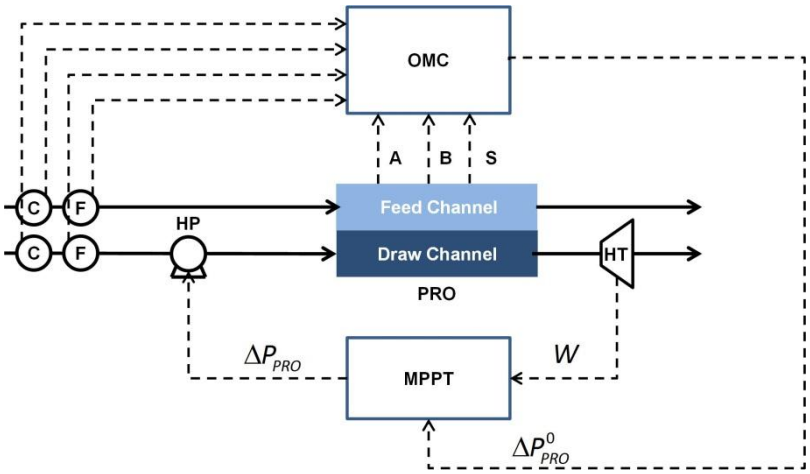

Figure 5.7: Schematic diagram of the PRO plant using MPPT and OMC.

5.4.2 Simulation of MPPT and OMC

Therefore, in this section, a series of simulation are developed to evaluate the performance of the osmotic power output tracking by using MPPT and OMC. Two step-sizes of MPPT using P&O and IMR, 0.5 and 0.1 bar, are used. Two models of OMC for the initial optimum hydraulic pressure, IPRO and DPRO which are represented by Equations (5.3) and (5.5), respectively, are also compared by simulation. Membrane M3 is selected for the simulations of the PRO plant. And other parameters are same as the parameters used in Section 5.2.2. For consistency with the simulation based on the same step-size in Section 5.3.3, the parameter ε_{IMR} is set to be 1×10^{-3} (the same parameter for the step-size 0.5 bar of IMR in Section 3.3) for all the MPPT using IMR algorithm.

The results are shown in Figure 5.8 in which osmotic power output with OMC and MPPT using P&O algorithm are presented in (a) and (c), and that with OMC and MPPT using IMR algorithm are plotted in (b) and (d). In addition, in (a) and (b), the step-size of the perturbation and increment is 0.5 bar and the step-size is 0.1 bar in (c) and (d).

First, the results indicate that the rise time of the MPPT is significantly reduced by using the OMC. With the step-size of 0.5 bar for the perturbation or incremental pressure, as shown

in Figure 5.6, the MPPT without OMC makes the PRO approach to its MPP more than 20 sample instants. In contrast, MPPT with OMC takes less than five sample instants for both algorithms. Moreover, the fast response time allows the MPPT applying a finer step-size to reduce the oscillation of the power output. As shown in Figure 5.8(c), the oscillation caused by P&O algorithm is considerably reduced by using 0.1 bar perturbation pressure and the rise time is still much quicker compared to the MPPT without OMC. In addition, the two models of OMC, IPRO and DPRO, show different performance of the MPPT. The results clearly indicate that the pressure estimated based on DPRO-OMC is closer to the MPP, and hence, a fast tracking is observed. As results shown in Figure 5.8, quicker tracking of OMC using estimated optimum pressure based on DPRO is found. Therefore, MPPT with DPRO-OMC is capable to employ a finer step-size to mitigate the oscillation around the MPP.

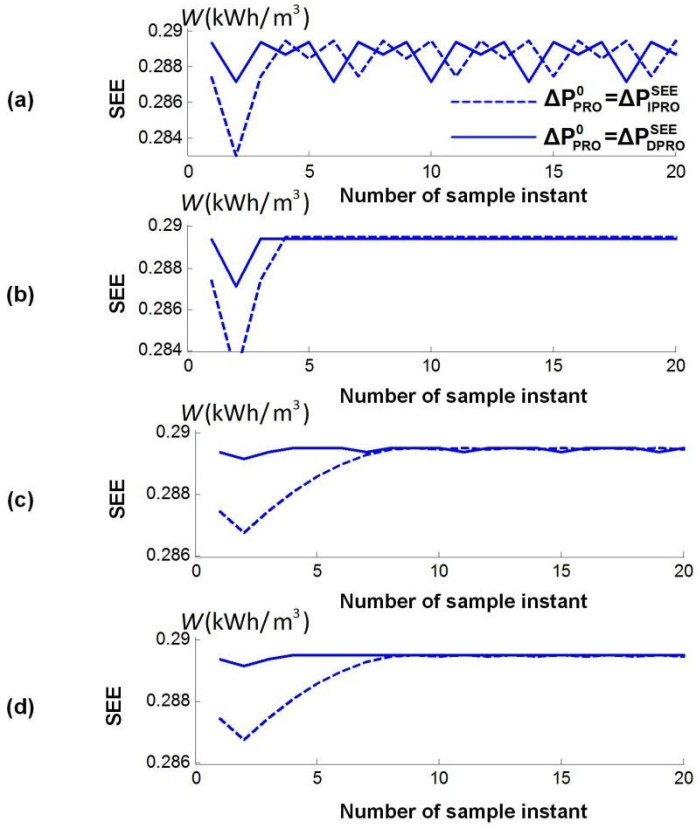

Figure 5.8: Osmotic power output with MPPT using P&O and IMR and OMC using Equation (5.3) and Equation (5.4). Osmotic power output with OMC and MPPT using P&O algorithm are presented in (a) and (c), and that with OMC and MPPT using IMR algorithm are plotted in (b) and (d). In addition, in (a) and (b), the step-size of the perturbation and increment is 0.5 bar and the step-size is 0.1 bar in (c) and (d).

In fact, the combination of the OMC and MPPT is efficient and robust to track the MPP of the PRO process. The OMC is a model-based controller to estimate the optimum operating

pressure for the PRO process based on the measured data. Therefore, the OMC aims to improve the performance by the knowledge of the process, which is efficient. In contrast, the MPPT is a general and robust method that is used to deal with the non-linear characteristics of the PRO and possible fluctuations.

5.4.3 Variations of flow rate and concentration of salinities

Furthermore, with the knowledge and information of the PRO plant, implementation of an OMC makes the PRO plant able to adjust the operation according to the rapid changes of the salinities. The combination of the OMC and MPPT is capable to respond quickly for the change of the concentration and flow rate of the salinities. A strategy to deal with these fluctuations is proposed based on the developed OMC and MPPT. The flowchart illustrating the strategy is shown in Figure 5.9. The MPPT operates starting at the optimum pressure estimated by the OMC. For tracking of the MPP with respect to the variations of the flow rate and concentration of the salinities, at the sample instant n, the estimated optimum pressure by OMC, $\Delta P_{PRO}^{SEE}(\mathrm{n})$, is compared to the potential current applied pressure applied by MPPT, $\Delta P_{PRO}(\mathrm{n})$. If the estimated pressure is close to the current applied pressure in which the vicinity can be controlled by the parameter ε_{OMC}^{1}, the pressure $\Delta P_{PRO}(\mathrm{n})$ is applied on the draw solution and the MPPT works around the current applied pressure. Conversely, if the estimated pressure deviates from the pre-defined vicinity of the current applied pressure, the decision is made based on the comparison between the current estimated optimum pressure and previous optimum pressure, $\Delta P_{PRO}^{SEE}(\mathrm{n}-1)$. If the current optimum pressure is close to the previous estimated pressure based on the parameter ε_{OMC}^{2}, the pressure $\Delta P_{PRO}(\mathrm{n})$ is applied on the draw solution and the MPPT works around the current applied pressure. Otherwise, the current pressure for the MPPT is set to be the current estimated pressure and is adjusted around the current estimated pressure by OMC.

The two parameters, ε_{OMC}^{1} and ε_{OMC}^{2}, are used to control the performance and cooperation between the MPPT and the OMC to deal with the rapid change of the environment and operating condition. As discussed above, the combination of OMC and MPPT provide efficient and robust solution to deal with the possible fluctuations. Due to the “imperfect” mathematical model of the PRO process, the selection of parameter ε_{OMC}^{1} allows the MPPT searching for and tracking the real MPP around the modelled MPP based on the OMC. In

addition, another parameter ε_{OMC}^{2} aims to identify the rapid and significant change of the environment or/and operating condition.

For the purpose of illustration of the proposed strategy of MPPT using OMC to deal with the variations of the salinities, two simple salinities fluctuation profiles of both the flow rate and concentration are shown in Figure 5.10. Specifically, we consider a 50 sample instants time window in which the dimensionless flow rate is used. For the first 25 sample instant, the dimensionless flow rate is 0.5, and then the dimensionless flow rate is reduced to 0.2 for the remaining 25 sample instant. For variations of the concentration, the draw concentration for the first 15 sample instants is 35 g/kg, increases to 55 g/kg from the 16th to the 35th sample instant, and then is reduced to 35 g/kg for the remaining 15 sample instants. Three case studies are carried out to evaluate the performance of the MPPT with OMC, including the individual variation of the flow rate of the draw, individual variation of the draw concentration, and the co-variations of the both flow rate and concentration. It is important to point out that the proposed strategy and associated analysis can be readily extended to deal with more complex salinities fluctuations profiles.

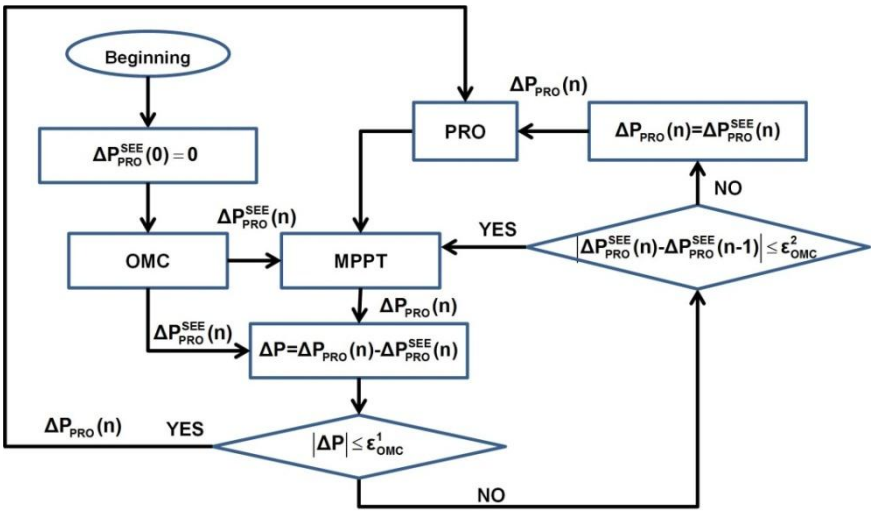

Figure 5.9: Flowchart of the strategy to operate MPPT and OMC subject to the variations of the flow rates and concentrations of the salinities.

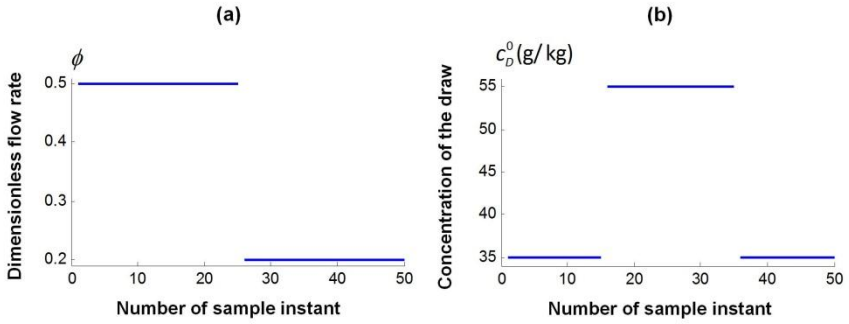

Figure 5.10: Variations of the concentration (in (a)) and flow rate (in (b)) of the salinities.

The results, shown in Figure 5.8, show very small oscillation of the osmotic power output around the MPP both algorithms compared to the large variation of the salinities as shown in Figure 5.10. Both the algorithms have very high performance. Therefore, for simplicity, only MPPT using P&O is considered in this section. First the performance of the MPPT with OMC is evaluated by dealing with variation of the flow rate of the draw. The results are shown in Figure 5.11 in which two strategies are evaluated. One is the simple combination of MPPT and OMC, in which OMC just provides the initial optimum pressure at the beginning and then the MPPT with P&O algorithm tracks the MPP. We call it SIM-MPPT-OMC strategy. Conversely, another is the optimum strategy illustrated in Figure 5.9. We call it OPT-MPPT-OMC strategy. In the simulation, 0.1 bar is selected for the perturbation pressure in OPT-MPPT-OMC, and two step-size, 0.1 and 0.5 bar, are studied for the perturbation pressure in SIM-MPPT-OMC. ε_{OMC}^{1} is set as ten times of the perturbation pressure and ε_{OMC}^{2} is set as 2 bar. The results clearly show the rapid response of the OPT-MPPT-OMC to track the changes of the flow rate of the draw solution and resulting varied osmotic power output. Compared to the SIM-MPPT-OMC strategy with two different step-sizes, the OPT-MPPT-OMC has fast tracking and small oscillation when the flow rate of the draw is suddenly changed. For SIM-MPPT-OMC, the trade-off of the rise time and the oscillation still exists. Larger step-size tacks the change fast but with a large oscillation around the MPP. In contrast, implementation of the small step-size results in long time-period to reach the MPP.

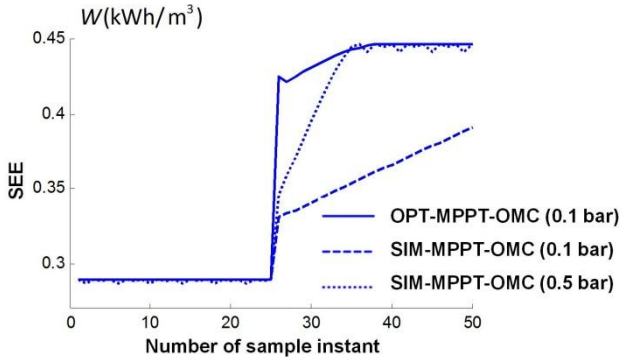

Figure 5.11. Osmotic power output with MPPT using P&O algorithm and OMC subject to the variation of the flow rate of the draw.

In addition, the performance of the MPPT with OMC is evaluated by dealing with variation of the draw concentration. The results are shown in Figure 5.12 in which the two strategies, OPT-MPPT-OMC and SIM-MPPT-OMC, are studied.

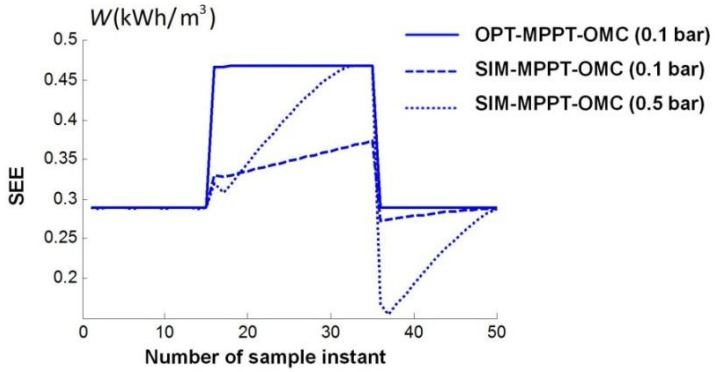

Figure 5.12: Osmotic power output with MPPT using P&O algorithm and OMC subject to the variation of the draw concentration.

As shown in Fig 5.10(b), the concentration of the draw changes two times within the studied period. According to the simulation, the OPT-MPPT-OMC strategy also has good performance to deal with the variations. It is found that fast tracking of the MPP for both the changes of the operations are achieved by OPT-MPPT-OMC. MPP is tracked and stable operation with negligible oscillation of PRO is simulated. In contrast, for the SIM-MPPT-OMC, the larger step-size causes larger fluctuation of the operation due to the changes of the operating condition. Although the SIM-MPPT-OMC with smaller perturbation pressure tracks the MPP slower, it has smaller fluctuation when the operating condition is changed rapidly.

Moreover, a more complex operating condition, co-varied concentration and the flow rate of the draw solution are evaluated. Both the varied profiles of the concentration and flow rate shown in Figure 5.10 are studied in a PRO plant with MPPT and OMC. The results are shown in Figure 5.13 in which both OPT-MPPT-OMC and SIM-MPPT-OMC strategies are considered. According to the results, the SIM-MPPT-OMC almost fails to track the MPP subject to such complicated varying operating conditions. Both of the two SIM-MPPT-OMC with two selections of the perturbation pressure cannot respond properly according to the co-varied concentration and flow rate of the draw solution. In contrast, the OPT-MPPT-OMC still performs well that it tracks the MPP fast subject to the rapid and various changes of the salinities. Therefore, based on the knowledge of the PRO process by implementing certain sensors, the performance of the MPPT can be further improved and the OPT-MPPT-OMC is capable to track the varied MPP with the fluctuating salinities.

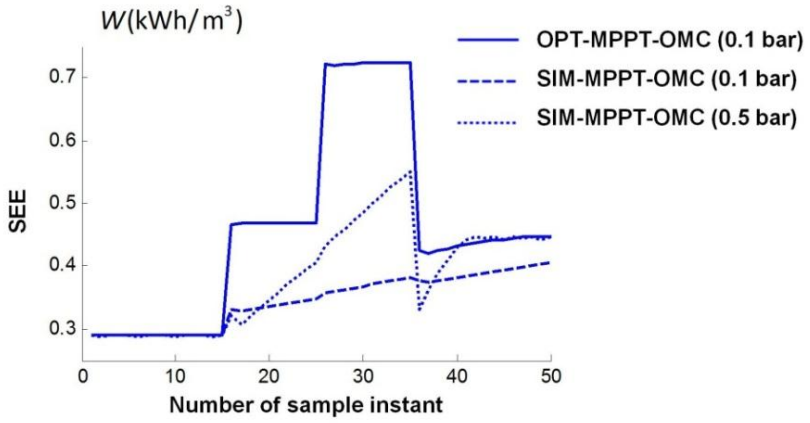

Figure 5.13: Osmotic power output with MPPT using P&O and OMC subject to co-variant of concentration and flow rate of the salinities.

5.5 SUMMARY

In order to increase the performance of a scale-up PRO application in practice, MPPT control to achieve the optimum osmotic power output is investigated. First, the process characteristics of the PRO process is studied and evaluated in terms of membrane properties, concentration and flow rate of the salinities. Then, two algorithms for MPPT in PRO are proposed and investigated, including P&O algorithm and IMR algorithm. These MPPT techniques are generic methods to track the MPP, and hence, for further improvement on the MPPT, a model-based OMC is proposed and operated with the MPPT techniques. Finally, a series of simulation are carried out to evaluate the performance of

the MPPT and OMC to operate the PRO track the MPP. Based on the results, several conclusions can be drawn: 1) process characteristic of the scale-up PRO process is affected by several factors, such as membrane properties, concentration and flow rate of the salinities etc. Therefore, it is necessary to develop and employ MPPT to ensure the optimum osmotic power output subject to the fluctuating operating conditions. 2) It is demonstrated by simulations that both P&O and IMR algorithms can be used to track the MPP of a PRO process. The trade-off between the rise time and the oscillation by selecting the step-size of the perturbation pressure or incremental pressure exists in both algorithms. Larger step-size results in fast response as well as larger oscillation, and vice versa. 3) With the availability of several measured variables, OMC is capable to further improve the performance of the MPPT. Based on the model of the scale-up PRO process, an estimated optimum pressure improves the convergence, allows MPPT using a smaller step-size and results in fast response and mitigated oscillation. 4) OMC is capable of quickly adjusting the operation to deal with the rapid changes of the salinities. In the simulation, the OPT-MPPT-OMC performs well to deal with the individual variations of the flow rate or concentration of the draw, and the co-variation of both the influential factors.

THERMODYNAMIC ANALYSIS OF A STAND-ALONE REVERSE OSMOSIS DESALINATION SYSTEM POWERED BY PRESSURE RETARDED OSMOSIS

6.1 INTRODUCTION

A systematic investigation on osmotic power extraction from different salinities is presented in Chapter 2-5. This chapter presents a study the feasibility of a PRO-based stand-alone salinity power driven RO desalination plant with zero brine discharge. First, a hybrid system is proposed to be the basis for this investigation. Then, the operation of the hybrid system is studied based on the thermodynamic analysis in which key states of the saline streams are discussed. The stand-alone feasibility of the hybrid RO-PRO system, including the objectives of zero carbon emission and brine discharge, is mathematically

interpreted. Furthermore, the required operations and the required membrane area of the PRO subsystem are studied. Finally, a case study on the feasible stand-alone operation is developed and the effects from the inefficiency of the pumps and energy recovery devices are also discussed.

6.2 STAND-ALONE SALINITY POWER DRIVEN REVERSE OSMOSIS SYSTEM BY PRESSURE RETARDED OSMOSIS

6.2.1 Hybrid RO-PRO membrane process

A proposed stand-alone salinity power driven RO desalination system is illustrated in Figure 6.1. The hybrid system consists of two sub-systems: desalination and power generation. In the first sub-system, seawater is desalinated using RO technology. The seawater is pressurized by the HP and the ERD before it flows into the RO membrane module in order to maintain the reverse water permeation from the high concentration side to the low concentration side. Accordingly, two streams flow from the RO module: the permeated water and the concentrated brine water. The brine is further used to pressurize the seawater in the ERD before it flows into the PRO sub-system, and the PW is the product of the hybrid system. In another sub-system, the salinity power is generated by the PRO process with the pressurized brine water from the RO plant as the draw solution. Usually, low concentration impaired water bodies include sewage and waste water from household and industries, brackish water, and other water with impurities [123]. These low concentration streams (secondary wastewaters and brackish water) or mixtures are potentially the candidates of the feed solution for the osmotic membrane process [100]. Among these water bodies, the salt concentration might no more than that of brackish water. In this chapter, the brackish water is selected as the feed solution for the early-stage investigation. The applied hydraulic pressure on the draw solution is controlled by adjusting the valve resistance on the draw solution flow channel. The feed solution flow rate is controlled by the boost pump (BP) and valves on the feed solution flow channel. Finally, the draw solution including the permeated water from the feed water is expanded in the HT to generate electricity.

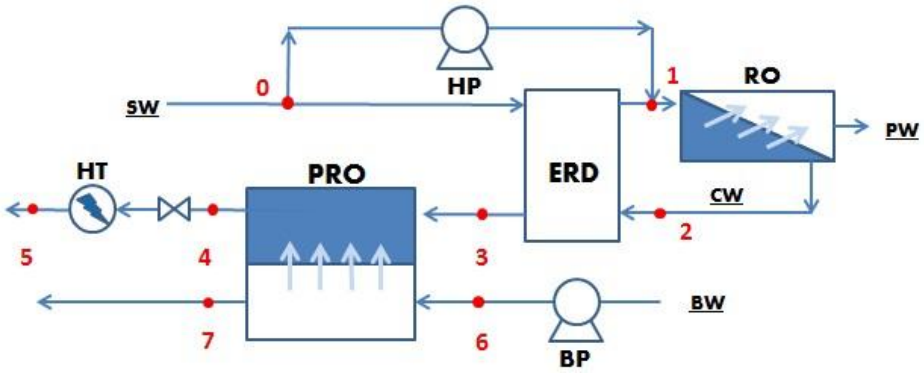

Figure 6.1: Schematic diagram of the proposed stand-alone salinity power driven RO desalination system.

6.2.2 Thermodynamic analysis of the stand-alone hybrid RO-PRO system

Before further analysis of the hybrid system, some key states of the saline streams are presented in the pressure-flow rate (P-Q) diagram as illustrated in Figure 6.2(a). At this stage, the pressure loss in the membrane and flow channels can be ignored and the efficiency of the pumps is assumed to be 100%. Also, the membrane is considered to be able to reject salt at a rate of 100% with no fouling or deformation effect. And due to the smaller amount of the energy consumed by the BP, in this chapter, the energy consumption is only considered as the work of the HP in the RO sub-system.

In Figure 6.2(a), the energy consumed, recovered and generated can be represented by the area of the states diagram i.e., the energy consumed by HP in pressurizing the seawater can be represented by the area covered by O-0-1-C, the energy recovered from the brine water in ERD can be represented by the area covered by 3-2-C-B and the energy generated by the PRO process can be represented by the areas covered by O-5-4-B. In the case concerning the energy recovery, the overall energy surplus between the generation and consumption of the hybrid system can be represented as the difference between the area of D-1-2-3 and 0-5-4-D. If the overall energy surplus is non-negative, theoretically, the hybrid system can be operated as stand-alone. Otherwise, the hybrid system needs an extra power source to cover the exceeding energy consumption. Therefore in the hybrid system, the distribution of the consumed, recovered and generated energy is determined by the states of the streams. If different state variables are chosen, the energy performance of the hybrid system is different. These key state variables include the states 2, 3 and 4 in which the operation are controlled by water recovery of the RO system, applied hydraulic pressure of draw solution and the flow rate of feed solution of the PRO

process, respectively. In addition, other states are determined by the local conditions or/and RO thermodynamic restrictions [124].

Additionally, the change of the osmotic pressure of the streams within the different states is also crucial. The variation describes the conversion of osmotic-hydraulic pressure between different states, which is the essence of this hybrid system. The change of the osmotic pressure is shown in Figure 6.2(b). When the osmotic pressure is increasing as shown in states transition 1-2, hydraulic energy releases and potential salinity energy increases. Conversely, when osmotic pressure decreases in the state transition such as transition 3-4, the salinity power is harvested. Because the osmotic pressure is mainly dependent on the concentration of the solution, the change of osmotic pressure is more about change of salinity concentration in the stand-alone RO-PRO system. Compared with a classical thermodynamic cycle, this 'salinity cycle' has similar attributes because it can generate power by the changing states of the salinity concentration. Furthermore, as the hybrid system is aimed at delivering zero brine discharge, the concentration of outlet streams of both the draw and feed solution from the PRO process should be less than the concentration of seawater. For example, in Figure 6.2(b), the osmotic pressure of state 4 (diluted draw solution) and 7 (concentrated feed solution) should be less than the osmotic pressure of state 0 and 1, π_{SW} , due to zero brine discharge constraint.

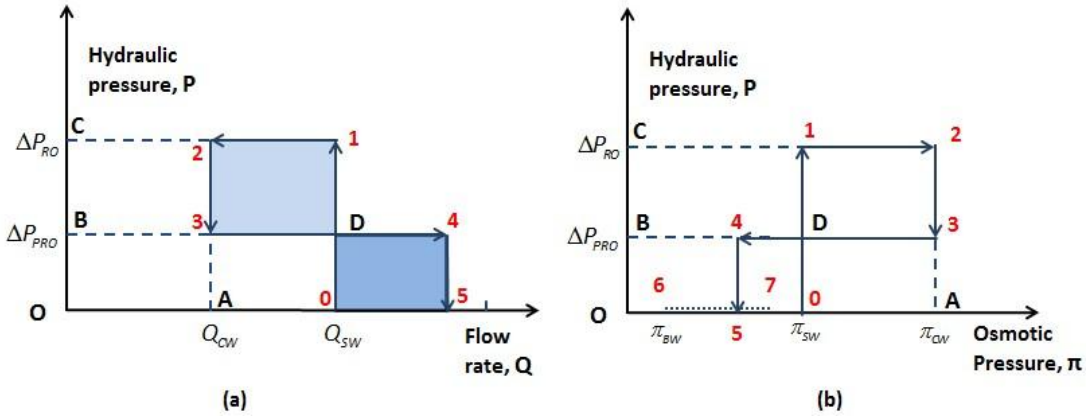

Figure 6.2: Diagrammatic analysis of the stand-alone salinity power driven RO system. Diagram of hydraulic pressure –flow rate (P-Q) is shown in (a). And Diagram of hydraulic pressure – osmotic pressure (P-π) is shown in (b).

Therefore in this study, the stand-alone RO-PRO system can be successfully operated only if the extra energy generated by the HT is no less than the overall energy consumed by the RO process. This can be expressed as

$$\dot{W}_{HT} \geq \dot{W}_{RO} \tag{6.1}$$

where $\dot{W}_{HT}$ represents the power generated by the HT which equals the area represented by O-5-4-B and can be further written as

$$\dot{W}_{HT} = Q_D \Delta P_{PRO} = (Q_{CW} + \Delta Q)\Delta \mathrm{P}_{PRO} = ((1-\mathrm{Y})\mathrm{Q}_{SW} + \Delta Q)\Delta \mathrm{P}_{PRO} \tag{6.2}$$

in which Q_D is the flow rate of the draw solution in the PRO process, ΔP_{PRO} is the hydraulic pressure applied on the draw solution, Q_{SW} is the flow rate of the seawater, Q_{CW} is the flow rate of concentrated brine water, ΔQ is the flow rate of the permeate through the PRO membrane. Considering the hydraulic energy recovery, furthermore, $\dot{W}_{RO}$, the power requirement of the RO system represented by the area of O-0-1-2-3-B can be further written as

$$\dot{W}_{RO} = Q_{SW}\Delta P_{RO} - Q_{CW}(\Delta P_{RO} - \Delta P_{PRO}) = Q_{SW}\Delta P_{RO} - Q_{SW}(1-\mathrm{Y})(\Delta \mathrm{P}_{RO} - \Delta P_{PRO}) \tag{6.3}$$

where ΔP_{RO} is the pressure applied on the feed water in the RO system.

Therefore, by substituting Equations (6.2) and (6.3) into Equation (6.1), the feasibility condition of the stand-alone 'salinity cycle' can be rewritten as

$$\Delta \dot{W} = \Delta P_{PRO}\Delta Q - \Delta P_{RO}(Q_{SW} - Q_{CW}) = Q_{SW}(\Delta P_{PRO} Y_P - \Delta P_{RO}\,\mathrm{Y}) \geq 0 \tag{6.4}$$

where Y_p is the dimensionless flow rate of the water permeation in the PRO process with respect to the inlet seawater stream to the RO system. The feasibility condition number, FC, can be defined as

$$FC = \frac{\Delta P_{PRO} Y_P}{\Delta P_{RO} Y} \tag{6.5}$$

In order to achieve the stand-alone hybrid system, certain variables are needed to be controlled to satisfy $FC \geq 1$. Based on the RO thermodynamic restriction, ΔP_{RO} is dependent on the RO water recovery and the seawater concentration which means it can be represented as

$$\Delta P_{RO} = \frac{\pi_{SW}}{1-Y} \tag{6.6}$$

where π_{SW} is the osmotic pressure of seawater and other three variables, ΔP_{PRO}, Y, and Y_P, can be controlled. This implies that, the selection of appropriate values for the three variables is crucial.

For a constant pressure PRO process, C-PRO, with enough membrane area available (allowable for full-scale PRO discharge), the applied pressure on the draw solution of the PRO process determines the termination of water permeation [32]. In other words, the termination happens when the osmotic pressure difference at the outlet equals the applied pressure [32]. For a co-current PRO process, because both the draw and feed solution flow toward the same direction, only one outlet needs to be considered. In contrast, for a counter-current PRO process, with a different applied pressure selected, the net driving force at either of the two outlets may satisfy the condition and terminate the water permeation [125-127]. Usually, the counter-current scheme performs better than the co-current scheme due to the high effectiveness [62]. For simplicity, the co-current PRO process is considered first.

In this chapter, similar to Chapter 2, I-PRO model and ideal solution are employed to identify the theoretical limit of the hybrid RO-PRO membrane process. And a further work addressing the detrimental effects is presented in Chapter 7. Therefore, the feed water desalinated by the RO system is assumed as the seawater that is a hypothetical solution with 35 g/L salinity and its osmotic pressure can be obtained according to the van't Hoff's law [32]. Thus, the osmotic pressure difference at the outlet of the membrane can be expressed as [32]

$$\Delta\pi_{Outlet} = \nu RT(c_{CW}^{Out} - c_{BW}^{Out}) = \nu RT\left(\frac{c_{CW} Q_{CW}}{Q_{CW} + \Delta Q} - \frac{c_{BW} Q_{BW}}{Q_{BW} - \Delta Q}\right) \tag{6.7}$$

where c_{CW} , c_{CW}^{out} , c_{BW} ,and c_{BW}^{out} are the inlet and outlet concentration of the brine and brackish water, respectively and Q_{BW} is the inlet flow rate of the brackish water stream. The inlet flow rate of draw solution is the flow rate of brine water from the RO system with leakage assumed to be negligible. With 100% rejection RO process, the concentration of the brine is determined by the water recovery that is $c_{CW} = c_{SW} / (1-Y)$. If a overall dimensionless flow rate, ϕ_h , is defined as the ratio of the inlet flow rate of brackish water to the sum of the inlet flow rate of brackish water and brine in the hybrid membrane process, which is $\phi_h = Q_{BW} / (Q_{BW} + Q_{CW})$, the osmotic pressure difference at the outlet of a co-current PRO process can be represented as

$$\Delta\pi_{Outlet} = \nu RT\left(\frac{\frac{c_{SW}}{1-Y}}{1+\frac{Y_P}{1-Y}} - \frac{c_{BW}\frac{\phi_h}{1-\phi_h}}{\frac{\phi_h}{1-\phi_h} - \frac{Y_P}{1-Y}}\right) \tag{6.8}$$

Accordingly, the applied pressure on the draw solution of the PRO process is determined by Y , Y_p and ϕ_h . It is noted that on the P-Q plot (Figure 6.2), the possible value of applied hydraulic pressure, ΔP_{PRO} , is from zero to the theoretical maximum, ΔP_{RO} . However, in practice, the PRO membrane cannot maintain as high hydraulic pressure as the commercial RO membranes [100]. Recently, the highest hydraulic pressure applied on the membrane to harvest the salinity energy by the PRO process is reported as 48 bar [128] and many other studies reported at the range of 15-24 bar [108, 129].

Furthermore, for the purpose of zero brine discharge, the maximum concentration of discharge streams is assumed to be less than the seawater salinity concentration. In this case, the conditions restricted the final concentration of both the draw and feed solutions, defined as 'zero brine discharge' (ZB) constraint which are represented as

$$\begin{aligned} c_{BW}^{out} &= \frac{c_{BW}Q_{BW}}{Q_{BW} - \Delta Q} \le c_{SW} \\ c_{CW}^{out} &= \frac{c_{CW}Q_{CW}}{Q_{CW} + \Delta Q} \le c_{SW} \end{aligned} \tag{6.9}$$

6.3 MODELLING OF THE STAND-ALONE RO-PRO SYSTEM

Accordingly, the hybrid RO-PRO system can be operated stand-alone only if $FC \geq 1$ with the appropriate cooperation between the RO and the PRO systems. In this section, the RO water recovery (Y), dimensionless water permeation (Y_p) and overall dimensionless flow rate (ϕ_h) are analysed to find the combination which will realise the feasibility of stand-alone. The analysis of feasible operation is presented in Figure 6.3.

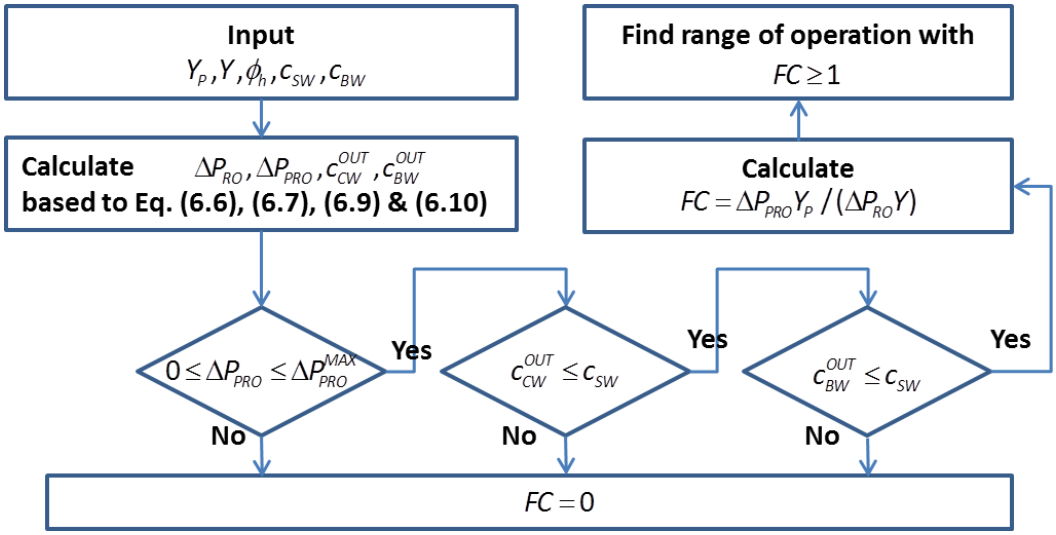

Figure 6.3: Schematic illustration of the calculation of FC number from possible operations of the RO-PRO system.

In the analysis, the main input variables consist of Y_p, Y, ϕ_h, c_{BW} and c_{SW}. Therefore the applied pressure required by the RO system can be obtained according to Equation (6.6). Combining Equations (6.8), the applied hydraulic pressure on the draw solution can be also obtained. In addition, based on Equation (6.9), the outlet concentration of both draw and feed solution in co-current PRO process can be obtained. Next, the constraints, including the constrained range of PRO applied pressure and the ZB constraint, are validated. For the validated operations, a further calculation of the stand-alone feasibility is developed to find the region with $FC \geq 1$.

6.3.1 The domain of input variables

The operation of the RO process in terms of water recovery is restricted to from 0% to 50% based on the practical operational range of the SWRO system. For the overall

dimensionless flow rate ϕ_h, the ratio is always restricted by the volume availability in a specific location. In this chapter, the range is considered to be between 0.2 and 0.8. Another important input is the dimensionless water permeation, Y_p. According to the definition of Y_p, it can be rewritten in terms of ϕ_h and Y as given below,

$$Y_P = \frac{\Delta Q}{Q_{SW}} = \frac{\Delta Q}{Q_{BW}} \frac{Q_{BW}}{Q_{CW}} \frac{Q_{CW}}{Q_{SW}} = \frac{\Delta Q}{Q_{BW}} \frac{\phi_h}{1-\phi_h}(1-\mathrm{Y}) \tag{6.10}$$

Theoretically, because the water permeation from the brackish water stream cannot exceed the mass available of the brackish water, such that $\Delta Q \le Q_{BW}$. Only if the process is operated reversibly, the permeation achieved would be close to the maximum. Actually, in a C-PRO plant the maximum permeation is further less. By applying a certain hydraulic pressure on the draw solution, the maximum permeation is given [32],

$$\Delta Q_{C-PRO}^{MAX} = \frac{\sqrt{c_{CW}} - \sqrt{c_{BW}}}{\sqrt{c_{CW}} + \frac{\phi}{1-\phi}\sqrt{c_{BW}}} Q_{BW} \tag{6.11}$$

where ΔQ_{C-PRO}^{MAX} represents the maximum water permeation in a C-PRO process. To this end, the range of Y_p is

$$\begin{aligned} &0 \le Y_P \le \frac{\phi_h}{1-\phi_h}(1-\mathrm{Y}) && \text{Reversible PRO} \\ &0 \le Y_P \le \frac{\Delta Q_{C-PRO}^{MAX}}{Q_{BW}} \frac{\phi_h}{1-\phi_h}(1-\mathrm{Y}) && \text{Constant-Pressure PRO} \end{aligned} \tag{6.12}$$

In this chapter, parameters are used same to those used in Chapter 2, to analyse the thermodynamic limiting performance of the stand-alone hybrid RO-PRO process.

6.3.2 Results and analysis

Results of the FC number with three conditions of Y_p are shown in Figure 6.4. The dotted lines represent the results with reversible PRO process that is the highest efficiency in osmotic energy recovery, and the solid lines denote the results of a C-PRO process. The results clearly indicate that the feasible operation of a C-PRO process is a part of the operations of a reversible PRO. As analysed above, the reversible PRO process represents

the theoretical maximum efficiency in the osmotic energy recovery. With the multi-stage C-PRO process treatment, the overall efficiency of salinity energy harvest will approach close to the reversible operation according to the study in Chapter 2. In other words, with a multi-stages PRO sub-system implemented in the hybrid system, the solid line would be approached to the dotted line by certain multi-stage treatment.

From the results of both reversible and C-PRO process, it is found that for constant dimensionless water permeation, lower RO water recovery results in higher FC number and larger validated range of overall dimensionless flow rate. In addition, greater values of Y_p move the curves with different RO water recovery towards the direction of increasing both FC number and the overall dimensionless flow rate.

It can be observed that the region with $FC > 1$ is restricted by the availability of the overall dimensionless flow rate in a reversible PRO process as depicted in Figure 6.4(a). It is a fact that higher Y_p requires higher overall dimensionless flow rate to validate the constraint based on Equation (6.12), and the upper bound is always restricted by the local environment. In addition, in a C-PRO process, the available operation is even more strictly restricted that only lower RO water recovery (Y=0.2 and 0.3) have very limited feasible operation. But the FC number can reach a higher value compared with that of lower Y_p which is advantageous in energy generation in both processes. When Y_p decreases, the validated range of overall dimensionless flow rate becomes larger, but also results in the decrease on the FC number. Comparing the results in Figure 6.4(b) with that in Figure 6.4(c), the decrease on the FC number at the same feed water condition of the PRO process and the RO operation can be observed.

Therefore, as discussed earlier the dimensionless flow rate is determined by the available volume of low concentration water bodies in a specific location. If there is large amount of low concentration water bodies available then high ϕ_h can be achieved, and a lager Y_p is more appropriate. If the low concentration stream volume is limited, a hybrid system operated at a smaller Y_p may be applicable. Otherwise, the hybrid system can hardly satisfy the stand-alone condition of $FC \geq 1$.

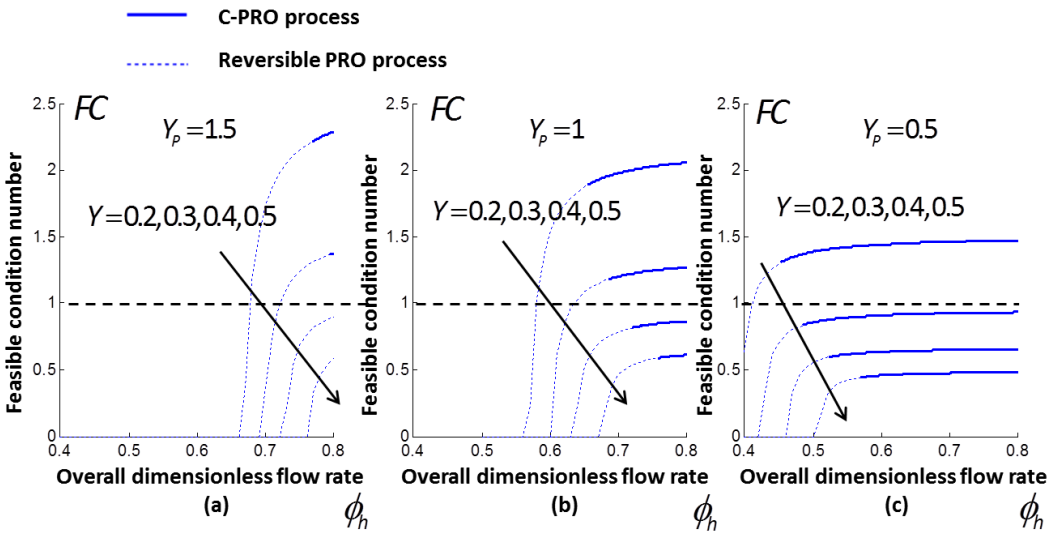

Figure 6.4: Result of the FC number with respect to several possible dimensionless water permeation, overall dimensionless flow rate and RO water recovery rates. Three different dimensionless permeation rates, 1.5, 1 and 0.5, are shown in (a), (b) and (c), respectively.

The way to control Y_p is to adjust the hydraulic pressure applied on the draw solution. Because the membrane area is assumed to satisfy the condition of full-scale water permeation in the PRO, different ΔP_{PRO} values can be controlled to reach different dimensionless water permeation. The relation between the applied pressure and the dimensionless water permeation is shown in Figure 6.5 with the same RO water recovery of 0.2. Lower Y_p values can be seen to require larger applied pressure on the draw solution to terminate the water permeation which is a result of relationship between the applied hydraulic pressure and the water permeation as represented in Equations (6.7).

Furthermore, according to the relation between the overall dimensionless flow rate and the dimensionless water permeation that the dimensionless water permeation Y_p is proportional to the overall dimensionless flow rate ϕ_h to achieve the condition, $FC \geq 1$. It appears more beneficial to use both the lower ϕ_h and Y_p values because less resources are required to maintain the stand-alone feasibility. However, a problem with this operation is that it requires a larger hydraulic pressure on the draw solution in a C-PRO process according to the results shown in Figure 6.5. The high applied pressure on the draw solution increases the risk of membrane deformation and the reverse salt permeation [130], and thus requires high performance of the membrane. Thus, to design a stand-alone RO-PRO system, an appropriate operation is needed to be selected according to the trade-off

between the membrane quality and the available water sources. Furthermore, if a counter-current configuration of PRO process is implemented, the feasibility would be further improved.

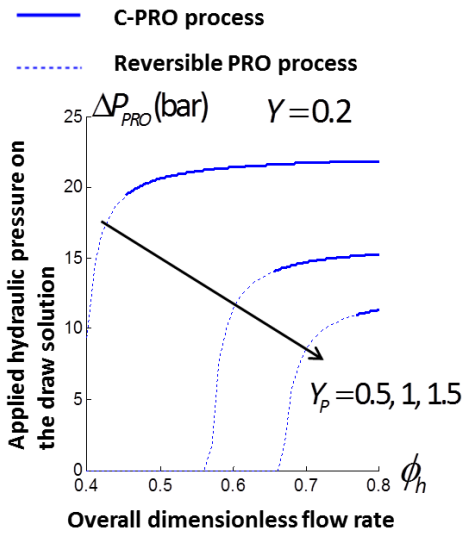

Figure 6.5: Schematic representation of the relation between the applied pressure on the draw solution and the water permeation.

6.3.3 A look inside the PRO

According to the above analysis, feasible operations of the hybrid system are mainly in the RO operations with low water recovery, approximately less than 0.3. In a PRO process, the volume of the permeated water from the feed is limited by its operation and the salinity gradients availability. In the hybrid system, as the flow rates and concentration of the salinity gradients including the seawater and brackish water are altered by the RO water recovery and/or the restricted overall dimensionless flow rate, in this chapter the feasible range of Y_p changes subject to the value of Y and ϕ_h. Accordingly, several possible pairs of RO water recovery and the overall dimensionless flow rates are selected such as RO water recovery at 0.1, 0.2 and 0.3 whilst an overall dimensionless flow rate from 0.2 to 0.8 is also investigated to find the variation of the water permeation inside the PRO subsystem. The results of FC number in the feasible range of Y_p are also presented in Figure 6.6.

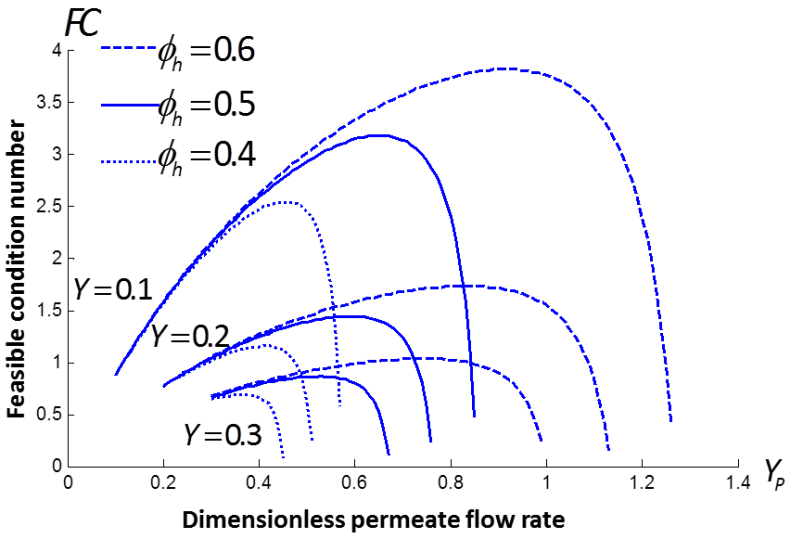

Figure 6.6: Variation of the dimensionless water permeation and resulting FC numbers.

In the figure, under a certain RO water recovery, all the curves with different overall dimensionless flow rates start at the same point. But with a larger overall dimensionless flow rate, the FC number increases more significantly and also the range of the feasible Y_p is enlarged. Compared with groups of curves with different RO water recovery ratios, this indicates that the lower water recovery improves the FC number. Furthermore, in the range of feasible Y_p of all the curves, the FC number initially increases, then reaches an optimum and finally decreases. If the maximum FC number, $FC_{MAX} > 1$, it means that the stand-alone feasibility can be achieved within the current operation which can also be improved by lowering RO water recovery and increasing the overall dimensionless flow rate. Consequently, the optimums of Y_p resulting in the maximum FC number are studied for different PRO operations. The optimisation is developed by searching all the values of FC number among the operations with RO water recovery ratio at 0.1, 0.2 and 0.3, and the range of the overall dimensionless flow rate from 0.2 to 0.8. All of the results of the optimum FC numbers and the optimum dimensionless permeate flow rates are illustrated in Figure 6.7.

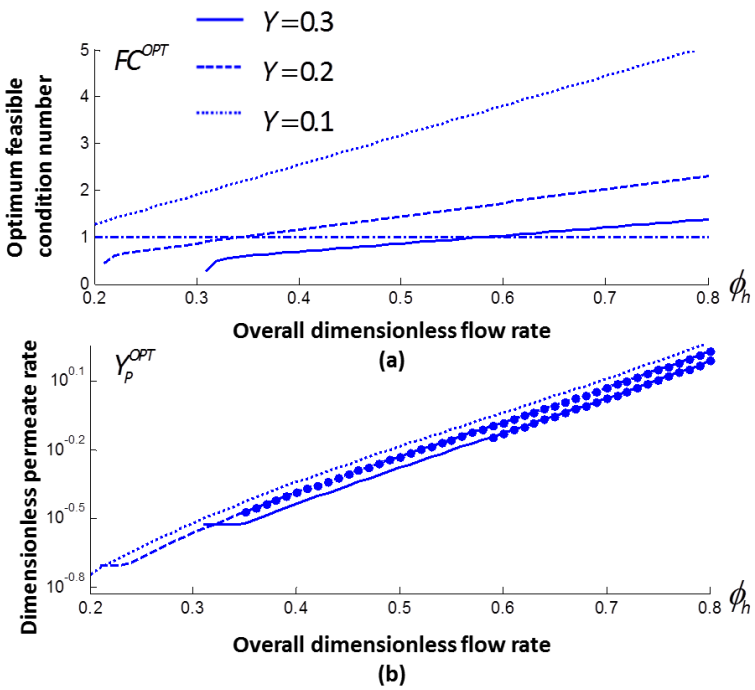

Figure 6.7: Optimisation results of the FC numbers (a) and the dimensionless water permeation flow rates (b). In the figure, Solid dots represent conditions which represent stand-alone systems.

The optimum FC numbers shown in Figure 6.7(a) are proportional to the overall dimensionless flow rate at each RO water recovery ratio. A lower RO water recovery ratio also improves the maximum FC numbers for all the overall dimensionless flow rates studied. Furthermore, with the increase on the Y, the feasible range of the overall dimensionless flow rates ($FC^{OPT} \geq 1$) diminishes. In Figure 6.7(b), the optimum dimensionless permeate flow rate is illustrated and the stand-alone feasible operations are marked by the solid dots (same representation in the later figures). The optimum dimensionless permeate flow rate also increases with the increase of ϕ_h, which means with a larger overall dimensionless flow rate ϕ_h, more water is needed to be transported from the brackish water stream to reach the maximum energy surplus. Furthermore, in the range of lower overall dimensionless flow rates, there is a stiff change on the slope in the curves with a constant RO water recovery of 0.2 and 0.3. In fact, the point connecting discrete slopes of the curve is determined by the ZB constraint which ensures the concentration of all the streams in the hybrid system. In the range of the dimensionless water flow rate before the point, the ZB constraint requires a certain level of flow of the permeation to dilute the brine stream and reduces the concentration to a level less than the level of the seawater stream at the

outlet. The constraint drives the PRO subsystem away from its optimum operation of energy generation. Until the overall dimensionless flow rate increases to the value, the PRO is able to operate at an optimum level under the ZB constraint.

Furthermore, the operations ensuring the PRO subsystem achieves optimum FC numbers are investigated, namely the hydraulic pressure applied on the draw solution. The results are presented in Figure 6.8.

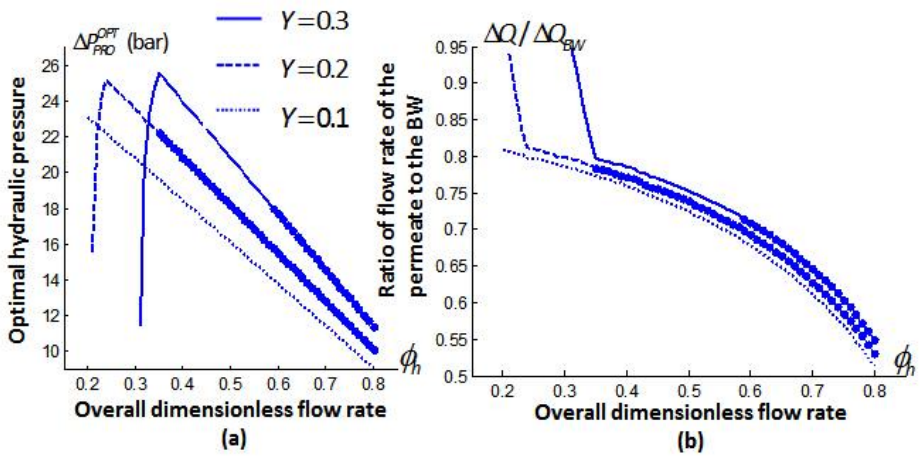

Figure 6.8: Operational parameters of the PRO subsystem to achieve the optimum FC numbers. Optimum operational pressures and ratios of flow rate of the permeation are plotted in (a) and (b), respectively.

The required hydraulic pressure to achieve optimal FC numbers is presented in Figure 6.8(a). It is found that in the range of stand-alone feasibility, the applied pressure is inversely proportional to the overall dimensionless flow rate. A larger ϕ_h results in a lower hydraulic pressure needed to apply on the brine stream from a certain RO operation. The decrease of the hydraulic pressure is mainly due to the decrease on the local dimensionless permeation flow rate of the PRO subsystem shown in Figure 6.8(b). This is a consequence of the addition to the flow rate of the brackish water stream by the control of the overall dimensionless flow rate ϕ_h. In addition, the significant changes of the slopes in the curves when RO water recovery is at 0.2 and 0.3 are also caused by the ZB constraint.

Furthermore, the required membrane area in the PRO subsystem is estimated based on the membrane water permeability of 1 $L \cdot bar^{-1} \cdot h^{-1} \cdot m^{-2}$. At this stage, I-PRO modelling is employed which means neither concentration polarisation effects nor reverse salt permeation is considered. Thus, the effective membrane requirement of full-scale water

permeation in a PRO process is determined by the water flux along the membrane from the inlet to the point that the water flux diminishes to negligibly small. Thus, the minimal the required membrane area of a full-scale PRO discharge can be determined by the equilibrium transport equation. With the brine from a RO system as the draw solution and the brackish water stream as the feed solution, water permeation can be expressed as

$$d(\Delta Q^{OPT}) = Q_{SW}\, \mathrm{d}(Y_P^{OPT}) = A(\nu RT(\frac{\frac{c_{SW}}{1-Y}(1-\phi)}{1-\phi(1-\frac{\Delta Q}{Q_{BW}})} - \frac{c_{BW}}{1-\frac{\Delta Q}{Q_{BW}}}) - \Delta P_{PRO}^{OPT})\, \mathrm{d}(A_M^{OPT}) \qquad (6.13)$$

where the superscript OPT represents the variable in the operations of optimum FC numbers. So, the required membrane area of the optimum operations can be obtained based on Equation (6.13) and the results are shown in Figure 6.9. The membrane area is estimated from the inlet to the area where the water flux decreased to 0.001 $L \cdot h^{-1} \cdot K^{-1}$. The results shown in Figure 6.9 is the minimal membrane area required per 1 g/L feed stream (seawater). From the Figure 6.9, with ϕ_h 0.6 and Y 0.1, the required membrane area is approximately 0.5 $m^2 \cdot L^{-1} \cdot h$. For instance, if the flow rate of feed solution (seawater) is 1 kg/s in practice, namely flow rate of brackish water 1.35 kg/s, about 1800 m^2 membrane would be required in PRO sub-system. Combining the results in Figs. 6.9 and 6.7(a), it is found that the required membrane area increases with increasing optimum FC. In order to reach a larger optimum FC number, a greater area of the membrane is required in a fixed RO water recovery ratio.

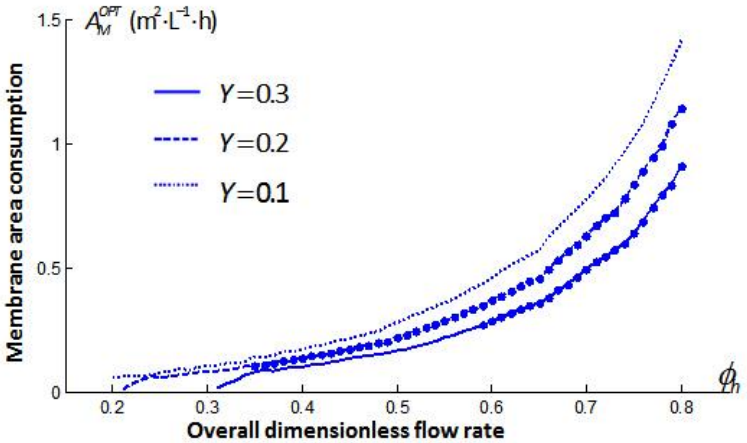

Figure 6.9: The required membrane area of the PRO subsystem in the operations of the optimum FC numbers

6.3.4 Energy performance of a stand-alone RO-PRO process

For a designed hybrid RO-PRO system, when Y_P and ϕ_h are maintained at selected values, different energy performance of the hybrid system can be obtained by adjusting RO water recovery, Y. A case study of $Y_P = 1$ and $\phi_h = 0.7$ is analysed and the results are shown in Figure 6.10 (a) in which work done the RO system considering the hydraulic energy recovery, and osmotic energy generated by the HT in the PRO system are included. The overall energy surplus of the hybrid system, $\Delta E_{Overall}$, which can be represented as, $E_{PRO-Generated} - E_{RO-Consumed}$. $E_{PRO\text{-}Generated}$ is the energy generated by the HT in PRO sub-system, and $E_{RO\text{-}Consumed}$ is the total energy consumed by the RO sub-system considering the hydraulic energy recovery. The results of the FC number are shown in Figure 6.10(b). Accordingly, if the energy difference is positive, the FC number satisfies $FC > 1$.

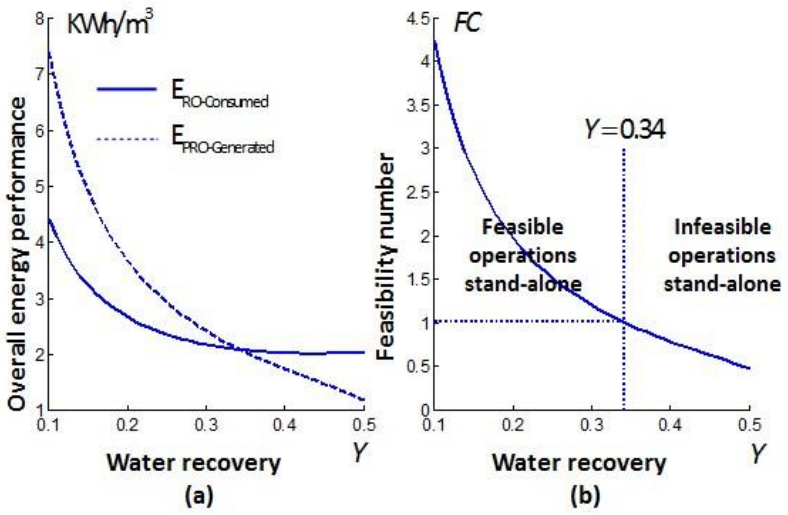

Figure 6.10: Energy performance of the stand-alone RO-PRO system with respect to different RO water recovery. Overall energy performance and feasibility number are shown in (a) and (b), respectively.

Figure 6.10(a) shows that both the energy consumed by RO considering recovered energy by ERD, and the energy generated by PRO decreases with the increase of RO water recovery. Furthermore, with the decreased overall energy surplus ($\Delta E_{Overall}$), the FC number decreases with respect to increasing RO water recovery. The limiting FC condition is achieved at Y = 0.34. In the range of RO water recovery between 0 and 0.34, the hybrid system can be operated stand-alone. For instance, with a RO water recovery value of 0.3 selected for a 10 m^3/day water production system, the power dynamic of the hybrid system

is shown in Table 6.1. In the table, the overall water recovery is the ratio of the flow rate of the permeation stream to the flow rate sum of the seawater and the brackish water streams.

Table 6.1 Energy performance of a case study of the stand-alone RO-PRO system with RO water recovery 0.3, overall dimensionless flow rate 0.7 and dimensionless water permeation 1. The system listed is under consideration of 10 m3/day capacity

Performance	Value	Representation by Area
Power generated by HT (kW)	1.0041	$S_{O\text{-}5\text{-}4\text{-}B}$
Power required by RO (kW)	0.9048	$S_{O\text{-}0\text{-}1\text{-}2\text{-}3\text{-}B}$
Work done by HP (kW)	1.6378	$S_{O\text{-}0\text{-}1\text{-}C}$
Energy recovered by ERD (kW)	0.7330	$S_{B\text{-}3\text{-}2\text{-}C}$
Overall energy surplus (kW)	0.0993	$S_{0\text{-}5\text{-}4\text{-}D}$-$S_{D\text{-}1\text{-}2\text{-}3}$
Overall water recovery	0.1139	
FC number	1.2021	

6.4 INFLUENCING FACTORS OF EFFICIENCY OF THE COMPONENTS AND SALINITY OF THE STREAMS

6.4.1 Effects of efficiency of pumps and energy recovery devices

The efficiency of all the components has so far been assumed to be 100%. In practice, however, this is not the case. In the hybrid RO-PRO process, if the efficiency of HP, η_{HP}, efficiency of ERD, η_{ERD}, and efficiency of HT, η_{HT} are considered, the work done by the RO, the power generated by the PRO and the FC number can be rewritten as

$$\dot{W}_{RO} = \frac{Q_{SW}\Delta P_{RO} - \eta_{ERD} Q_{CW}(\Delta P_{RO} - \Delta P_{PRO})}{\eta_{HP}} = \frac{Q_{SW}\Delta P_{RO} - \eta_{ERD} Q_{SW}(1-\mathrm{Y})(\Delta \mathrm{P}_{RO} - \Delta P_{PRO})}{\eta_{HP}} \tag{6.14}$$

$$\dot{W}_{HT} = \eta_{HT} Q_D \Delta P_{PRO} = \eta_{HT}((1-\mathrm{Y})\mathrm{Q}_{SW} + \Delta Q)\Delta \mathrm{P}_{PRO} \tag{6.15}$$

$$FC = \frac{\Delta P_{PRO}[(1-\mathrm{Y})(\eta_{HT} - \frac{\eta_{ERD}}{\eta_{HP}}) + \mathrm{Y}_P]}{\Delta P_{RO}[\frac{1-\eta_{ERD}(1-\mathrm{Y})}{\eta_{HP}}]} \tag{6.16}$$

The effects of the inefficiency of the pumps and ERD is considered in the previous case study of the hybrid RO-PRO system with dimensionless water permeation of 1 and overall

dimensionless flow rate of 0.7. Two categories of efficiencies are considered and the results are presented in Figure 6.11. It is observed that the inefficiency reduces the extra energy gained by the hybrid system and shortened the feasible region of the stand-alone condition. This means that the feasible range of RO water recovery is shortened significantly or becomes unavailable, and the power surplus also decreases. In fact, the inefficiency drives the hybrid system to more consumption of the RO subsystem and less generation from the PRO system. As a consequence, the decreased energetic performance requires larger water permeation and corresponding more available volume of feed solution. As such in Figure 6.11, the red curve with larger Y_p and ϕ_h values has a larger overall energy surplus (a greater FC number) and a larger domain of stand-alone feasible operation. After all, for the purpose of achieving stand-alone feature in consecutive operations in practice, the high efficiency of the pumps and ERD is preferred.

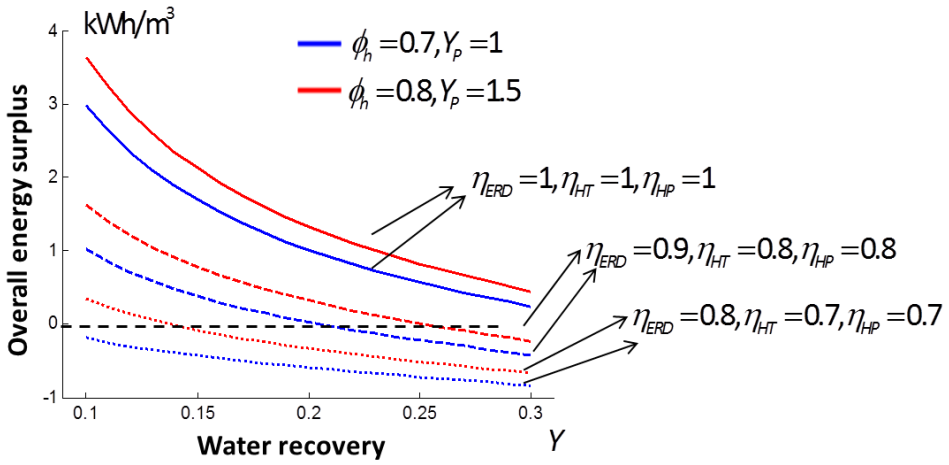

Figure 6.11: The energy performance of the case study with respect to the efficiency of the pumps and ERD.

6.4.2 Effects of the concentration of the saline streams

For a salinity power driven SWRO system by the PRO technology, the concentration of the feed solution affects the performance of the salinity power generation. Previously, in this chapter, the feed solution is assumed as the brackish water whose concentration is high in the potential feed solutions. In fact, the smaller concentration of the feed solution, the larger net driving force of the water permeation achieved, improving the salinity power generation. In fact, the pre-treated sewage and wastewater from the household and industries have much lower salts concentration. Because of the negligible difference

between the concentrations of the freshwater and the wastewater, the expected performance of the PRO will be significantly improved thanks to the enhanced water permeation. But the fouling propensity of the membrane using reclaimed wastewater is also enhanced. In order to prolong the lifetime of the membrane and maintain the system performance, reclamation of the wastewater specified for the PRO osmotic energy generator should be studied, such as bio-fouling and possible contaminants in the wastewater. Therefore, two kinds of feed water are studied and the results of the reversible PRO process are shown in Figure 6.12. The two feed solutions represent the brackish water and the freshwater or wastewater (with the same concentration of freshwater) from private households and industries. And the dimensionless water permeation Y_P is 1. The figure shows that the feed solution with lower concentration requires lower overall dimensionless flow rate and achieves larger FC number. This means that the stand-alone hybrid RO-PRO system is capable of desalinating more seawater with less usage of the dilute stream.

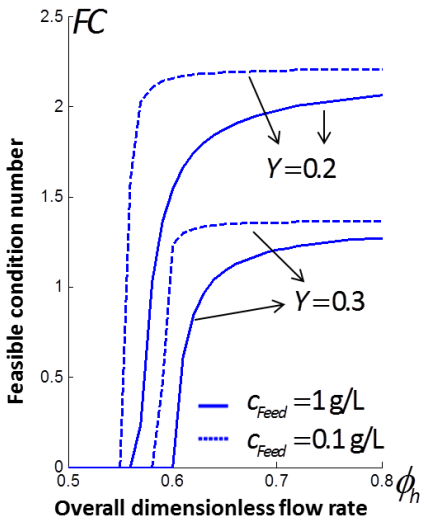

Figure 6.12: The energy performance of the case study with respect to the concentration of the saline streams.

The system is based on module design. An appropriate size of the module system is designed and the scale-up of the whole plant can be achieved by increasing the number of the modules. Furthermore, in order improve overall performance of the system, optimisation of both components and system need to be developed. Components, such as membrane module, pump, turbine and pressure exchanger, significantly influence the

osmotic energy generation. Also, how to design an appropriate configuration subject to the available salinities' condition is also essential.

6.5 SUMMARY

A hybrid RO-PRO system is investigated to find a possible solution of the stand-alone salinity power driven desalination process. First, a thermodynamic analysis of the saline streams using P-Q and P-π plot is presented (Figure 6.2). Based on the analysis, a methodology to determine the stand-alone feasibility of the hybrid system is developed mathematically including the feasible constant that represents the availability of the stand-alone RO-PRO, zero brine discharge constraint and other variables restricted in practice. Secondly, an investigation into the PRO subsystem is developed to study its required operations. Finally, a case study of the possible operation is validated and two influencing factors, the efficiency of the components and the salinity of the feed water, are discussed. Based on the results obtained, the following conclusions can be drawn: 1) The stand-alone feasibility of the hybrid RO-PRO can be determined by checking the value of the FC number; 2) The dimensionless water permeation Y_p is proportional to the overall dimensionless flow rate ϕ_h in order to increase the FC number at certain RO water recovery Y ; 3) Lower RO water recovery and higher ratio of the PRO feed volumetric flow rate to the combined PRO feed and draw flow rates improve the stand-alone feasibility of the hybrid system and the feasible range of the dimensionless water permeation; 4) For the same water recovery of the RO system, higher applied hydraulic pressure, but lower membrane area, is required to achieve the optimum FC numbers at the lower dimensionless water permeation rates; 5) With the decrease of the pump efficiency the FC number of the hybrid system reduces and the feed solution with lower concentration benefits the system in higher FC number and larger feasible operation.

STAND-ALONE SEAWATER REVERSE OSMOSIS (RO) DESALINATION POWERED BY PHOTOVOLTAIC (PV) AND PRESSURE RETARDED OSMOSIS (PRO)

7.1 INTRODUCTION

Renewable energy powered RO desalination and the optimum operation management have been widely reported literature [131-136]. Among the renewable energy powered RO desalination applications, stand-alone PVRO plant has been demonstrated to be feasible both in terms of techniques and costs in lab-scale and pilot-scale systems [20, 137-139]. At present, it is considered as a proper solution for small-scale desalination applications in rural areas with high solar insulation [140]. The effectiveness of the stand-alone plant depends on the location, geographical conditions, topography of the site, and the capacity of the plant. Bilton et al. presented a generalised methodology to evaluate the feasibility of

small-scale PVRO systems in challenging environment [141]. Their findings indicate that the freshwater cost of PVRO is economically feasible for most remote areas with high availability of solar energy [142]. Fraidenraich et al. proposed a simple and general theoretical procedure for estimating the SEC to evaluate feasibility of a PVRO plant and validate the methodology with experiments [143]. During the last decade, with the significant development in optimal designs [144, 145] and control strategies [146, 147] for PVRO plants, the cost of freshwater has considerably reduced. However, the sunshine is not available at night. In order to prolong the operational hours, and to increase the renewable energy supply, alternative power sources need to be identified and integrated to the designs for night time operation. Previous investigations have focused on a hybrid system combining solar and wind energy to power RO desalination processes [148, 149]. An estimation of energy and water production during a large-scale time frame from photovoltaic-wind hybrid system coupled with RO desalination unit was developed based on the local solar and wind data [150]. Their results demonstrated the appropriation of the proposed hybrid system to produce water from brackish water (6 g/L) in southern Tunisia. Novosel et al. evaluated the impact of desalination in combination with water pump storage and penetration of wind and solar energy [151]. The analysis of the case study in Jordan demonstrated that the integration of water and renewable energy generation could provide a real benefit to the country water supply, energy security and ecology [151]. Recently, osmotic energy from water with different salinities has emerged as a viable alternative. Compared with other renewable energy sources, osmotic energy is less periodic and has no significant operational hazards. It therefore has the potential to formulate a hybrid energy system to supplement the power supply. However, as suggested in the literature, no research has addressed the potential integration of the salinity energy with other renewable energy sources. Thus, this chapter aims to investigate the integration of salinity power and solar power and to identify the optimum operations of this hybrid renewable system in a desalination application.

Although Chapter 6 has focused on the theoretical feasibility salinity energy powered RO desalination plant, it is still a challenge to develop the stand-alone salinity power driven desalination based on the current PRO membrane performance. Moreover, the detrimental effects, namely ICP, ECP and RSP, and the energy losses caused by the pressurisation and de-pressurisation machines decrease the performance of PRO process and these effects aim to be considered in the chapter. In fact, to deal with the problems in a stand-alone

renewable energy powered system, a hybrid renewable energy source is a promising solution [152-154]. There are a large number of examples of stand-alone renewable energy powered systems at off-grid locations. An experimental study of hybrid energy generation including PV, wind emulator, battery, and controller was constructed and demonstrated to be capable to operate stand-alone mode and grid-connected mode [155]. A work of the solar PV and the solar/hydro schemes for rural electrification was evaluated and shown to be more reliable and sustainable than the use of a diesel genset [156]. A similar application for off-grid rural electrification by hybrid diesel power plant with high-penetration renewable and compressed air energy storage was also found in literatures [157]. Moreover, optimum design and control of the integrated PV and wind powered RO desalination plant was illustrated by a series of simulations to demonstrate applicability and effectiveness [158, 159]. Therefore this chapter focuses on investigating the hybrid solar-salinity energy supply in a RO desalination application to improve the freshwater production. In fact, the hybrid solar-salinity power generation has several advantages: i) the salinity power improves the energy efficiency of the solar powered system by the recovery of osmotic energy during daytime and by prolonging the operational hours over night through salinity power harvest; ii) the solar power helps improve the total water production of the hybrid RO-PRO system by providing external power to compensate the lack of commercially high performance PRO membrane in osmotic energy extraction currently in practice. Therefore, in the hybrid system, the stand-alone feasibility can be realised by two operations: hybrid power source of salinity power from PRO and solar power from PV array during daytime, and only salinity power at night. With the osmotic energy generation, more freshwater can be treated under the available solar radiation. Conversely, at lower RO water recovery, salinity power generated by PRO is potentially capable to sustain continuous operation when the sun is unavailable. Such integration of power supplies ensures that the desalination plant meets the demand for the freshwater production. To this end, a study on the stand-alone RO desalination plant powered by PV and PRO is developed in this chapter. First, the hybrid plant is proposed and thermodynamically analysed using a state-diagram. Following this, the stand-alone feasibility of the plant is studied and derived mathematically. Based on the models, the performance of the RO plant and the entire hybrid system is evaluated. The feasible operational windows of the two operations are identified and discussed. Finally, with the known hourly solar data available for Perth, Australia, over duration of a year, a case study of the proposed hybrid powered RO desalination is presented.

7.2 STAND-ALONE SEAWATER RO DESALINATION PLANT POWERED BY HYBRID SYSTEM OF PV AND PRO

A proposed stand-alone solar-salinity power driven RO desalination system is illustrated in Figure 7.1 and it shows the three main sub-systems in this hybrid plant. The hybrid system consists of RO desalination and renewable power generation including solar and salinity power; the two parts are closely interacted. The renewable energy generation supplies the power to the desalination plant and the brine from the RO desalination is the source of the chemical potential for salinity power generation. In operations of solar-salinity powered RO (SSRO) during daytime, both the PV array and the PRO plant are working to generate electricity. In contrast, at night in operations of salinity powered RO (SRO), only the PRO plant is working. In Figure 7.1(b), the detail diagram of the hybrid plant is plotted. seawater is pressurised by a HP and a hydraulic ERD before it flows into a RO membrane module. The HP is driven by the induction motor. The freshwater is produced from the seawater in the RO plant. Accordingly, two streams flow out from the RO module: the permeation and the brine. The brine is further used to pressurise the seawater in the ERD before it flows into the PRO plant, and the permeation is the product of the hybrid system.

In another sub-system, the solar power is harvested by solar PV technology and the salinity power is generated by the PRO plant. In this chapter, impaired water (IW) is selected as the feed solution for the early-stage investigation. In order to overcome the pressure loss along the flow channel, the IW is pressurised by a BP which is also driven by the induction motor. Finally, the draw solution including the permeated water from the PRO feed solution is expanded in a HT to generate electricity. Both renewable energy generators, the PV array and the PRO plant, are interconnected to an AC bus through DC/DC/AC and AC/DC/AC converters. For simplicity, the efficiencies of all the converters and motors are assumed to be 100%.

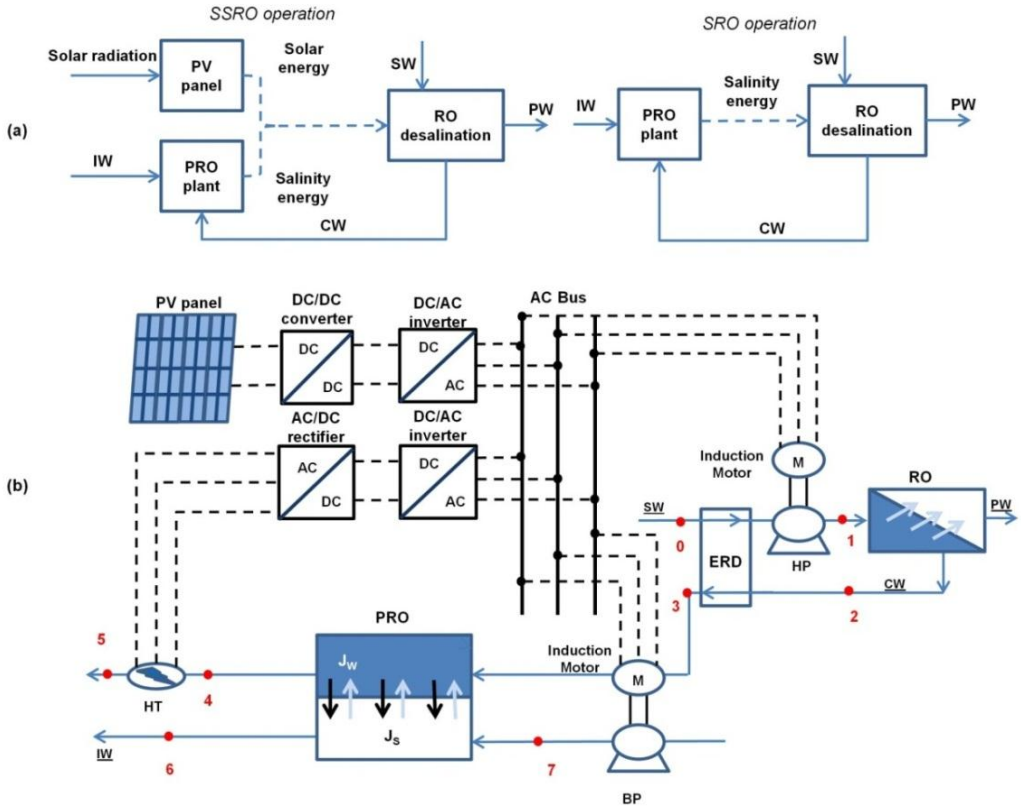

Figure 7.1: Illustration of two operations in the proposed solar-salinity power driven RO desalination plant is presented in (a) and schematic diagram of the solar-salinity power driven seawater RO desalination plant is presented in (b).

7.2.1 Thermodynamic analysis of the stand-alone salinity-solar power driven seawater RO plant

Before further analysis of the hybrid system, some key states of the saline streams are presented in the pressure-flow rate (P-Q) diagram as illustrated in Figure 7.2. As can be seen from the diagram, the pressure loss in the membrane and flow channels is negligible compared with the hydraulic pressure applied on the saline streams. So the applied pressure is considered as constant. Also, it is assumed that no fouling or membrane deformation is occurred. And because a very small amount of energy is used by the BP compared to the energy consumed by the HP, in this study, the energy consumption is only considered as the work of the HP in the RO sub-system.

Similar to the thermodynamic analysis in Chapter 6, in the P-Q diagram, the energy consumption by the RO plant and the energy generation by the PRO plant can be represented by the areas illustrated in Figure7.2, i.e., the energy consumed can be

represented by the area O-0-1-C, the energy recovered by ERD can be represented by the area 3-2-C-B and the energy generated by the PRO plant can be represented by the area O-5-4-B. These areas are determined by the specific states of the saline streams, namely states 2, 4 and 5 in Figure 7.2. Moreover, these states of the saline streams can be controlled by the operations of the RO and PRO plants. Other states are usually determined by the local conditions or/and RO thermodynamic restrictions [124]. Therefore, this 'salinity cycle' has similar attributes as the classical thermodynamic cycles by changing states of the salinity concentration and due to the integration of the solar PV, the selection of the salinity states becomes more flexible.

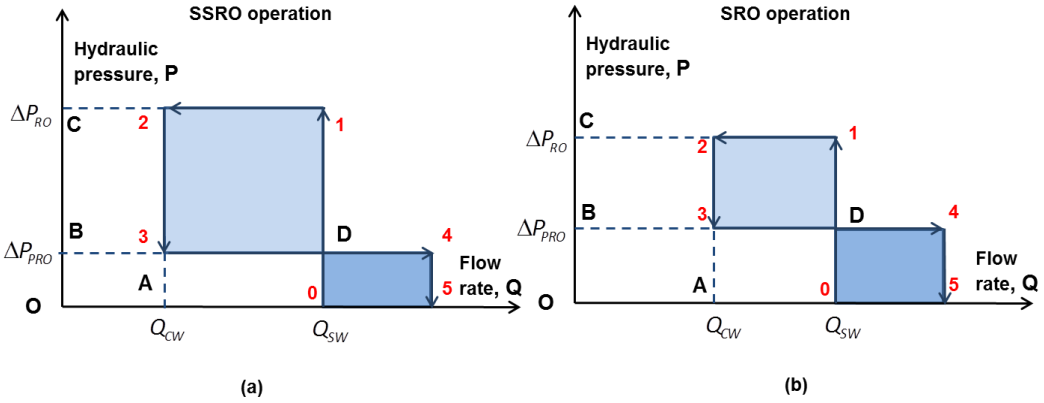

Figure 7.2: Thermodynamic analysis of the hybrid salinity-solar power driven RO desalination plant in hydraulic pressure and flow rate diagram, P-Q diagram. Two operations, SSRO operation and SRO operation, are plotted in (a) and (b), respectively.

Two operational strategies in this hybrid power system are hybrid power of salinity and solar and stand-alone salinity power, namely SSRO and SRO operation. In the SRO operation, without the solar energy harvesting, the overall energy surplus between the generation and consumption by the hybrid system can be represented as the difference between the areas D-1-2-3 and 0-5-4-D. In contrast, in SSRO operation, the overall energy surplus includes the electricity generated from the PV array. Therefore, the overall energy surplus can be represented as

$$\begin{aligned} \Delta E^{SSRO} &= E_{PV} + E_{PRO} - W_{RO} \\ \Delta E^{SRO} &= E_{PRO} - W_{RO} \end{aligned} \tag{7.1}$$

where E_{PV}, is the energy generated from the PV array. If the overall energy surplus is non-negative, theoretically, the hybrid system can be operated as stand-alone. Otherwise, the hybrid system needs an extra power source to cover the exceeding energy consumption. Therefore in the hybrid system, the stand-alone feasibility is determined by the states of

the streams and the availability of the solar irradiation. In the SSRO operation, due to the availability of the solar PV power, more freshwater can be separated from the saline stream as illustrated in Figure 7.2(a). Thus, it allows higher applied hydraulic pressure in RO, and the energy consumption in the RO plant is higher than the energy generated by the PRO plant. In contrast, without the solar PV power, the stand-alone feasibility of a RO desalination plant with osmotic energy generation by the PRO plant can be realized by operating it at a lower water recovery ratio. In such an operation, the energy consumption by the RO plant is fully covered by the energy generation of the PRO plant. As illustrated in Figure 7.2(b), at the limiting condition of the SRO operation, the area 3-D-1-2 equals to the area 0-5-4-D.

7.2.2 RO and PRO membrane process

The mathematical model describing energy consumption of RO and osmotic energy generation of PRO membrane process are derived in Chapter 6. The mathematical models and the framework for modelling a process considering the CP and RSP effects are presented in Chapter 3. Generally, during the mass transfer in a real PRO, the water permeates across the membrane. On one hand, the feed solutes are selectively retained by the active layer and accumulated in the support layer, resulting ICP. On the other hand, the permeated water dilutes the draw solution near another side of membrane active layer and causes ECP. In addition, RSP exists because of the non-perfect rejection of the current PRO membrane.

7.2.3 Solar PV array

Datasheets of a PV array provide the information of the performance of PV devices with respect to standard test condition (STC), namely irradiation 1,000 W/m^2 with an ambient temperature of 25 ^{o}C (298 K). However, practical PV arrays are not always operated at STC. The performance of a PV array depends on the solar irradiation level and the ambient temperature. In this study, single-diode model of a PV array is used to find the non-linear current-voltage equation with the parameters from the product datasheet. In the single-diode PV model, the effect of the series and parallel resistances are considered and it is warranted that the maximum power of the model matches with the maximum power of the real array [160]. The current-voltage ($I-V$) characteristics of the single-diode PV cell is given by [161]

$$I = I_{PV} - I_0[\exp(\frac{\mathrm{V}+\mathrm{R}_S I}{V_t a}) - 1] - \frac{V + R_S I}{R_P} \quad (7.2)$$

where I_{PV} and I_0 are the PV and saturation currents of the array, respectively. V_t is the thermal voltage of the array and is given by $V_t = N_S kT / q$. N_S is the number of cell connected in series, k is the Boltzmann constant (1.3806503×10^{-23} J/K), q is electron charge (1.60217646×10^{-19} C), T is the temperature. R_S and R_P are the equivalent series and the parallel resistance of the array, respectively. Detailed derivation and numerical algorithm to adjust the $I-V$ mode can be found in [160]. The technical data of solar array Bosch M2453BB used in this work is listed in Table 7.1.

Table 7.1 The technical data of solar array Bosch M2453BB

Short-circuit current [A], I_{SC}	8.7	**Nominal output [W],** P_{mpp}	245
Open-circuit voltage [V], V_{OC}	37.7	**Voltage/temperature coefficient [V/K],** K_V	-0.1206
Nominal current [A], I_{mpp}	8.2	**Current/temperature coefficient [A/K],** K_I	0.0028
Nominal voltage [V], V_{mpp}	30.1	**Number of series cell,** N_S	60

7.3 STAND-ALONE SALINITY-SOLAR POWER DRIVEN RO DESALINATION PLANT

7.3.1 Stand-alone solar PV powered RO desalination plant

Works investigating the SEC in steady-state operation of the RO plant are available in the literature [17, 120, 162]. But different from the RO plants powered by the electric grid in which the power input is constant, PV powered RO plants are operated along a large variety of power supplies subject to the availability of intermittent solar energy. To deal with the intermittent power input, operation of the RO plant is needed to change for the high effectiveness. The SEC performance of the RO plant has been investigated in previous studies [17, 162]. The outcomes of the SEC of the RO plant operated at thermodynamic restriction with hydraulic energy recovery are shown in Figure 7.3(a) in which three sets of the efficiencies of devices in the RO plant are considered, including the HP and the ERD.

The inefficiency of the devices shifts the monotonically ideal SEC profile and the inefficiency increase of the devices increases the SEC. In the ideal case with devices of 100%

efficiency, the lowest SEC occurs and the SEC increases with the increase of the water recovery in all the range of the ratio studied. In contrast, in the cases with real devices which are not 100% efficient, the profile of the SEC has a minimum among the water recovery ratio. The reason is that at very low water recovery, the energy loss due to the inefficient HP and ERD is relatively large. And hence, the optimum SEC moves to the high water recovery ratio. For instance, the solid line representing the HP efficiency 85% and the ERD efficiency 95% has the optimum SEC approximately 1.3 in the water recovery around 0.18. Actually, the thermodynamic restriction operation is the limiting case when the high permeable membrane or/and sufficient area of the membrane is used. In practice, the higher SEC is required when the operation of the RO plant does not meet the thermodynamic restriction (non-thermodynamic restriction). For instance, based on the ε-MTU model of the RO plant, with the membrane permeability 3.61×10^{-6} kg m^{-2} kPa^{-1} s^{-1}, flow rate of feed solution 1 kg s^{-1}, and area 100, 200 and 300 m^2, the SEC is presented in Figure 5(b). The efficiency of the HP is 90%, and efficiency of the ERD is 98%.

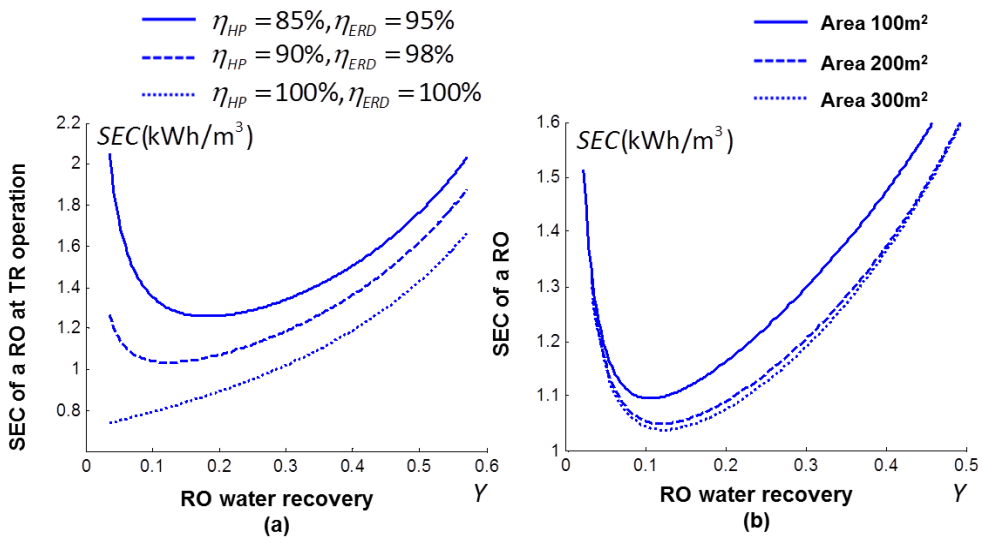

Figure 7.3: SEC profile of the RO plant. The SEC profiles of the RO operated at the thermodynamic restriction condition are presented in (a). The SEC profiles of the RO plant with different membrane area usage are shown in (b).

In Figure 7.3(b), the results clearly indicate that the profiles of the SEC are different with different areas. For areas 100, 200 and 300 m^2, less the area requires, more the SEC in RO desalination. The optimums of the SEC are shifted towards the lower water recovery ratio with the decrease on the membrane area. In addition, comparing the profile of area 300 m^2 with the SEC profile of a thermodynamic restriction RO plant in Figure 5(a) with the devices with same efficiency, it is found that the profile of area 300 m^2 approximately have the

same values in all the range of water recovery. Consequently, in this case, with the usage of 300 m^2 area, the thermodynamic restriction operation of the RO can be achieved.

Based on the results shown in Figure 7.3, with different parameters (conditions and usages of devices and membrane), the RO plant performs differently. But at each fixed condition, a minimum SEC can be found, thus the RO plant can be operated optimally. To this end, to deal with the variable load from the solar PV array, the flow rate of the feed solution can be adjusted to ensure that the RO plant is operated most efficiently with respect to energy consumption. Thus, in a PVRO plant (operation with thermodynamic restriction and non-thermodynamic restriction), with certain power supply from the solar PV array, the maximum water production rate can be expressed as

$$q_P^{MAX} = \frac{E_{PV}}{SEC^{MIN}} \tag{7.3}$$

where SEC^{MIN} denotes the minimum SEC of the RO plant and q_P^{MAX} is the maximum water production under certain solar energy supply, E_{PV}.

Previous studies have investigated the operation of RO plants under variable-load and suggested that the RO desalination plant can operate successfully under varying flow rate and pressure without any technical problems [20, 138]. In addition, it has been pointed out that relatively short time is needed for the transition from one steady state to another steady state for a RO process [122]. Therefore, it is practical to study the RO plant in this work with the hourly data of solar irradiation and ambient temperature. In this work the optimal strategy of the PVRO plant is to control the flow rate of the feed solution and the pressure, ensuring that the RO plant is operated at the available minimum SEC state.

7.3.2 Dynamics of the hybrid RO-PRO system

When the osmotic energy recovery is considered in the RO desalination plant, the net SEC (SEC_{net}) that is the overall SEC considering the specific energy generation in the PRO plant, can be expressed as

$$SEC_{net} = \frac{W_{RO} - E_{PRO}}{Q_{PW}} \tag{7.4}$$

Based on equations of energy consumed by the RO plant and energy generated by the PRO, the net SEC can be obtained. In the salinity energy harvesting by the PRO, the CP and RSP

cannot be avoided in real applications. As a result, with the reduced energy generation in the PRO, the net SEC is increased. According to the framework of simulating the CP and RSP effect in salinity energy generation as presented in Chapter 2, the net SEC considering the overall detrimental effects in the PRO plant and the reduced performance can also be obtained. The results of the optimum net SEC of the RO desalination plant with the osmotic energy generation are presented in Figure 7.4(a). The optimum net SEC of the RO-PRO plant without the CP and RSP is obtained through the maximum salinity energy harvest from the mixture of brine and IW by applying the optimum hydraulic pressure on the brine [32]. The optimum net SEC of the RO-PRO plant considering the CP and RSP effects is numerically obtained. The parameters used in the simulations of the salinity power harvest by the PRO are: water permeability 1.74 L m^{-2} $h^{-1}$$bar^{-1}$, salt permeability 0.16 L m^{-2} h^{-1}, and structural parameter 307 μm. Other parameters used are same to those used in Chapter 3. The efficiency of the HP is 90%, efficiency of the ERD is 98% and efficiency of the HT is 90%.

The results clearly indicate that the optimum net SEC of RO desalination with osmotic energy recovery by the PRO is significantly decreased compared to that of the SEC of the RO plant without osmotic energy recovery. Furthermore, the detrimental effects raise the optimum net SEC in all studied RO operations. Considering the CP and RSP effects, less the osmotic energy is generated from the PRO plant, more the net SEC is required.

At the lower range of the water recovery, the negative net SEC indicates that the salinity power generated by the PRO is larger than the energy consumed by the RO. Therefore, the operations at RO water recovery ratios with non-positive optimum net SEC are the feasible operations for the SRO operation of the hybrid plant. In Figure 7.4(a), the feasible operational window for the SRO operation is O-B-E-C and considering the detrimental effects the feasible operational window becomes O-A-D-C. Moreover, with the increase of the RO water recovery, the optimum net SEC increases as well. In the range of the water recovery ratio with positive optimum net SEC, the osmotic energy generated by the PRO cannot fully cover the energy consumed by the RO desalination. The power shortage can be supplemented by the energy from solar PV array in the proposed hybrid system. Thus, these RO water recovery ratios belong to the SSRO operation. Under the constrained range of the RO water recovery, from 0.1 to 0.5, in Figure 7.4(a), the maximum feasible operational window of the SSRO operation is restricted by the window E-F-H-G for the ideal PRO salinity harvest and by the window D-F-J-I for the PRO salinity harvest considering the CP and RSP effects.

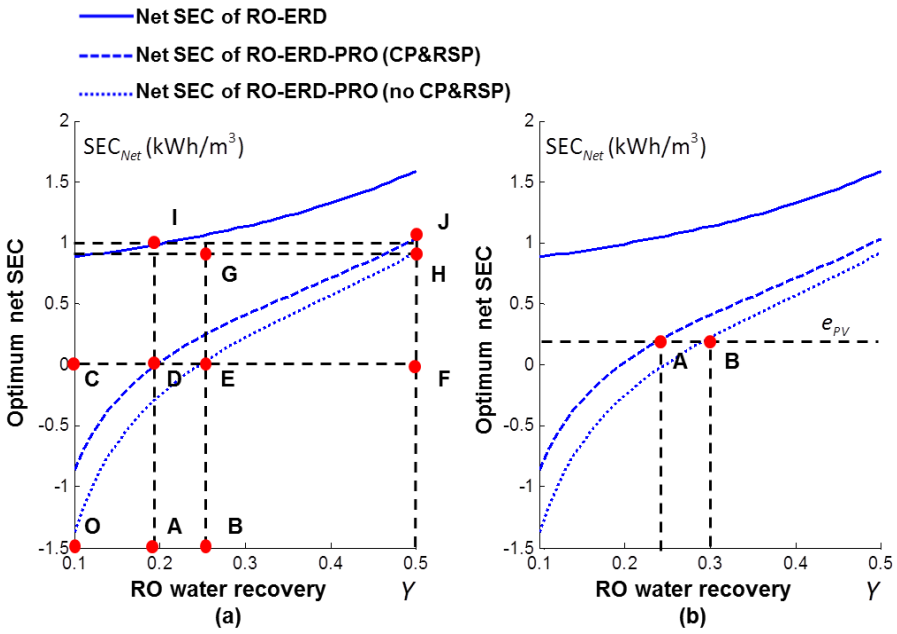

Figure 7.4: SEC profiles of RO desalination with osmotic energy recovery by PRO. Two operations, SRO operation and SSRO operation, are shown in (a) and (b), respectively.

The upper and lower limits of the feasible operational windows are determined by different factors in the two operational schemes. In the feasible operational window of the SRO operation, the lower limits of both operations with or without the CP and RSP effects are restricted by the lowest RO water recovery ratio. But the upper limits are different due to the performance limiting effects. The upper limit is significantly decreased when the CP and RSP effects are considered. Conversely, theoretically the lower limit of the SSRO operation is the upper limit of the SRO operation in both cases. The upper limit depends on the specific available solar power per unit production water, $e_{PV} = E_{PV} / V_{PW}$. If the required water recovery by the specific available solar power is lower than the maximum water recovery ratio studied (0.5), the upper limit of the SSRO operation is the required water recovery ratio by the specific available solar power. Otherwise, with the enough energy from the PV array, the upper limit is restricted by the maximum water recovery 0.5. One specific SSRO operation with a certain specific solar power is illustrated in Figure 7.4(b). The upper limit of the RO water recovery is less than 0.5, namely state A for the PRO salinity extraction considering the CP and RSP effects and state B for the ideal PRO salinity extraction.

Actually, similar to the PVRO plant, the water is needed to be optimally produced by the PVROPRO plant. The optimum operation of the SRO and SSRO schemes are achieved at

their upper limits of the RO water recovery ratio. From the perspective of the optimum operation, the detrimental effects reduce the upper limit of the RO water recovery ratio in both the SRO and SSRO schemes. In Figure 7.4(a), in the window of the SRO operation, the optimum operation of the RO with ideal PRO power generation is the state E, whilst the optimum is state D due to the real CP and RSP effects. In the SSRO operational window, under certain specific available solar power (e_{PV}), the upper limit is also further restricted by the detrimental effects as illustrated in Figure 7.4(b). The optimum operation of the RO with ideal PRO power generation is the state B. In contrast, the optimum ratio is reduced to state A due to the real CP and RSP effects. The resulting lower maximum water recovery ratio, accordingly, causes the lower water production rate at the constant flow rate of the seawater or the higher required flow rate of the seawater to produce a certain volume of the permeation.

7.3.3 Simulation framework of the stand-alone salinity-solar power driven RO desalination plant

A flow chart illustrating the simulation framework is shown in Figure 7.5. In order to simulate the PVROPRO hybrid power desalination plant, several inputs are needed, including the input parameters of the system and the environmental data of solar and salinity. The input parameters of the PV array are the efficiency of the PV panel which is 15% and the number of the PV panels which is 20. The parameters of the PRO membrane are the same as that in Section 7.3.2. The RO plant is assumed to be operated at the thermodynamic restriction operation. The yearly data of solar irradiation and ambient temperature of Perth, Australia is provided by Meteonorm 7 software [163] and used in this study for a case study of the proposed hybrid power RO desalination plant. The concentration of seawater is 35 g/kg and the concentration of the IW is assumed to be 0.1 g/kg.

In the simulation, firstly the performance of the stand-alone PVRO plant is evaluated. The PVRO plant is optimised to find the appropriate flow rate of the seawater to ensure the minimum SEC. Then, with the same devices (e.g. HP pumps) within the PV array and the RO plant, the proposed hybrid powered RO desalination plant is modelled. The same pumps implementation denotes that the maximum flow rate in the PVROPRO plant is restricted by the maximum flow rate in the PVRO plant. In the simulation, the solar PV power generation is assumed to be operated with maximum power point tracking that the available

maximum power is supplied to the desalination plant under certain environmental condition.

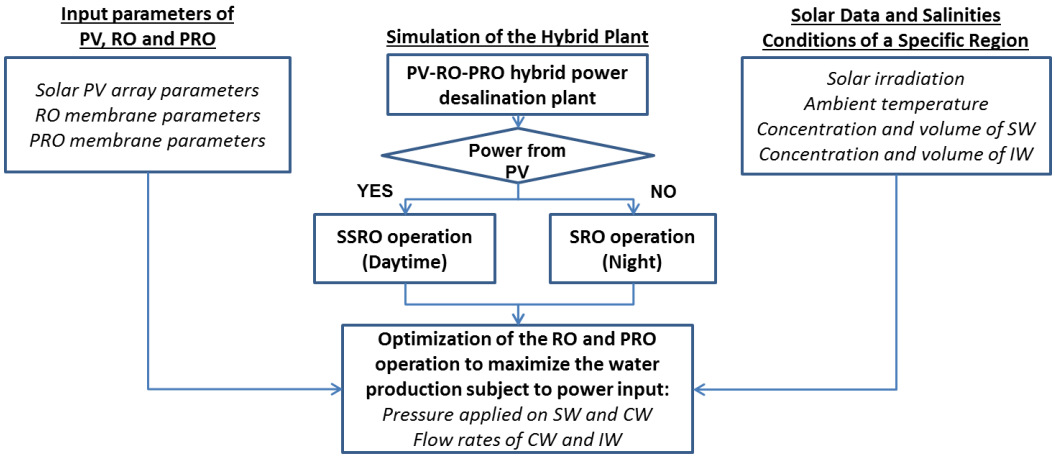

Figure 7.5: Illustration of the simulation framework.

7.4 RESULTS AND ANALYSIS

A stand-alone RO desalination plant powered by PV array is first modelled with predefined parameters. The RO plant is operated at its minimum SEC, and then the maximum water production is obtained under certain level of solar PV power based on Equation (7.3). In addition, with the same scale of flow rate of the seawater used in the PVRO plant, the hybrid solar-salinity powered RO desalination plant is modelled. Because the stand-alone feasibility of the hybrid solar-salinity powered RO desalination system depends on the relation between the flow rates of the seawater and the IW, another advantage of the PVROPRO plant is that it can be operated at a larger seawater flow rate if the volume of IW is sufficient. In this chapter, the total dimensionless flow rate which is the ratio of the IW flow rate to the sum of the seawater and the IW flow rate is assumed as 0.5 in modelling both the processes with and without osmotic energy generation. The flow rate of the seawater is selected as the maximum flow rate of the seawater required in the stand-alone PVRO plant. Thus, the same flow rate of the IW is required to meet the predefined overall dimensionless flow rate. In both the SSRO and SRO schemes, the maximum RO water recovery ratio can be obtained by solving Equation (7.1) with the limiting zero overall energy surplus. Moreover, the effects of the CP and RSP are investigated with the same flow operation, namely the flow rate of the seawater and the IW.

7.4.1 Overall optimum production rates of the permeation

The objective is to maximise the flow rate of permeation in the PVRO and the PVROPRO plants. With hourly PV solar power calculated, both the SSRO and SRO operations are optimised. During the search, with the step-size of the RO water recovery ratio 0.01 (1%), all the operations in the range of RO water recovery (0.1 – 0.5) are calculated and compared. Then, the hourly optimum RO operation for the maximum water production is obtained. The results, as presented in Figure 7.6, show the increased water production by the osmotic power generation and the water reduction due to the CP and RSP effects. These two influences are represented by the relative permeation increase and decrease, respectively, which are defined as

$$q_{PW}^{+} = \frac{q_{PW}^{PVROPRO} - q_{PW}^{PVRO}}{q_{PW}^{PVRO}}; \qquad q_{PW}^{-} = \frac{q_{PW}^{PVROPRO} - q_{PW}^{PVROPRO,CPRSP}}{q_{PW}^{PVROPRO}} \tag{7.5}$$

where q_{PW}^{+} and q_{PW}^{-} are the relative permeation increase due to osmotic energy generation and the relative water decrease due to the CP and RSP effects in PRO salinity power harvest, respectively. q_{PW}^{PVRO}, $q_{PW}^{PVROPRO}$, and $q_{PW}^{PVROPRO,CPRSP}$ are the flow rates of the permeation in the stand-alone PVRO plant and the stand-alone PVROPRO plant with and without the detrimental effects.

The results clearly indicate the dependence of the permeation flow rate on the available PV solar power. The water production rate varies with respect to different solar power availability in both the PVRO and PVROPRO plants. However, with the salinity power generation, the permeation water production rate is considerably increased and less fluctuated. Comparing Figure 7.6(a) and 7.6(b), the hourly production rate of the PVROPRO plant is much larger than that of the PVRO plant. In the PVROPRO plant, due to the salinity power generation, the desalination plant can be operated continuously. In the SRO operation, a constant water production is achievable at the upper limit of the RO water recovery as shown in Figure 7.4(a) (state E). In addition, during daytime, with the available solar power, more permeation can be treated in the stand-alone desalination plant as illustrated in Figure 7.4(b) (state B). The relative permeation increase is presented in Figure 7.6(c) with respect to weekly permeation production. The results show significant increase in permeation production due to incorporation of the salinity power harvesting technology

in the PVRO desalination plant. It is observed in Figure 7.6(c) that, the permeation production rate of the most improved week is almost 20 times the rate in PVRO plant. On average, the yearly permeation production of the PVROPRO plant is increased more than nine times the stand-alone PVRO plant. Furthermore, the profile of the relative permeation production increase shows that the more increase occurs when the permeation rate in the PVRO plant are less, i.e. hour 4000 – 5000 in Figure 7.6(a) and week 20 – 30 in Figure 7.6(c). Because there was less irradiation in magnitude and shorter daytime during such periods in the year, the PV solar power is reduced. Simultaneously, the continuous osmotic power generation which is less periodic, plays a more important role to sustain the plant when the solar PV power is relatively lower.

When the overall performance limiting effects in PRO salinity energy harvest are considered, the salinity power generation decreases. Thus, the overall permeation production of the hybrid desalination decreases as well. The weekly relative permeation decrease is shown in Figure 7.6(d). According to the simulations with the membrane studied, the weekly permeation production rates are decreased in the range of 16-20%. Annually, the overall permeation production is reduced by 18.07% due to the CP and RSP effects. In addition, it is found that the most significant reduction also occurs when the solar power is less. In the SSRO operation, the optimum RO water recovery ratio is lower when the solar power is less. And for the proposed hybrid desalination plant, lower RO water recovery rate causes more energy loss due to the detrimental effects. As shown in Figure 7.4(b), with the increase of the RO water recovery rate, the deviation between the two dotted lines become less at the same water recovery rate. Therefore, during the period with less solar irradiation, more reduction due to the CP and RSP effect may result in.

7.4.2 Optimum operations of the stand-alone RO desalination plant

The optimum operation of the stand-alone RO desalination plants is studied, including the stand-alone PVRO plant and the stand-alone PVROPRO plant with and without consideration of the detrimental effects. The optimum flow rate of the seawater and the optimum water recovery ratio are shown in Figure 7.7. A summer day with 24 hours (from the 25^{th} to 48^{th} hours, as shown in Figure 7.6), is considered to compare the different optimum operation of the stand-alone RO desalination plant.

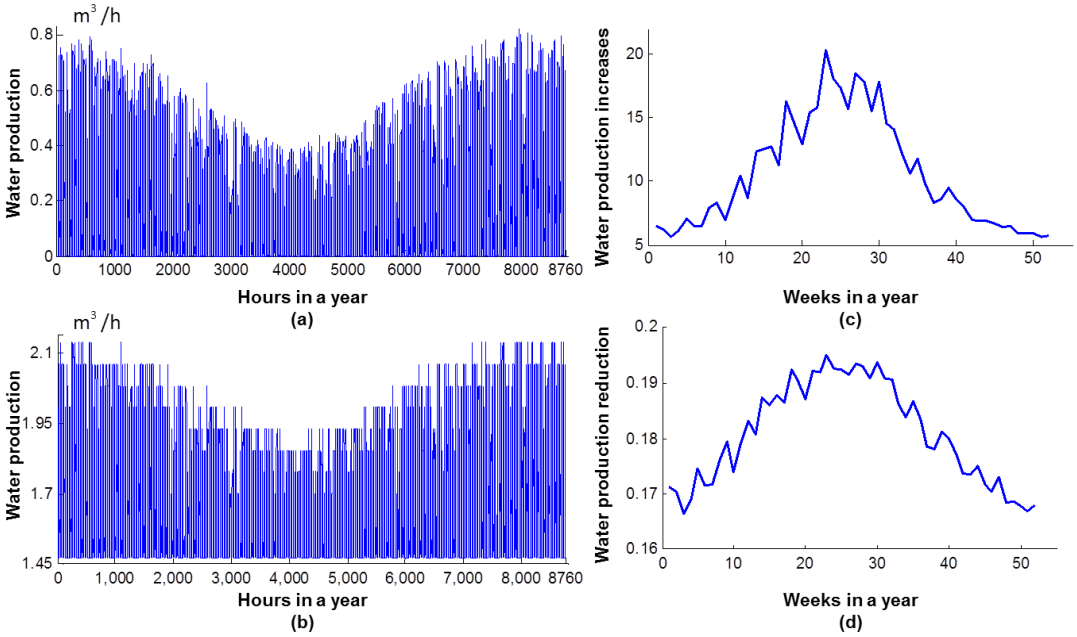

Figure 7.6: The stand-alone RO desalination plant. In (a), the hourly water production of the stand-alone PVRO desalination plant are presented. In (b), the hourly water production of the stand-alone PVROPRO desalination plant is shown. The water production increase due to the osmotic energy generation is presented in (c), and the water production reduction due to the CP and RSP effects in PRO plant are presented in (d).

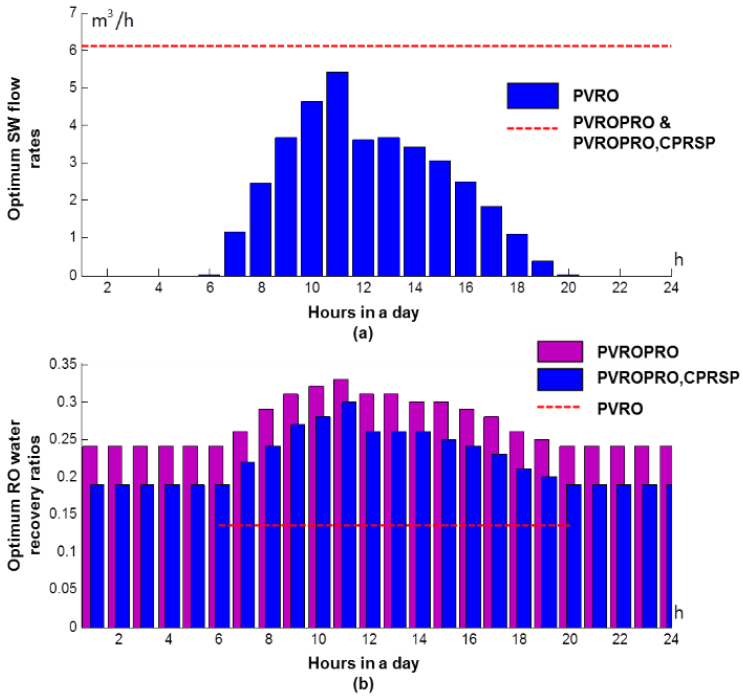

Figure 7.7: The optimum operations of the RO plant. In (a), the optimum flow rates of the seawater are presented. In (b), the optimum RO water recovery ratios are shown.

The results clearly indicate different optimum operation required for the two RO desalination plants. The seawater flow rate of the PVRO plant clearly indicates the varying optimum flow rate with respect to the available solar power. In the range of hours without solar power (hour 1-5 and hour 21-24), the flow rate of the seawater are zero and also zero treated freshwater is produced. In contrast, during daytime, the flow rate is changed in order to ensure the RO plant operated at its minimum SEC operation as shown in Figure 7.7(b). The optimum water recovery ratio of the PVRO plant is 0.13. It can be controlled by the hydraulic pressure applied on the seawater based on the thermodynamic restriction condition.

Conversely, the simulations of the PVROPRO plant are developed with the constant flow rate of the seawater as presented in Figure 7.7(a). All the flow rates during a day are constant. In the PVROPRO plant, the flow rate of the seawater is selected as the maximum in the PVRO plant for the entire year. With the osmotic energy generation by the PRO plant, the RO desalination plant can be operated consecutively over night at a low water recovery, as shown in Figure 7.7(b). However, the performance limiting effects reduce the optimum water recovery ratio in both the SSRO and SRO operation. In Figure 7.7(b), the optimum states discussed in Figure 7.4 can be identified in the 24 hours operation. It is noted that the PVROPRO without the CP and RSP effects, operation of hours 1-5 and hours 21-24, is carried out at the state E shown in Figure 7.4(a), and operation of hours 6-20 is carried out at the state B shown in Figure 7.4(b) subject to different solar power. In addition, when the CP and RSP effects are considered, operation of hours 1-5 and hours 21-24 is carried out at the state D as shown in Figure 7.4(a), and operation of hours 6-20 is carried out at the state A as shown in Figure 7.4(b).

7.4.3 Optimum operations of the PRO plant

In the PRO plant, the flow rate of the brine is determined by the RO water recovery ratio in the RO plant. The flow rate of the IW might be restricted by the local condition of the low concentration streams. Because compared to available seawater in coastal regions, the availability of low concentration stream is always limited. In this chapter, the overall dimensionless flow rate is assumed to be 0.5 that the IW flow rate is same to that of the seawater. Therefore, in order to extract the maximum salinity energy from the given volume of the seawater and the IW, the hydraulic pressure applied on the brine should be optimised. In the ideal PVROPRO plant in which the CP and RSP effects are ignored, the

maximum osmotic energy extraction can be analytically obtained [32]. But for a PRO plant with the CP and RSP effects considered, the maximum extractable energy cannot be easily calculated. It needs simulation by certain step-size of the pressure and comparison between the results to search for the optimum. With different membrane used (water and salt permeability coefficients, structural parameter, and et al.) and flow parameters (flow rates, flow directions et al.), the phenomena and detrimental effects of the CP and RSP are different. Based on the membrane and flow parameters selected, the results of the optimum operations are shown in Figure 7.8 in which both the PVROPRO plant with and without consideration of the CP and RSP effects are included.

The results indicate the optimum operational window during a day subject to the availability of solar power. Higher hydraulic pressure is required during daytime for both PVROPRO plants. It is a result of the more concentrated brine caused by the higher water recovery in the RO plant with the PV array in operation. Moreover, the overall detrimental effect on the optimum applied pressure is also studied. The results show that, when the CP and RSP effects are considered, the required optimum pressure is lower in both the SSRO and SRO operation, which is a result of the reduced osmotic energy generation.

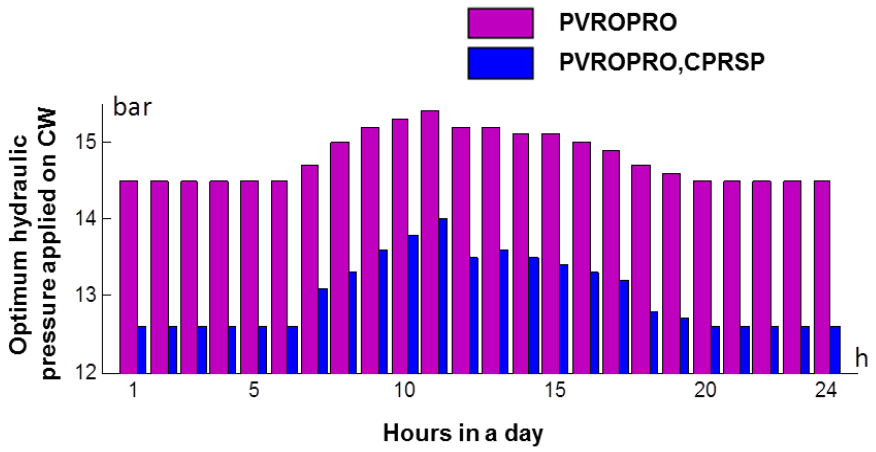

Figure 7.8: Optimum hydraulic pressure applied on the brine in the PRO plant.

7.5 SUMMARY

An investigation into the development of a novel stand-alone RO seawater desalination plant powered by a solar PV and a PRO is carried out. Two stand-alone schemes, the SSRO

and SRO operation, are proposed and investigated using a state-diagram. With the mathematical models describing the membrane process of the RO, the PRO and the solar PV energy harvest, the stand-alone feasibility is studied numerically and both the feasible operational windows of the SSRO and SRO operation are analysed. In addition, the detrimental effects, the CP and the RSP, are also investigated. Finally, with the hourly solar data of Perth, Australia in a year, the production rates of the PVROPRO plant during a year is modelled and the optimum operational windows are identified and discussed. Based on the results, some conclusions can be drawn: 1) the feasibility of the PVROPRO plant can be realized by the SSRO operation during the daytime and by the SRO operation over night when sun is unavailable; 2) the operational windows are identified in the case of both the SRO and SSRO operation in the PVROPRO plant, and the upper limit in each operational window is the optimum operation; 3) the production rate is significantly increased by the integration of the salinity power generation by the PRO plant. The highest weekly production rate of the PVROPRO plant is almost 20 times the rate in PVRO at the same week. Annual production of the PVROPRO plant is increased more than nine times that of the stand-alone PVRO plant; 4) the CP and RSP effects in the PRO plant reduce the performance of the PVROPRO plant. The weekly permeation production rate is decreased in the range of 16-20% due to the detrimental effects. Annually, the overall production is reduced by 18.07%.

Conclusion

Osmotic energy is a promising renewable energy source which is environmental friendly and less intermittent. Its enormous capacity of energy release when river water flows into and mixes with seawater makes it a great candidate to further improve the portfolio of the current renewable energy generation. Furthermore, osmotic energy recovery/generation is capable of significantly reducing the intensive energy consumption in the various desalination plants. PRO as one of the main technologies to extract the osmotic energy has rapidly developed in recent decade. On the basis of the significantly improved membrane performance, this thesis aims to develop a systematic investigation on the scale-up process of PRO by simulation, optimisation and control. First, mathematical model of a scale-up PRO process is developed based on the previously validated membrane transport equations. Then, the flow and mass transfer (including water permeation and reverse solute permeation) in a PRO process from a coupon-scale (lab-scale) to full-scale are systematically investigated in terms of power density, specific extractable energy, and

detrimental effects (ICP, ECP and RSP). In order to realise the optimum operation of the PRO process, strategies and controllers for MPPT of PRO are studied. Two MPPT controllers based on the P&O and IMR algorithms and a model-based controller are proposed and studied to track the MPP of the PRO process subject to the fluctuations and disturbances of the operation. Finally, the hybrid RO-PRO membrane process, a significant application of osmotic energy in desalination, is studied. The theoretical feasibility and performance of the hybrid system is first analysed and discussed. Additionally, integrating with solar PV, the performance of the overall water production in the two alternative operations in the hybrid solar-osmotic power driven RO desalination plant is investigated and the detrimental effects in both operations are identified.

Therefore, based on the results, some conclusions can be drawn:

- Mathematical model and modelling framework developed in this study can be used to estimate the overall performance of a scale-up PRO process. Both thermodynamic limiting performance and the detrimental effects of CP and RSP in the mass transfer can be estimated in a scale-up PRO by simulation.
- There are inherent inconsistencies in the operational conditions with regard to achieving maximal power density and available energy. It is due to different physical representations of the quantities based on the PRO discharge behaviour and the inherent trade-off between the power density and specific extractable energy in a PRO process with the increase on the membrane area.
- The results indicate favourable energetic performance of the two-stage versus the one-stage PRO process in terms of the reduced frictional loss and unused energy involved in the process. The extra energy generated by a continuous feed two-stage PRO and separated feed two-stage process are observed compared to the maximum extracted energy by the single-stage PRO. The maximum extra energy generation of the continuous feed and separated feed two-stage PRO are approximately 0.07 and 0.06 kWh/m^3 , which increases about 20% and 18% of the maximum energy generation of the single stage PRO.
- The capacity of extractable energy of the scale-up PRO discharge is significantly reduced due to the ICP, ECP and RSP effects.
- In a scale-up PRO process, the performance of the scale-up PRO process is significantly dependent on the dimensionless flow rate. Furthermore, with the increase of the

specific membrane scale, the accumulated solute leakage becomes important. The preferred membrane to achieve the optimal performance moves to the low permeability in order to reduce the detrimental effect of the reverse solute permeation. In co-current flow scheme, the optimum membrane permeability is nearly 8 $L \cdot m^{-2} \cdot h^{-1} \cdot bar^{-1}$ in PRO scale 0.01 $m^2/(L \cdot h^{-1})$, is nearly 4 $L \cdot m^{-2} \cdot h^{-1} \cdot bar^{-1}$ in PRO scale 0.05 $m^2/(L \cdot h^{-1})$, and is slightly higher than 2 $L \cdot m^{-2} \cdot h^{-1} \cdot bar^{-1}$ in PRO scale 0.1 $m^2/(L \cdot h^{-1})$ at the structural parameter 10 μm. For the counter-current, with the increased scale from 0.01 to 0.1 $m^2/(L \cdot h^{-1})$, the optimum membrane permeability coefficients are approximately 8, 5 and 3.5 $L \cdot m^{-2} \cdot h^{-1} \cdot bar^{-1}$. Therefore, counter-current flow scheme results in more evenly distributed water permeation across the membrane in a scale-up PRO process, compared to the co-current flow scheme. The counter-current flow scheme is capable to increase the process performance with a higher permeable and less selectable membrane compared to the co-current flow scheme. However, in the range of high average power density, there is no obvious difference in the osmotic energy performance between the co-current and counter-current flow schemes.

- The machines' inefficiencies drive the maximum average power density occurring at a higher dimensionless flow rate to reduce the energy losses in pumping and pressurisation and a higher specific membrane scale to increase the salinity energy generation. The energy losses caused by the inefficiencies shrunk the salinity energy generation, especially at the small dimensionless flow in a small scale process. It is observed that using the set of components with (90%, 90%, 98%) efficiencies, maximum average power density of PRO at dimensionless flow rate 0.2 is achieved at around 0.05 $m^2/(L \cdot h^{-1})$ rather than the theoretical infinitesimal specific membrane scale. The stand-alone feasibility of a hybrid RO-PRO process can be improved with lower RO water recovery and higher dimensionless flow rate. In the PRO subsystem, the optimum applied hydraulic pressure is found to be inversely proportional to the dimensionless flow rate in the range of feasible stand-alone operations and more area of membrane is required by a larger FC number.
- The stand-alone feasibility of the RO-PRO system can be significantly improved with the integration of solar PV arrays using the identified two feasible operational windows for the two operation schemes, SSRO and SRO operation. According to the case study of the proposed PVROPRO plant developed based on the hourly solar data

of Perth Australia in a year, the highest weekly production rate is found to be almost 20 times the rate in PVRO in the same week. Annual production is increased more than nine times compared to the stand-alone PVRO plant.

- The detrimental effects, CP and RSP in the mass transfer, on the operational windows are also found to decrease the performance of the hybrid PVROPRO system. It is found that, due to detrimental effects the weekly permeation production rate is decreased in the range of 16-20% and the overall annual reduction is 18.07% in the case study of Perth.
- Both the MPPT algorithms, P&O and IMRC, are demonstrated to be capable of tracking the MPP. However, in both cases the trade-off between the rise time and the oscillation is found requiring further consideration on the selection of the step-size for perturbation pressure or incremental pressure.
- The performance of the MPPT is improved significantly with the cooperation with OMC. It is demonstrated to deal with the rapid variations of the salinities.

Future work

Osmotic energy extraction and PRO are still at the early stage. It needs extensive and in-depth investigations to increase the membrane power density and specific extractable energy, and to reduce the economic cost. Scientists in material science, environmental science and chemistry are focusing on new types of materials to increase the performance of the membrane because the RO membranes and FO membranes are inappropriate for the PRO applications because of different operational conditions. The bulky support layers of the RO membranes cause severe ICP and significant decrease in water flux. In contrast, the highly open substrate of the FO membranes does not possess the sufficient mechanical strength to withstand the pressure applied in the PRO process. The objectives of the membrane development are to maximise the permeability and selectivity of the membrane and minimise the structure parameter. Furthermore, selection of draw solutions and feed solutions and interaction between solutions and membranes are also needed to be

considered. High net driving force is preferred in the PRO using highly concentrated draw solution, which is calling for easy generation and recovery of appropriate draw solution. In addition, mechanisms of fouling and salt leakage of the membrane with different feed solutions are also not clear at the moment.

Taking advantages from high performance membrane development in collaboration with engineers in chemical engineering, as an engineer in mechanical engineering, further investigations are needed for accurate modelling, optimum configuration and operation of the PRO process. In addition robust and stable control strategies are also needed to develop and implement to ensure the desired performance.

The mathematical model and modelling framework of the scale-up PRO is to estimate the overall performance of the process. The average effects of hydrodynamic conditions of the flow in the draw and feed flow channels are affected in the model to influence the water flux and solute flux across the membrane. In future, in order to capture the interaction between the hydrodynamics and the mass transfer of the PRO, a detailed mathematical model and modelling framework need to be developed. Computational fluid dynamics (CFD) modelling is a promising approach in this context. In fact, CFD based modelling has been used in several membrane systems, such as RO membrane system. Therefore, the objective of future work may be to extend the current semi-analytical model which describes the transport process in PRO process into CFD model to study the coupled hydrodynamic effect on CP and performance of the osmotic energy generation. On the basis of the developed CFD model, effects of CP and hydrodynamic conditions can be investigated in detail. For example, coupled effects of the cross-flow velocities of the draw and feed solution and the operational hydraulic pressures can be investigated. Moreover, a comparison between the semi-analytic model and CFD based model can be developed in terms of both the membrane performance and process performance.

As stated earlier, hybrid membrane process of RO and PRO has several advantages, further studies focusing on the operational analysis and optimisation should be carried out. Due to highly interacted operation between the RO and the PRO, the identification of the steady-state of the hybrid system and the dynamics of the transitions between the steady-states should be addressed. First, based on the steady-state models of the two processes, the analysis and identification of the steady-states of the hybrid system can be developed. The optimum steady operation of the hybrid system should be identified and validated by the

experimental facility or pilot systems. In addition, the dynamic modelling of the hybrid system should be carried out. Start-up, shutdown and transition of the states are the main targets. Strategies of these dynamic behaviour and specific controllers need to be investigated and developed.

Also currently, due to the lack of the high performance specific membrane for the PRO process, the efficiency of the unit membrane in the osmotic-driven mass transfer between the seawater and the river is not satisfactory. Additionally, the inefficiency of the hydro-turbine and the pumps further reduce the applicability of the salinity energy harvest by the PRO. Therefore, in future, several methodologies need to be proposed and aimed to be studied for potential applications of the PRO with the currently available membrane. First, the design and optimisation of the components need to be carried out. In order to increase the membrane performance in PRO, with the development on the fabrication of the membrane by material scientist, novel design and optimisation of the membrane module should also be accompanied. Currently, studies still focus on fundamental flow schemes, such as co-current and counter-current flow scheme, to evaluate the mass transfer behaviour in the membrane module. In fact, these basic flow schemes are viable for the local flow and approximation of the flow in a scale-up PRO process. Therefore, geometry of the membrane module should be designed. It may include the flat sheet or tubular shape, and this configuration determines the geometry of the membrane module. Inspired by the membrane modules in RO desalination, the possible membrane module may include plate-and-frame module, plate-and-frame module, spiral wound module, tubular module, hollow fibre module, and envelope-type module. The analysis and optimisation of the possible geometries of the membrane modules should be carried out. Furthermore, for the pressurisation and energy recovery and generation device, advanced and efficient devices need to be designed and manufactured. In a PRO, due to the operating media which includes a wide range of the salinities, specific design and selection criteria should be addressed. For different capacity of the PRO processes used as an osmotic power plant or an osmotic ERD in water desalination, different devices should be designed according to the different flow rates, concentrations of the flowing streams.

Moreover, as a part of the renewable energy and an inherent water treatment technology, PRO is a promising candidate to deal with the water, energy and environmental problems simultaneously. In order to further increase and accelerate applications of the PRO process, integration of the osmotic energy with other renewable energy sources, such as wind, tidal

and wave energy, are promising and straightforward. The optimisation of the design and operation of the hybrid renewable energy system subject to fluctuated environmental conditions and electricity price in the market, need to be developed. For the control of such a system, model predictive control (MPC) with preceding horizon is a solution to ensure the performance of the system. A MPC approach needs to be studied to allocate the resources for operating osmotic energy generation to supply the fluctuating load at the minimum cost. The value of having the prediction and direct control over all variables renewable resources need to be quantified. In a hybrid energy sources, such as solar/osmotic and solar/wind/osmotic, methodology to treat the intermittence of the relevant energy sources should be developed. Then, expected load consumption and expected renewable energy output are analysed at each optimisation loop in order to demand side fluctuation. Moreover, as a water treatment process, integration with other water treatment and desalination processes also results in decrease on the energy consumption of water production. The MPC approach is promising in coordinating these water treatment systems, such as RO/PRO, FO/PRO, and RO/FO/PRO, to produce water to follow the water demand in an efficient and optimum way. Furthermore, operational analysis of these water treatment systems considering the varying water price during the day might be developed. And MPC approach can be used to compensate for the time-varying effects during the operation of the hybrid water treatment system and ensure the improved performance and to reduce cost.

Bibliography

[1] Kalogirou SA. Seawater desalination using renewable energy sources. Progress in Energy and Combustion Science. 2005;31:242-81.

[2] Owen Anderson MA, Mary Livingstone. 'Smart City' - Intelligent energy integration for London's decentralised energy projects. 2012.

[3] Agency E. The city of London - London State of the Environment report. November 2011.

[4] Shannon MA, Bohn PW, Elimelech M, Georgiadis JG, Marinas BJ, Mayes AM. Science and technology for water purification in the coming decades. Nature. 2008;452:301-10.

[5] Elimelech M, Phillip WA. The Future of Seawater Desalination: Energy, Technology, and the Environment. Science. 2011;333:712-7.

[6] Mousa K, Diabat A, Fath H. Optimal design of a hybrid solar-wind power to drive a small-size reverse osmosis desalination plant. Desalin Water Treat. 2013;51:3417-27.

[7] Supply WT. Thames Gateway Water Treatment Plant, http://waterprojectsonline.com/case_studies/2010/Thames_Beckton_2010.pdf 2010.

[8] Lauren F. Greenleea, Desmond F. Lawlerb, , Benny D. Freemana, , Benoit Marrotc, , Philippe Moulinc. Reverse osmosis desalination: Water sources, technology, and today's challenges. Water Researcj 2009;43:2317-48.

[9] Thomas Manth, , Michael Gabora, Eli Oklejas Jr. Minimizing RO energy consumption under variable conditions of operation. Desalination. 2003;157:9-21.

[10] Klinko MWaK. OPTIMIZATION OF SEAWATER RO SYSTEMS DESIGN. Desalination. 2005:1-12.

[11] Wilf M. The Emergence of High Permeable Membrane. Desalination. 1997;113.

[12] Fan LTC, C. Y.; Erickson, L. E.; Hwang, C. L. . The Optimal Desaign of Reverse Osmosis Systems. Desalination. 1967;3.

[13] Fan LTC, C. Y.; Ho, L. Y. S.; Hwang, C. L. Erickson, L. E. . Analysis and Optimization of a Reverse Osmosis Water Purification System - Part I. Process Analysis and Simulation Desalination 1968;5.

[14] Fan LTC, C. Y.; Ho, L. Y. S.; Hwang, C. L. Erickson, L. E. . Analysis and Optimization of a Reverse Osmosis Water Purification System - Part I. Optimization. Desalination. 1969;6.

[15] Aihua Zhu PDC, * and Yoram Cohen. Effect of Thermodynamic Restriction on Energy Cost Optimization of RO Membrane Water Desalination. Industrial and Engineering Chemistry Research 2009;48.

[16] Zhu A, Christofides PD, Cohen Y. On RO membrane and energy costs and associated incentives for future enhancements of membrane permeability. Journal of Membrane Science. 2009;344:1-5.

[17] Zhu A, Rahardianto A, Christofides PD, Cohen Y. Reverse osmosis desalination with high permeability membranes — Cost optimization and research needs. Desalination and Water Treatment. 2010;15:256-66.

[18] Guirguis MJ. Energy Recovery Devices in Seawater Reverse Osmosis Desalination Plants with Emphasis on Efficiency and Economical Analysis of Isobaric versus Centrifugal Devices: University of South Florida; 2011.

[19] Narayan GP, St John MG, Zubair SM, Lienhard VJH. Thermal design of the humidification dehumidification desalination system: An experimental investigation. Int J Heat Mass Transf. 2013;58:740-8.

[20] Thomson M, Infield D. A photovoltaic-powered seawater reverse-osmosis system without batteries. Desalination. 2003;153:1-8.

[21] Qiblawey H, Banat F, Al-Nasser Q. Performance of reverse osmosis pilot plant powered by Photovoltaic in Jordan. Renew Energy. 2011;36:3452-60.

[22] Goetzberger A, Hebling C, Schock H-W. Photovoltaic materials, history, status and outlook. Materials Science and Engineering: R: Reports. 2003;40:1-46.

[23] D. P. Clarke YMA-AaGK. Modelling Small-Scale Stand-Alone (PV) Energy Systems with Reverse Osmosis Integration. 19th International Congress on Modelling and Simulation,. Perth, Australia2011.

[24] Ma QF, Lu H. Wind energy technologies integrated with desalination systems: Review and state-of-the-art. Desalination. 2011;277:274-80.

[25] Park GL, Schäfer AI, Richards BS. Potential of wind-powered renewable energy membrane systems for Ghana. Desalination. 2009;248:169-76.

[26] Park GL, Schäfer AI, Richards BS. Renewable energy powered membrane technology: The effect of wind speed fluctuations on the performance of a wind-powered membrane system for brackish water desalination. Journal of Membrane Science. 2011;370:34-44.

[27] Gao PH, Zhou GQ. Analysis of an evaporation-condensation desalination system in vacuum driven by geothermal energy. Desalin Water Treat. 2012;43:76-83.

[28] Tomaszewska B, Bodzek M. Desalination of geothermal waters using a hybrid UF-RO process. Part I: Boron removal in pilot-scale tests. Desalination. 2013;319:99-106.

[29] Kershman SA, Rheinländer J, Gabler H. Seawater reverse osmosis powered from renewable energy sources - hybrid wind/photovoltaic/grid power supply for small-scale desalination in Libya. Desalination. 2003;153:17-23.

[30] Li W, Krantz WB, Cornelissen ER, Post JW, Verliefde ARD, Tang CY. A novel hybrid process of reverse electrodialysis and reverse osmosis for low energy seawater desalination and brine management. Applied Energy. 2013;104:592-602.

[31] She Q, Jin X, Tang CY. Osmotic power production from salinity gradient resource by pressure retarded osmosis: Effects of operating conditions and reverse solute diffusion. Journal of Membrane Science. 2012;401–402:262-73.

[32] Yip NY, Elimelech M. Thermodynamic and Energy Efficiency Analysis of Power Generation from Natural Salinity Gradients by Pressure Retarded Osmosis. Environmental Science & Technology. 2012;46:5230-9.

[33] Yip NY, Elimelech M. Performance Limiting Effects in Power Generation from Salinity Gradients by Pressure Retarded Osmosis. Environmental Science & Technology. 2011;45:10273-82.

[34] Ramon GZ, Feinberg BJ, Hoek EMV. Membrane-based production of salinity-gradient power. Energy & Environmental Science. 2011;4:4423-34.

[35] Achilli A, Childress AE. Pressure retarded osmosis: From the vision of Sidney Loeb to the first prototype installation — Review. Desalination. 2010;261:205-11.

[36] Logan BE, Elimelech M. Membrane-based processes for sustainable power generation using water. Nature. 2012;488:313-9.

[37] La Mantia F, Pasta M, Deshazer HD, Logan BE, Cui Y. Batteries for Efficient Energy Extraction from a Water Salinity Difference. Nano Letters. 2011;11:1810-3.

[38] Pattle RE. Production of Electric Power by mixing Fresh and Salt Water in the Hydroelectric Pile. Nature. 1954;174:660-.

[39] WEINSTEIN JN, LEITZ FB. Electric Power from Differences in Salinity: The Dialytic Battery. Science. 1976;191:557-9.

[40] Post JW, Hamelers HVM, Buisman CJN. Influence of multivalent ions on power production from mixing salt and fresh water with a reverse electrodialysis system. Journal of Membrane Science. 2009;330:65-72.

[41] Veerman J, de Jong RM, Saakes M, Metz SJ, Harmsen GJ. Reverse electrodialysis: Comparison of six commercial membrane pairs on the thermodynamic efficiency and power density. Journal of Membrane Science. 2009;343:7-15.

[42] Veerman J, Post JW, Saakes M, Metz SJ, Harmsen GJ. Reducing power losses caused by ionic shortcut currents in reverse electrodialysis stacks by a validated model. Journal of Membrane Science. 2008;310:418-30.

[43] Yip NY, Elimelech M. Comparison of Energy Efficiency and Power Density in Pressure Retarded Osmosis and Reverse Electrodialysis. Environmental Science & Technology. 2014.

[44] Loeb S, Norman RS. Osmotic Power Plants. Science. 1975;189:654-5.

[45] Li X, Chung T-S. Thin-film composite P84 co-polyimide hollow fiber membranes for osmotic power generation. Applied Energy. 2014;114:600-10.

[46] GMVP. Global MVP, http://www.globalmvp.org/. 2015.

[47] Park M, Kim JH. Numerical analysis of spacer impacts on forward osmosis membrane process using concentration polarization index. Journal of Membrane Science. 2013;427:10-20.

[48] Kim YC, Kim Y, Oh D, Lee KH. Experimental Investigation of a Spiral-Wound Pressure-Retarded Osmosis Membrane Module for Osmotic Power Generation. Environmental Science & Technology. 2013;47:2966-73.

[49] Jin X, She QH, Ang XL, Tang CYY. Removal of boron and arsenic by forward osmosis membrane: Influence of membrane orientation and organic fouling. J Membr Sci. 2012;389:182-7.

[50] Kim YC, Elimelech M. Potential of osmotic power generation by pressure retarded osmosis using seawater as feed solution: Analysis and experiments. Journal of Membrane Science. 2013;429:330-7.

[51] McCutcheon JR, McGinnis RL, Elimelech M. A novel ammonia—carbon dioxide forward (direct) osmosis desalination process. Desalination. 2005;174:1-11.

[52] Xu Y, Peng XY, Tang CYY, Fu QSA, Nie SZ. Effect of draw solution concentration and operating conditions on forward osmosis and pressure retarded osmosis performance in a spiral wound module. J Membr Sci. 2010;348:298-309.

[53] She QH, Wong YKW, Zhao SF, Tang CYY. Organic fouling in pressure retarded osmosis: Experiments, mechanisms and implications. J Membr Sci. 2013;428:181-9.

[54] Post JW, Veerman J, Hamelers HVM, Euverink GJW, Metz SJ, Nymeijer K, et al. Salinity-gradient power: Evaluation of pressure-retarded osmosis and reverse electrodialysis. J Membr Sci. 2007;288:218-30.

[55] Thorsen T, Holt T. The potential for power production from salinity gradients by pressure retarded osmosis. J Membr Sci. 2009;335:103-10.

[56] Gerstandt K, Peinemann KV, Skilhagen SE, Thorsen T, Holt T. Membrane processes in energy supply for an osmotic power plant. Desalination. 2008;224:64-70.

[57] Zhou Z, Lee JY, Chung T-S. Thin film composite forward-osmosis membranes with enhanced internal osmotic pressure for internal concentration polarization reduction. Chemical Engineering Journal. 2014;249:236-45.

[58] Yip NY, Tiraferri A, Phillip WA, Schiffman JD, Hoover LA, Kim YC, et al. Thin-Film Composite Pressure Retarded Osmosis Membranes for Sustainable Power Generation from Salinity Gradients. Environmental Science & Technology. 2011;45:4360-9.

[59] Lin S, Straub AP, Elimelech M. Thermodynamic Limits of Extractable Energy by Pressure Retarded Osmosis. Energy & Environmental Science. 2014.

[60] Straub AP, Lin S, Elimelech M. Module-Scale Analysis of Pressure Retarded Osmosis: Performance Limitations and Implications for Full-Scale Operation. Environmental Science & Technology. 2014.

[61] Banchik LD, Sharqawy MH, Lienhard V JH. Effectiveness-mass transfer units (ε-MTU) model of a reverse osmosis membrane mass exchanger. Journal of Membrane Science. 2014;458:189-98.

[62] Sharqawy MH, Banchik LD, Lienhard V JH. Effectiveness–mass transfer units (ε–MTU) model of an ideal pressure retarded osmosis membrane mass exchanger. Journal of Membrane Science. 2013;445:211-9.

[63] Banchik LD, Sharqawy MH, Lienhard V JH. Limits of power production due to finite membrane area in pressure retarded osmosis. Journal of Membrane Science. 2014;468:81-9.

[64] Feinberg BJ, Ramon GZ, Hoek EMV. Scale-up characteristics of membrane-based salinity-gradient power production. Journal of Membrane Science. 2015;476:311-20.

[65] Sivertsen E, Holt T, Thelin WR, Brekke G. Iso-watt diagrams for evaluation of membrane performance in pressure retarded osmosis. Journal of Membrane Science. 2015;489:299-307.

[66] Touati K, Tadeo F, Hänel C, Schiestel T. Effect of the operating temperature on hydrodynamics and membrane parameters in pressure retarded osmosis. Desalination and Water Treatment. 2015:1-13.

[67] Touati K, Hänel C, Tadeo F, Schiestel T. Effect of the feed and draw solution temperatures on PRO performance: Theoretical and experimental study. Desalination. 2015;365:182-95.

[68] Kim J, Park M, Snyder SA, Kim JH. Reverse osmosis (RO) and pressure retarded osmosis (PRO) hybrid processes: Model-based scenario study. Desalination. 2013;322:121-30.

[69] Prante JL, Ruskowitz JA, Childress AE, Achilli A. RO-PRO desalination: An integrated low-energy approach to seawater desalination. Applied Energy. 2014;120:104-14.

[70] Achilli A, Prante JL, Hancock NT, Maxwell EB, Childress AE. Experimental Results from RO-PRO: A Next Generation System for Low-Energy Desalination. Environmental Science & Technology. 2014;48:6437-43.

[71] Yeong-Chan K, Tsorng-Juu L, Jiann-Fuh C. Novel maximum-power-point-tracking controller for photovoltaic energy conversion system. Industrial Electronics, IEEE Transactions on. 2001;48:594-601.

[72] Jain S, Agarwal V. A new algorithm for rapid tracking of approximate maximum power point in photovoltaic systems. Power Electronics Letters, IEEE. 2004;2:16-9.

[73] Femia N, Petrone G, Spagnuolo G, Vitelli M. Optimization of perturb and observe maximum power point tracking method. Power Electronics, IEEE Transactions on. 2005;20:963-73.

[74] Pandey A, Dasgupta N, Mukerjee AK. Design Issues in Implementing MPPT for Improved Tracking and Dynamic Performance. IEEE Industrial Electronics, IECON 2006 - 32nd Annual Conference on2006. p. 4387-91.

[75] Kumar G, Trivedi MB, Panchal AK. Innovative and precise MPP estimation using P–V curve geometry for photovoltaics. Applied Energy. 2015;138:640-7.

[76] Ahmed J, Salam Z. A Maximum Power Point Tracking (MPPT) for PV system using Cuckoo Search with partial shading capability. Applied Energy. 2014;119:118-30.

[77] Bizon N. On tracking robustness in adaptive extremum seeking control of the fuel cell power plants. Applied Energy. 2010;87:3115-30.

[78] Bizon N. Energy harvesting from the FC stack that operates using the MPP tracking based on modified extremum seeking control. Applied Energy. 2013;104:326-36.

[79] Lin C-H, Huang C-H, Du Y-C, Chen J-L. Maximum photovoltaic power tracking for the PV array using the fractional-order incremental conductance method. Applied Energy. 2011;88:4840-7.

[80] Salam Z, Ahmed J, Merugu BS. The application of soft computing methods for MPPT of PV system: A technological and status review. Applied Energy. 2013;107:135-48.

[81] Xu Y, Peng X, Tang CY, Fu QS, Nie S. Effect of draw solution concentration and operating conditions on forward osmosis and pressure retarded osmosis performance in a spiral wound module. Journal of Membrane Science. 2010;348:298-309.

[82] Hancock NT, Cath TY. Solute Coupled Diffusion in Osmotically Driven Membrane Processes. Environmental Science & Technology. 2009;43:6769-75.

[83] Fimbres-Weihs GA, Wiley DE. Review of 3D CFD modeling of flow and mass transfer in narrow spacer-filled channels in membrane modules. Chemical Engineering and Processing: Process Intensification. 2010;49:759-81.

[84] McCutcheon JR, Elimelech M. Modeling water flux in forward osmosis: Implications for improved membrane design. AIChE Journal. 2007;53:1736-44.

[85] McCutcheon JR, Elimelech M. Influence of concentrative and dilutive internal concentration polarization on flux behavior in forward osmosis. Journal of Membrane Science. 2006;284:237-47.

[86] Loeb S, Titelman L, Korngold E, Freiman J. Effect of porous support fabric on osmosis through a Loeb-Sourirajan type asymmetric membrane. Journal of Membrane Science. 1997;129:243-9.

[87] Achilli A, Cath TY, Childress AE. Power generation with pressure retarded osmosis: An experimental and theoretical investigation. Journal of Membrane Science. 2009;343:42-52.

[88] Gruber MF, Johnson CJ, Tang CY, Jensen MH, Yde L, Hélix-Nielsen C. Computational fluid dynamics simulations of flow and concentration polarization in forward osmosis membrane systems. Journal of Membrane Science. 2011;379:488-95.

[89] Jalilvand Z, Zokaee Ashtiani F, Fouladitajar A, Rezaei H. Computational fluid dynamics modeling and experimental study of continuous and pulsatile flow in flat sheet microfiltration membranes. Journal of Membrane Science. 2014;450:207-14.

[90] Radu AI, Vrouwenvelder JS, van Loosdrecht MCM, Picioreanu C. Modeling the effect of biofilm formation on reverse osmosis performance: Flux, feed channel pressure drop and solute passage. Journal of Membrane Science. 2010;365:1-15.

[91] Sivertsen E, Holt T, Thelin W, Brekke G. Modelling mass transport in hollow fibre membranes used for pressure retarded osmosis. Journal of Membrane Science. 2012;417–418:69-79.

[92] Spiegler KS, Kedem O. Thermodynamics of hyperfiltration (reverse osmosis): criteria for efficient membranes. Desalination. 1966;1:311-26.

[93] Geise GM, Park HB, Sagle AC, Freeman BD, McGrath JE. Water permeability and water/salt selectivity tradeoff in polymers for desalination. Journal of Membrane Science. 2011;369:130-8.

[94] Wang R, Shi L, Tang CY, Chou S, Qiu C, Fane AG. Characterization of novel forward osmosis hollow fiber membranes. Journal of Membrane Science. 2010;355:158-67.

[95] Tiraferri A, Yip NY, Phillip WA, Schiffman JD, Elimelech M. Relating performance of thin-film composite forward osmosis membranes to support layer formation and structure. Journal of Membrane Science. 2011;367:340-52.

[96] Song X, Liu Z, Sun DD. Nano Gives the Answer: Breaking the Bottleneck of Internal Concentration Polarization with a Nanofiber Composite Forward Osmosis Membrane for a High Water Production Rate. Advanced Materials. 2011;23:3256-60.

[97] Phillip WA, Yong JS, Elimelech M. Reverse Draw Solute Permeation in Forward Osmosis: Modeling and Experiments. Environmental Science & Technology. 2010;44:5170-6.

[98] Han G, Wang P, Chung T-S. Highly Robust Thin-Film Composite Pressure Retarded Osmosis (PRO) Hollow Fiber Membranes with High Power Densities for Renewable Salinity-Gradient Energy Generation. Environmental Science & Technology. 2013;47:8070-7.

[99] Chou S, Wang R, Shi L, She Q, Tang C, Fane AG. Thin-film composite hollow fiber membranes for pressure retarded osmosis (PRO) process with high power density. Journal of Membrane Science. 2012;389:25-33.

[100] Zhang S, Chung T-S. Minimizing the Instant and Accumulative Effects of Salt Permeability to Sustain Ultrahigh Osmotic Power Density. Environmental Science & Technology. 2013;47:10085-92.

[101] Zhu A, Christofides PD, Cohen Y. Effect of thermodynamic restriction on energy cost optimization of RO membrane water desalination. Industrial & Engineering Chemistry Research. 2008;48:6010-21.

[102] Kim J, Park M, Snyder SA, Kim JH. Reverse osmosis (RO) and pressure retarded osmosis (PRO) hybrid processes: Model-based scenario study. Desalination. 2013;322:121-30.

[103] van't Hoff JH. The role of osmotic pressure in the analogy between solutions and gases. Journal of Membrane Science. 1995;100:39-44.

[104] Guggenheim E. The theoretical basis of Raoult's law. Transactions of the Faraday Society. 1937;33:151-6.

[105] Wiley DE, Fletcher DF. Techniques for computational fluid dynamics modelling of flow in membrane channels. Journal of Membrane Science. 2003;211:127-37.

[106] Fletcher DF, Wiley DE. A computational fluids dynamics study of buoyancy effects in reverse osmosis. Journal of Membrane Science. 2004;245:175-81.

[107] Fimbres-Weihs GA, Wiley DE. Numerical study of two-dimensional multi-layer spacer designs for minimum drag and maximum mass transfer. Journal of Membrane Science. 2008;325:809-22.

[108] Song X, Liu Z, Sun DD. Energy recovery from concentrated seawater brine by thin-film nanofiber composite pressure retarded osmosis membranes with high power density. Energy & Environmental Science. 2013;6:1199-210.

[109] He W, Wang Y, Shaheed MH. Modelling of osmotic energy from natural salt gradients due to pressure retarded osmosis: Effects of detrimental factors and flow schemes. Journal of Membrane Science. 2014;471:247-57.

[110] He W, Wang Y, Shaheed MH. Energy and thermodynamic analysis of power generation using a natural salinity gradient based pressure retarded osmosis process. Desalination. 2014;350:86-94.

[111] Banchik LD, Sharqawy MH, Lienhard V JH. Limits of power production due to finite membrane area in pressure retarded osmosis. Journal of Membrane Science.

[112] Zhang S, Sukitpaneenit P, Chung T-S. Design of robust hollow fiber membranes with high power density for osmotic energy production. Chemical Engineering Journal. 2014;241:457-65.

[113] McCool BC, Rahardianto A, Faria J, Kovac K, Lara D, Cohen Y. Feasibility of reverse osmosis desalination of brackish agricultural drainage water in the San Joaquin Valley. Desalination. 2010;261:240-50.

[114] Anastasio DD, Arena JT, Cole EA, McCutcheon JR. Impact of temperature on power density in closed-loop pressure retarded osmosis for grid storage. Journal of Membrane Science. 2015;479:240-5.

[115] Achilli A, Prante JL, Hancock NT, Maxwell EB, Childress A. Experimental Results from RO-PRO: A Next Generation System for Low-Energy Desalination. Environmental Science & Technology. 2014.

[116] Wan CF, Chung T-S. Osmotic power generation by pressure retarded osmosis using seawater brine as the draw solution and wastewater retentate as the feed. Journal of Membrane Science. 2015;479:148-58.

[117] Chen SC, Wan CF, Chung T-S. Enhanced fouling by inorganic and organic foulants on pressure retarded osmosis (PRO) hollow fiber membranes under high pressures. Journal of Membrane Science. 2015;479:190-203.

[118] Kim YC, Lee JH, Park S-J. Novel crossflow membrane cell with asymmetric channels: Design and pressure-retarded osmosis performance test. Journal of Membrane Science. 2015;476:76-86.

[119] Han G, Ge Q, Chung T-S. Conceptual demonstration of novel closed-loop pressure retarded osmosis process for sustainable osmotic energy generation. Applied Energy. 2014;132:383-93.

[120] Bartman AR, Zhu A, Christofides PD, Cohen Y. Minimizing energy consumption in reverse osmosis membrane desalination using optimization-based control. Journal of Process Control. 2010;20:1261-9.

[121] Bartman AR, Christofides PD, Cohen Y. Nonlinear model-based control of an experimental reverse-osmosis water desalination system. Industrial & Engineering Chemistry Research. 2009;48:6126-36.

[122] Sassi KM, Mujtaba IM. Optimal operation of RO system with daily variation of freshwater demand and seawater temperature. Computers & Chemical Engineering. 2013;59:101-10.

[123] Gude VG, Nirmalakhandan N, Deng S. Renewable and sustainable approaches for desalination. Renewable and Sustainable Energy Reviews. 2010;14:2641-54.

[124] Zhu A, Christofides PD, Cohen Y. Energy Consumption Optimization of Reverse Osmosis Membrane Water Desalination Subject to Feed Salinity Fluctuation. Industrial & Engineering Chemistry Research. 2009;48:9581-9.

[125] Wang KY, Chung T-S, Amy G. Developing thin-film-composite forward osmosis membranes on the PES/SPSf substrate through interfacial polymerization. AIChE Journal. 2012;58:770-81.

[126] Sagiv A, Semiat R. Finite element analysis of forward osmosis process using NaCl solutions. Journal of Membrane Science. 2011;379:86-96.

[127] Jung DH, Lee J, Kim DY, Lee YG, Park M, Lee S, et al. Simulation of forward osmosis membrane process: Effect of membrane orientation and flow direction of feed and draw solutions. Desalination. 2011;277:83-91.

[128] Straub AP, Yip NY, Elimelech M. Raising the Bar: Increased Hydraulic Pressure Allows Unprecedented High Power Densities in Pressure-Retarded Osmosis. Environmental Science & Technology Letters. 2013.

[129] Kim YC, Elimelech M. Adverse Impact of Feed Channel Spacers on the Performance of Pressure Retarded Osmosis. Environmental Science & Technology. 2012;46:4673-81.

[130] She Q, Hou D, Liu J, Tan KH, Tang CY. Effect of feed spacer induced membrane deformation on the performance of pressure retarded osmosis (PRO): Implications for PRO process operation. Journal of Membrane Science. 2013;445:170-82.

[131] Xia GH, Sun QX, Cao X, Wang JF, Yu YZ, Wang LS. Thermodynamic analysis and optimization of a solar-powered transcritical CO2 (carbon dioxide) power cycle for reverse osmosis desalination based on the recovery of cryogenic energy of LNG (liquefied natural gas). Energy. 2014;66:643-53.

[132] Antipova E, Boer D, Cabeza LF, Guillén-Gosálbez G, Jiménez L. Uncovering relationships between environmental metrics in the multi-objective optimization of energy systems: A case study of a thermal solar Rankine reverse osmosis desalination plant. Energy. 2013;51:50-60.

[133] Blanco-Marigorta AM, Masi M, Manfrida G. Exergo-environmental analysis of a reverse osmosis desalination plant in Gran Canaria. Energy. 2014;76:223-32.

[134] Calise F, d'Accadia MD, Piacentino A. A novel solar trigeneration system integrating PVT (photovoltaic/ thermal collectors) and SW (seawater) desalination: Dynamic simulation and economic assessment. Energy. 2014;67:129-48.

[135] El-Emam RS, Dincer I. Thermodynamic and thermoeconomic analyses of seawater reverse osmosis desalination plant with energy recovery. Energy. 2014;64:154-63.

[136] Ghobeity A, Mitsos A. Optimal time-dependent operation of seawater reverse osmosis. Desalination. 2010;263:76-88.

[137] de Carvalho PCM, Riffel DB, Freire C, Montenegro FFD. The Brazilian experience with a photovoltaic powered reverse osmosis plant. Progress in Photovoltaics: Research and Applications. 2004;12:373-85.

[138] Thomson M, Miranda MS, Infield D. A small-scale seawater reverse-osmosis system with excellent energy efficiency over a wide operating range. Desalination. 2003;153:229-36.

[139] Joyce A, Loureiro D, Rodrigues C, Castro S. Small reverse osmosis units using PV systems for water purification in rural places. Desalination. 2001;137:39-44.

[140] Aybar HŞ, Akhatov JS, Avezova NR, Halimov AS. Solar powered RO desalination: Investigations on pilot project of PV powered RO desalination system. Appl Sol Energy. 2010;46:275-84.

[141] Bilton AM, Kelley LC, Dubowsky S. Photovoltaic reverse osmosis — Feasibility and a pathway to develop technology. Desalination and Water Treatment. 2011;31:24-34.

[142] Bilton AM, Wiesman R, Arif AFM, Zubair SM, Dubowsky S. On the feasibility of community-scale photovoltaic-powered reverse osmosis desalination systems for remote locations. Renewable Energy. 2011;36:3246-56.

[143] Fraidenraich N, Vilela OC, Lima GA. Specific energy consumption of PV reverse osmosis systems. Experiment and theory. Progress in Photovoltaics: Research and Applications. 2013;21:612-9.

[144] Poullikkas A. An optimization model for the production of desalinated water using photovoltaic systems. Desalination. 2010;258:100-5.

[145] Kelley LC, Dubowsky S. Thermal control to maximize photovoltaic powered reverse osmosis desalination systems productivity. Desalination. 2013;314:10-9.

[146] Ben Chaabene A, Sellami A. A novel control of a Reverse Osmosis Desalination system powered by photovoltaic generator. Electrical Engineering and Software Applications (ICEESA), 2013 International Conference on2013. p. 1-6.

[147] Bialasiewicz JT. Renewable Energy Systems With Photovoltaic Power Generators: Operation and Modeling. Industrial Electronics, IEEE Transactions on. 2008;55:2752-8.

[148] Ipsakis D, Voutetakis S, Seferlis P, Stergiopoulos F, Elmasides C. Power management strategies for a stand-alone power system using renewable energy sources and hydrogen storage. International Journal of Hydrogen Energy. 2009;34:7081-95.

[149] Bekele G, Tadesse G. Feasibility study of small Hydro/PV/Wind hybrid system for off-grid rural electrification in Ethiopia. Applied Energy. 2012;97:5-15.

[150] Cherif H, Belhadj J. Large-scale time evaluation for energy estimation of stand-alone hybrid photovoltaic-wind system feeding a reverse osmosis desalination unit. Energy. 2011;36:6058-67.

[151] Novosel T, Ćosić B, Krajačić G, Duić N, Pukšec T, Mohsen M, et al. The influence of reverse osmosis desalination in a combination with pump storage on the penetration of wind and PV energy: A case study for Jordan. Energy. 2014;76:73-81.

[152] Garcia HE, Mohanty A, Lin W-C, Cherry RS. Dynamic analysis of hybrid energy systems under flexible operation and variable renewable generation – Part I: Dynamic performance analysis. Energy. 2013;52:1-16.

[153] Garcia HE, Mohanty A, Lin W-C, Cherry RS. Dynamic analysis of hybrid energy systems under flexible operation and variable renewable generation – Part II: Dynamic cost analysis. Energy. 2013;52:17-26.

[154] Ali Ehyaei MR, M.; Ahmadi. Meeting the Electrical Energy Needs of a Residential Building with a Wind-Photovoltaic Hybrid System. In Proceedings of the 4th World Sustain Forum: Sciforum Electronic Conference Series; 2015.

[155] Dali M, Belhadj J, Roboam X. Hybrid solar–wind system with battery storage operating in grid-connected and standalone mode: Control and energy management – Experimental investigation. Energy. 2010;35:2587-95.

[156] Ibrahim H, Younès R, Basbous T, Ilinca A, Dimitrova M. Optimization of diesel engine performances for a hybrid wind–diesel system with compressed air energy storage. Energy. 2011;36:3079-91.

[157] Abdullah MO, Yung VC, Anyi M, Othman AK, Ab. Hamid KB, Tarawe J. Review and comparison study of hybrid diesel/solar/hydro/fuel cell energy schemes for a rural ICT Telecenter. Energy. 2010;35:639-46.

[158] Qi W, Liu J, Christofides PD. A distributed control framework for smart grid development: Energy/water system optimal operation and electric grid integration. Journal of Process Control. 2011;21:1504-16.

[159] Qi W, Liu J, Christofides PD. Supervisory predictive control for long-term scheduling of an integrated wind/solar energy generation and water desalination system. Control Systems Technology, IEEE Transactions on. 2012;20:504-12.

[160] Villalva MG, Gazoli JR, Filho ER. Comprehensive Approach to Modeling and Simulation of Photovoltaic Arrays. Power Electronics, IEEE Transactions on. 2009;24:1198-208.

[161] Villalva MG, Gazoli JR, Filho ER. Modeling and circuit-based simulation of photovoltaic arrays. Power Electronics Conference, 2009 COBEP '09 Brazilian2009. p. 1244-54.

[162] Zhu A, Christofides PD, Cohen Y. Minimization of energy consumption for a two-pass membrane desalination: Effect of energy recovery, membrane rejection and retentate recycling. Journal of Membrane Science. 2009;339:126-37.

[163] Meteonorm Software 7 (http://meteonorm.com/). Access in September 2014.